



SATELLITE ANTENNA PATTERN DISTORTION  
DUE TO GROUND PLANE EDGES

Charles L. Moore, Jr. and Gary A. Thiele

12

FC

AD A 026184

The Ohio State University  
**ElectroScience Laboratory**

Department of Electrical Engineering  
Columbus, Ohio 43212

FINAL REPORT 4091-2

October 1975

Contract N00014-75-C-0313

DDC  
RECEIVED  
JUN 20 1976  
C

*[Signature]*

Reproduction in whole or in part is permitted for any  
purpose of the United States Government.

Department of the Navy  
Office of Naval Research  
Arlington, Virginia 22217

APPROVED FOR PUBLIC RELEASE  
DISTRIBUTION UNLIMITED

## NOTICES

When Government drawings, specifications, or other data are used for any purpose other than in connection with a definitely related Government procurement operation, the United States Government thereby incurs no responsibility nor any obligation whatsoever, and the fact that the Government may have formulated, furnished, or in any way supplied the said drawings, specifications, or other data, is not to be regarded by implication or otherwise as in any manner licensing the holder or any other person or corporation, or conveying any rights or permission to manufacture, use, or sell any patented invention that may in any way be related thereto.

ADDITIONAL FOR

THIS  
COPY  
DATE 8/1/50  
JANUARY 1951

WHY SECTION  
BUT SECTION

BY  
DATE

1

UNCLASSIFIED

SECURITY CLASSIFICATION OF THIS PAGE (When Data Entered)

REPORT DOCUMENTATION PAGE		READ INSTRUCTIONS BEFORE COMPLETING FORM
1. REPORT NUMBER	2. GOVT ACCESSION NO.	3. RECIPIENT'S CATALOG NUMBER (1 Jul 74-30 Sep 75)
4. TITLE (and Subtitle) SATELLITE ANTENNA PATTERN DISTORTION DUE TO GROUND PLANE EDGES.		5. TYPE OF REPORT & PERIOD COVERED Final Report. 7/74-9/30/75
7. AUTHOR(s) Charles L./Moore, Jr. and Gary A./Thiele		6. PERFORMING ORG. REPORT NUMBER ESL-4091-2
9. PERFORMING ORGANIZATION NAME AND ADDRESS The Ohio State University ElectroScience Laboratory, Department of Electrical Engineering Columbus, Ohio 43		8. CONTRACT OR GRANT NUMBER(s) Contract N00014-75-C-0313
11. CONTROLLING OFFICE NAME AND ADDRESS Department of the Navy Office of Naval Research Arlington, Virginia 22217		10. PROGRAM ELEMENT, PROJECT, TASK AREA & WORK UNIT NUMBERS NRL Req. N000173-75-C-0313
14. MONITORING AGENCY NAME & ADDRESS (if different from Controlling Office) 12 141p.		12. REPORT DATE October 1975
		13. NUMBER OF PAGES 136
		15. SECURITY CLASS. (of this report) Unclassified
		15a. DECLASSIFICATION/DOWNGRADING SCHEDULE
16. DISTRIBUTION STATEMENT (of this Report) Reproduction in whole or in part is permitted for any purpose of the United States Government.		
17. DISTRIBUTION STATEMENT (of the abstract entered in Block 20, if different from Report)		
18. SUPPLEMENTARY NOTES		
19. KEY WORDS (Continue on reverse side if necessary and identify by block number) Antenna Satellite Antenna Method of Moments Geometrical Theory of Diffraction		
20. ABSTRACT (Continue on reverse side if necessary and identify by block number) The hybrid technique, which combines the Method of Moments with the Geometrical Theory of Diffraction, is used to investigate the radiation patterns of a UHF satellite antenna at various locations on a 28" by 28" square ground plane. Due to the diffraction which takes place at the edges of the ground plane, the radiation patterns are quite sensitive to the location of the antenna. It is concluded that, for the type of radiation coverage desired, it is best that the antenna be located close to one edge of the ground plane.		

DD FORM 1 JAN 73 1473

EDITION OF 1 NOV 65 IS OBSOLETE

UNCLASSIFIED 4, 12 251  
SECURITY CLASSIFICATION OF THIS PAGE (When Data Entered)

LB

## ACKNOWLEDGMENTS

The author would like to express special thanks to Professor Gary A. Thiele for serving as his adviser and providing greatly appreciated guidance and assistance throughout this endeavor. He also thanks Professor Carlton H. Walter for reviewing the manuscript and serving on the reading committee. Thanks also go to George K. Chan for his help and to the faculty and staff of the ElectroScience Laboratory.

The work reported herein was supported in part by Contract N00014-75-C-0313 between Department of the Navy, Office of Naval Research, Arlington, Virginia, and The Ohio State University Research Foundation.

The material contained in this report is also used as a thesis submitted to the Department of Electrical Engineering, The Ohio State University as partial fulfillment for the degree Master of Science.

## CONTENTS

Chapter	Page
I INTRODUCTION.....	1
II METHOD OF MOMENTS.....	4
A. Introduction	4
B. Galerkin's Method	6
C. Point-Matching	8
D. The Reaction Method	9
III THE GEOMETRICAL THEORY OF DIFFRACTION.....	16
A. Introduction	16
B. Wedge Diffraction	16
IV A HYBRID TECHNIQUE COMBINING THE METHOD OF MOMENTS AND THE GEOMETRICAL THEORY OF DIFFRACTION.....	23
A. Introduction	23
B. Far-Zone Field Pattern Calculation	26
C. Single Monopole on a Ground Plane	31
D. Two Monopoles on a Ground Plane	40
V SUMMARY AND CONCLUSIONS.....	85
REFERENCES.....	86
APPENDIX	
I .....	88
II .....	122

## CHAPTER I INTRODUCTION

The subject of this thesis is the development of a satellite communications antenna. The fundamental requirement is that the radiation pattern of the antenna be broad enough to cover the entire portion of the earth visible to it in the optical sense as illustrated in Fig. 1-1. The desired radiation pattern should have a maximum at the horizon while a local minimum is permissible mid-way between the horizon look angles. This minimum is allowable due to the increased path distance to the horizon as compared to the shortest distance between the satellite and the earth's surface. The local minimum can be as much as 6 dB below the maximum radiation in the direction of the horizon. The desired bandwidth for this antenna is 800-1000 MHz.

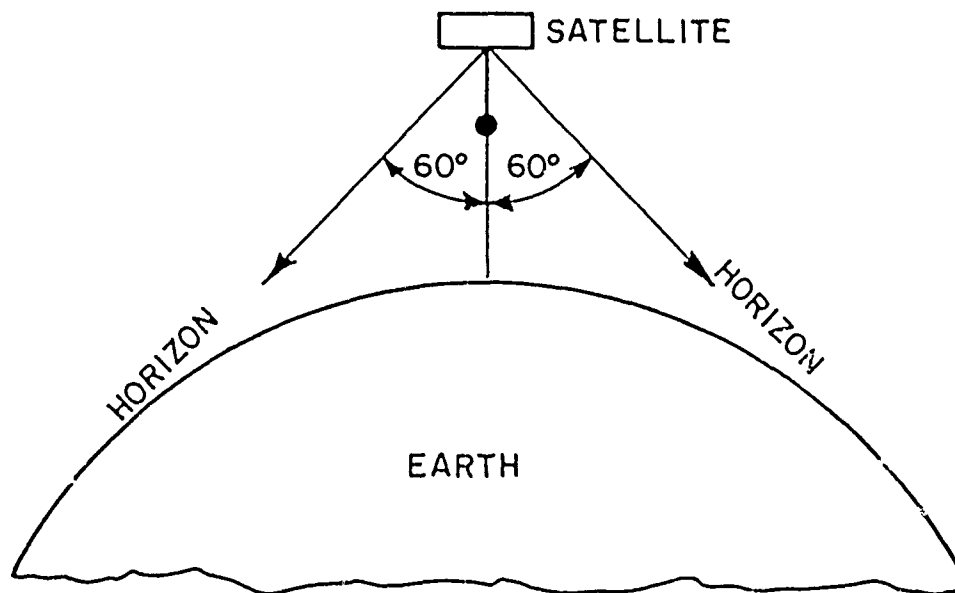


Fig. 1-1. Satellite above the earth with a 60° look angle to the horizon.

The UHF satellite antenna under investigation is shown in the photograph in Fig. 1-2. The antenna consists of four base-fed monopoles fed in phase quadrature which produces circular polarization on the axis of the antenna. Three major factors controlling the radiation pattern produced by this antenna are the flare angle of the blades, the spacing between the blades, and the location of the blades on the ground plane. Results for various flare angles, spacings, and locations are presented in Chapter IV. The results in Chapter IV are calculated using the Hybrid Technique which combines the Method of Moments and the Geometrical Theory of Diffraction [1,2].

The Method of Moments [3] is discussed in Chapter II along with Galerkin's Method [3], Point-matching [3], and the Reaction Method [4,5].

An introduction to the Geometrical Theory of Diffraction [6] is presented in Chapter III. Particular attention is focused on the equations for the diffracted field from a perfectly conducting wedge. The edge diffracted field from a ground plane which is electrically small is of great importance to the radiation pattern shape.

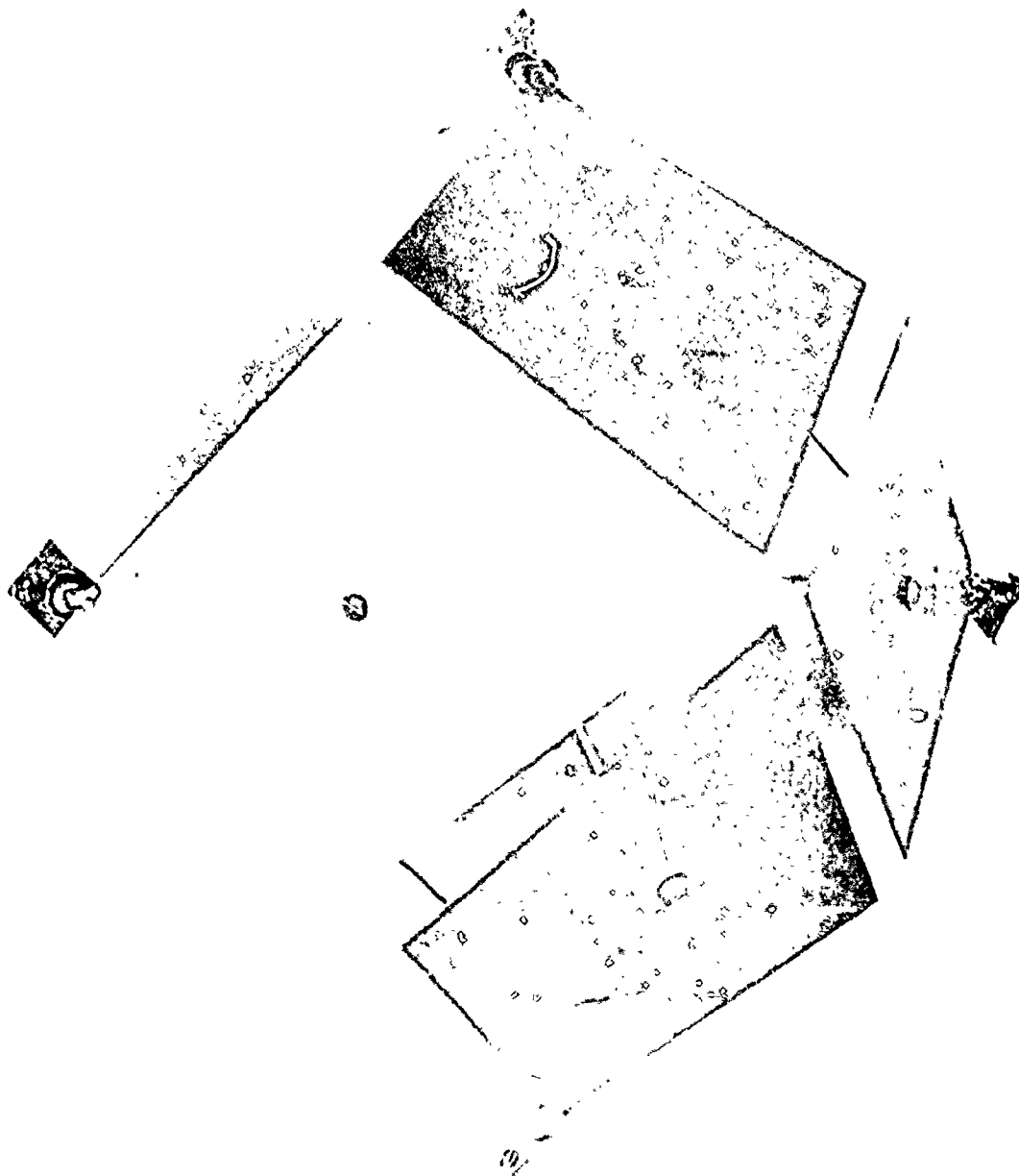


Fig. 1-2. Photograph of UHF experimental satellite antenna.



## CHAPTER II

### METHOD OF MOMENTS

#### A. Introduction

Associated with any general radiation problem there is an appropriate integral equation. With the Method of Moments it is possible to approximate the solution to the integral equation by a system of linear algebraic equations.

Consider a metallic body with current density  $\underline{J}$  on it. If the body is a perfect conductor, then the boundary conditions require that the tangential electric field be zero on the body's surface as follows:

$$(2-1) \quad \underline{E}_{\text{tan}}^S + \underline{E}_{\text{tan}}^i = 0$$

$\underline{E}_{\text{tan}}^S$  is a scattered electric field generated by the current density  $\underline{J}$ .  $\underline{E}_{\text{tan}}^i$  is the tangential component of an incident electric field generated by a source anywhere on or outside the body. Throughout the remainder of this chapter, the tan subscript will be dropped, and it will be understood that the tangential component is used unless otherwise specified.

Equation (2-1) may be rewritten as,

$$(2-2) \quad -\underline{E}^S = \underline{E}^i$$

The relationship between the current density  $\underline{J}$  and the scattered field  $\underline{E}^S$  may be written as

$$(2-3) \quad L_{\text{op}}(\underline{J}) = -\underline{E}^S$$

where  $L_{\text{op}}$  is defined as an operator which must be determined for the particular problem of interest. The concept of linear vector spaces and operators can be used to write

$$(2-4) \quad L_{\text{op}}(\underline{J}) = \underline{E}^i$$

In this equation,  $\underline{E}^i$  is a known excitation function, and  $\underline{J}$  is an unknown response function to be determined. For the problem considered in this thesis,  $L_{op}$  is an integral operator on the current density  $\underline{J}$ . For a given source, it is assumed that  $\underline{J}$  is unique and may be expressed as

$$(2-5) \quad \underline{J} = L_{op}^{-1} (\underline{E}^i) .$$

For a given problem, the space of functions or the domain of definition of the operator must be determined along with the functions resulting from the operation or range. If  $\underline{J}$  is unique, then the operator must perform a one-to-one mapping in going from a subset containing  $\underline{J}$  to one containing  $\underline{E}^i$ .

In addition to finding the domain and range of the operator, it is necessary to formulate an inner product or reaction [7],  $\langle \underline{J}, \underline{E} \rangle$ . The reaction is a scalar quantity which satisfies the following conditions:

$$(2-6) \quad \langle \underline{J}, \underline{E} \rangle = \langle \underline{E}, \underline{J} \rangle$$

$$(2-7) \quad \langle \alpha \underline{J} + \beta \underline{J}, \underline{E} \rangle = \alpha \langle \underline{J}, \underline{E} \rangle + \beta \langle \underline{J}, \underline{E} \rangle$$

if

$$(2-8) \quad \langle \underline{J}^*, \underline{J} \rangle > 0, \text{ then } \underline{J} \neq 0$$

if

$$(2-9) \quad \langle \underline{J}^*, \underline{J} \rangle = 0, \text{ then } \underline{J} = 0$$

where  $\alpha$  and  $\beta$  are scalars and  $*$  denotes the complex conjugate. The reaction is discussed in detail in Section D.

There are four basic steps in solving Eq. (2-5) by the technique known as the Method of Moments:

1.  $\underline{J}$  is expanded in a series of basis functions,  $\underline{J}_n$  which span  $\underline{J}$  in the domain of  $L_{op}$ .
2. A set of testing or weighting functions are defined and a suitable inner product determined.
3. The inner product is taken and a matrix equation formed.
4. The matrix equation is solved for the unknown, the current.

Once the current is found, then the far-zone field pattern and impedance may be calculated in a straightforward manner.

Depending upon how the basis functions, testing functions and inner product are chosen, several different types of solutions are obtained. If the basis and testing functions are chosen to be identical, we have Galerkin's method. If Dirac Delta functions are used for testing function, we have a method known as point-matching. If we use the Reaction Integral Equation and piecewise sinusoidal basis functions, we have Richmond's Reaction method [4], which is equivalently a Galerkin formulation. The remainder of this chapter is a discussion of each of these methods. The Reaction Method is subsequently used to obtain the results in Chapter IV.

#### B. Galerkin's Method

In the first step of the general Method of Moments solution, the response function  $\underline{J}$  in Eq. (2-4) is expanded in a series of basis functions  $\underline{J}_1, \underline{J}_2, \underline{J}_3, \dots$  on a surface  $S$  and defined in the domain of the operator  $L_{op}$ .

$$(2-10) \quad \underline{J} = \sum_n I_n \underline{J}_n$$

The  $I_n$ 's are unknown complex coefficients. The solution for these gives the amplitude and phase of the current on the radiator. Substituting Eq. (2-10) into Eq. (2-4) yields

$$(2-11) \quad L_{op} \left( \sum_n I_n \underline{J}_n \right) = \underline{E}^i$$

or, using the linearity of  $L_{op}$ ,

$$(2-12) \quad \sum_n I_n L_{op} (J_n) = \underline{E}^i$$

The second step in the solution is to define a set of weighting or testing functions  $\underline{W}_1, \underline{W}_2, \dots$  in the range of  $L_{op}$ . Next, the inner product is formed

$$(2-13) \quad \sum_n I_n \langle \underline{W}_m, L_{op} J_n \rangle = \langle \underline{W}_m, \underline{E}^i \rangle$$

If  $\underline{W}_m$  is set equal to  $\underline{J}_m$ , then the formulation of the problem is known as Galerkin's method, and Eq. (2-13) becomes

$$(2-14) \quad \sum_n I_n \langle \underline{J}_m, L_{op} J_n \rangle = \langle \underline{J}_m, \underline{E}^i \rangle$$

In the third step, the inner products or reactions are calculated and the matrix equation formed:

$$(2-15) \quad \begin{bmatrix} \langle \underline{J}_1, L_{op} J_1 \rangle & \langle \underline{J}_1, L_{op} J_2 \rangle & \dots \\ \langle \underline{J}_2, L_{op} J_2 \rangle & & \\ \vdots & & \ddots \end{bmatrix} \begin{pmatrix} I_1 \\ I_2 \\ \vdots \\ I_n \end{pmatrix} = \begin{pmatrix} \langle \underline{J}_1, \underline{E}^i \rangle \\ \langle \underline{J}_2, \underline{E}^i \rangle \\ \vdots \\ \langle \underline{J}_n, \underline{E}^i \rangle \end{pmatrix}$$

In compact matrix notation,

$$(2-16) \quad [Z] (I) = (V)$$

$[Z]$  represents the generalized impedances,  $(I)$  the generalized currents and  $(V)$  the generalized voltages. Solving Eq. (2-16) for  $(I)$ :

$$(2-17) \quad (I) = [Z]^{-1} (V)$$

where  $(I)$  is a column matrix containing the  $I_n$ 's in Eq. (2-10).

At least two integrations must be performed for each impedance element in Eq. (2-15). One of these integrations can be avoided by using point-matching.

### C. Point-Matching

In Galerkin's method, it is necessary to evaluate the generalized impedance elements

$$(2-18) \quad Z_{mn} = \langle \underline{J}_m, L_{op}(\underline{J}_n) \rangle$$

If numerical integrations are involved, they may be tedious and computationally expensive. This problem can be remedied by choosing Dirac delta functions as weighting functions in Eq. (2-15) such that

$$(2-19) \quad \begin{bmatrix} \langle \delta(\underline{S}-\underline{S}_1), L_{op}(\underline{J}_1) \rangle & \langle \delta(\underline{S}-\underline{S}_1), L_{op}(\underline{J}_2) \rangle & \dots \\ \langle \delta(\underline{S}-\underline{S}_2), L_{op}(\underline{J}_1) \rangle & & \\ \vdots & & \\ \vdots & & \end{bmatrix} \begin{pmatrix} I_1 \\ I_2 \\ \vdots \\ I_n \end{pmatrix}$$

$$= \begin{pmatrix} \langle \delta(\underline{S}-\underline{S}_1), \underline{E}_1^i \rangle \\ \langle \delta(\underline{S}-\underline{S}_2), \underline{E}_2^i \rangle \\ \vdots \\ \langle \delta(\underline{S}-\underline{S}_n), \underline{E}_n^i \rangle \end{pmatrix}$$

where  $\underline{S}$  is the distance to some reference point and  $\underline{S}_n$  is the distance to the point at which the boundary condition is being applied.  $\underline{E}_1^i$  indicates that matching is being done at point 1,  $\underline{E}_2^i$  indicates that matching is being done at point 2, and so forth. Any further integrations remaining are those due to  $L_{op}$ .

The use of Dirac Delta functions is physically a relaxation of the electric field boundary condition. Now the boundary condition is only applied at discrete points on the surface and not continuously over the entire surface, thus the term point-matching describes the process. Accurate solutions are obtained if a sufficient number of points are picked to match boundary conditions. The location of these points is also important for accuracy. Equispaced points yield good results for scattering problems or far-field patterns where the observer is far-removed from the radiator. For near-field problems, however, the number and location of the match points is more critical.

#### D. The Reaction Method

Richmond [4] utilizes the reaction integral equation (RIE) to derive the impedance matrix for the thin-wire radiators or scatterers in his thin-wire computer program [8]. The unknown quantity in the RIE is the current distribution of the wire structure. To arrive at the impedance matrix from this viewpoint, it is necessary to define suitable test sources and expansion modes. The purpose of this section is to define the RIE and illustrate its solution for the impedance matrix with the use of test sources and expansion modes.

Consider a closed surface,  $S$ , of a wire structure with interior volumetric region,  $V$ . There is an external source ( $\underline{J}_i, \underline{M}_i$ ) in the vicinity of the wire structure which generates the fields ( $\underline{E}, \underline{H}$ ). If the wire structure is removed, and the source is in a homogeneous medium ( $\mu, \epsilon$ ), then the incident fields ( $\underline{E}_i, \underline{H}_i$ ) are generated. The scattered fields are defined as the difference between the fields ( $\underline{E}, \underline{H}$ ) and ( $\underline{E}_i, \underline{H}_i$ ) with the wire structure present.

$$(2-20) \quad \underline{E}_s = \underline{E} - \underline{E}_i$$

$$(2-21) \quad \underline{H}_s = \underline{H} - \underline{H}_i$$

These are time-harmonic fields at the same frequency with the time-dependence term  $e^{j\omega t}$  suppressed.

From the surface-equivalence theorem of Schelkunoff [9], the following surface-current densities can be assumed on  $S$ :

$$(2-22) \quad \underline{J}_s = \hat{n} \times \underline{H}$$

$$(2-23) \quad \underline{M}_S = \underline{E} \times \hat{n}$$

The fields  $(\underline{E}, \underline{H})$  interior to  $S$  can be assumed to be zero, while the exterior fields  $(\underline{E}, \underline{H})$  remain unchanged, allowing the wire structure to be replaced by homogeneous medium  $(\mu, \epsilon)$ . The unit vector  $\hat{n}$  is directed outward from the surface.

$\underline{J}_S$  and  $\underline{M}_S$  generate the fields  $(\underline{E}_S, \underline{H}_S)$  exterior to the area that once contained the wire structure. Since  $\underline{E}$  and  $\underline{H}$  are zero interior to the region once containing the wire structure, from Eqs. (2-20) and (2-21) these interior fields are  $-\underline{E}_i$  and  $-\underline{H}_i$ .

The Carson reciprocity theorem [10] is defined as

$$(2-24) \quad \iiint_{V_1} (\underline{J}_1 \cdot \underline{E}_2 - \underline{M}_1 \cdot \underline{H}_2) dv_1 = \iiint_{V_2} (\underline{J}_2 \cdot \underline{E}_1 - \underline{M}_2 \cdot \underline{H}_1) dv_2$$

$(\underline{J}_1, \underline{M}_1)$  and  $(\underline{J}_2, \underline{M}_2)$  are source, or impressed, current densities and  $(\underline{E}_1, \underline{H}_1)$  are the fields from source 1 radiating in the presence of source 2, and vice versa for  $(\underline{E}_2, \underline{H}_2)$ . Either side of Eq. (2-24) is known as a reaction:

$$(2-25) \quad <1, 2> = \iiint_{V_1} (\underline{J}_1 \cdot \underline{E}_2 - \underline{M}_1 \cdot \underline{H}_2) dv_1$$

If reciprocity conditions are satisfied, then

$$(2-26) \quad <1, 2> = <2, 1>$$

Equation (2-26) can be expanded to yield Eq. (2-24) (the Carson reciprocity theorem). Reaction is considered as a measure of the coupling between two sources, 1 and 2.

Going back to our original problem, a test source  $(\underline{J}_m, \underline{M}_m)$  is placed in the interior region. The reaction of this test source with the other sources is desired. Applying the Carson reciprocity theorem and integrating over the surface of the test source:

$$(2-27) \quad \iint (\underline{J}_m \cdot \underline{E}_S - \underline{M}_m \cdot \underline{H}_S) ds = - \iint (\underline{J}_m \cdot \underline{E}_i - \underline{M}_m \cdot \underline{H}_i) ds$$

where  $(\underline{E}_s, \underline{H}_s)$  are the fields generated by  $(\underline{J}_s, \underline{M}_s)$ , and the origin of  $(\underline{E}_i, \underline{H}_i)$  was discussed previously. Eq. (2-27) is one form of the reaction integral equation (RIE). Eq. (2-27) states that the interior test source has zero reaction with the other sources. Another form of the RIE may be obtained from Eq. (2-27) and the reciprocity theorem:

$$(2-28) \quad \oint_S (\underline{J}_s \cdot \underline{E}^m - \underline{M}_s \cdot \underline{H}^m) ds + \iiint (\underline{J}_i \cdot \underline{E}^m - \underline{M}_i \cdot \underline{H}^m) dv = 0.$$

$(\underline{E}^m, \underline{H}^m)$  are the fields generated by the test source. The volume integral is over that region which used to be occupied by the wire structure. Electric test sources are used with Eq. (2-28) to determine the surface current distributions  $\underline{J}_s$  and  $\underline{M}_s$  for thin-wire problems. With electric test sources applied to Eq. (2-28), a less general form of the RIE is found known as the electric-field integral equation (EFIE).

In the wire structure, let each segment have a circular cylindrical surface. A circular-cylindrical coordinate system with unit vectors  $(\hat{\rho}, \hat{\phi}, \hat{z})$  is set up. The integral equation is simplified by assuming the wire radius  $a$  to be much less than the wavelength  $\lambda$ , and that the length of the wire is much greater than its radius. Therefore, if the wire is thin, the integrations over the ends of the wire can be neglected along with the circumferential component of the surface-current density  $J_\phi$ . Furthermore, the axial component of the current density  $J_z$  can be assumed independent of  $\phi$ . By these assumptions, the current density on the thin wire structure is related to the total current by

$$(2-29) \quad \underline{J}_s(z) = \frac{\hat{z} I(z)}{2\pi a} = \frac{I(z)}{2\pi a}$$

$z$  is a metric coordinate measuring position along the wire axis and  $I(z)$  is the total current including conduction and displacement. If one wire is within a few diameters of another or the wire is bent to form a small acute angle, then a more elaborate formulation than Eq. (2-29) is required.

If the wire structure is perfectly conducting, then  $\underline{M}_s$  is zero. Substituting Eq. (2-29) into the RIE (Eq. (2-28)), Eq. (2-28) reduces to

$$(2-30) \quad - \int_0^L I(z) E_z^m dz = V_m$$



where  $L$  is the entire length of the wire.

$$(2-31) \quad V_m = \iiint (\underline{J}_i \cdot \underline{E}^m - \underline{M}_i \cdot \underline{H}^m) dv$$

and

$$(2-32) \quad E_z^m = \frac{1}{2\pi} \int_0^{2\pi} \hat{z} \cdot \underline{E}^m d\phi$$

The sinusoidal reaction formulation for thin wires is based on Eq. (2-30). The known quantities in this equation are  $\underline{E}^m$  and  $V_m$ . The unknown is the current distribution  $I(z)$ . To solve for  $I(z)$ , suitable test sources and expansion modes need to be defined.

A good choice for a test source for a perfectly conducting thin wire is a filamentary electric dipole with a sinusoidal current distribution. The piecewise-sinusoidal function is similar to the natural current distribution of the perfectly conducting thin wire. Also, the sinusoidal dipole represents a finite electric line source in a homogeneous medium with simple closed-form expressions for the near-zone fields, while the mutual impedance between two such dipoles can be represented in terms of exponential integrals.

A V dipole, with different arm lengths and terminals at the vertex, makes a typical test source. The current is a maximum at the terminals and decreases sinusoidally to zero at the endpoints. The terminal current is one ampere, and the current distribution has a slope discontinuity at the terminals. The linear test dipole along with its current distribution is shown in Fig. 2-1.

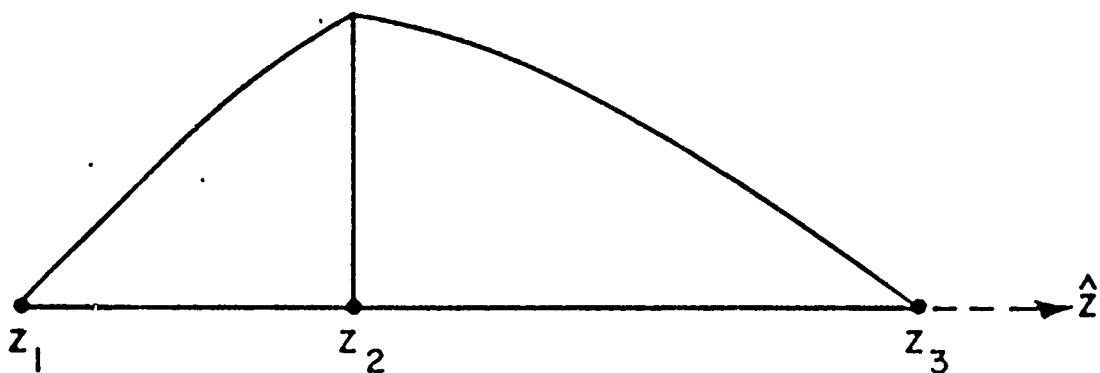


Fig. 2-1. A linear test dipole and its sinusoidal current distribution. The endpoints are at  $z_1$  and  $z_3$  with terminals at  $z_2$ .

The current distribution  $\underline{I}(z) = \underline{F}(z)$  can be represented as

$$(2-33) \quad \underline{I}(z) = \frac{\hat{z} P_1 \sin k(z-z_1)}{\sin k(z_2-z_1)} + \frac{\hat{z} P_2 \sin k(z_3-z)}{\sin k(z_3-z_2)}$$

where  $P_1 = 1$  on the interval  $z_1 < z < z_2$  and zero elsewhere and  $P_2 = 1$  for  $z_2 < z < z_3$  and is zero elsewhere.  $k$  is the complex propagation constant of the homogeneous exterior medium:

$$(2-34) \quad k = j\omega\sqrt{\mu\epsilon}$$

This value of  $k$  is necessary for the assumptions made earlier regarding the test source.

To simplify the integration in Eq. (2-32), the test dipole is placed on the wire axis rather than elsewhere in the interior region of the wire structure.

A practical problem may require many test dipoles located at different positions along the wire axis to form an overlapping array. A particular test dipole  $m$  will generate the fields  $(\underline{E}^m, \underline{H}^m)$  in the homogeneous medium. Each of the test dipoles must satisfy Eq. (2-30). Also, each dipole must radiate at the same frequency as the wire structure's true source. Thus, enforcing Eq. (2-30) requires each test dipole in the array to have the correct reaction with the true source. If there are  $N$  test dipoles, then Eq. (2-30) represents a system of  $N$  simultaneous integral equations.

The current distribution on the wire structure may be expanded in a finite series:

$$(2-35) \quad \underline{I}(z) = \sum_{n=1}^N I_n \underline{F}_n(z)$$

$\underline{F}_n(z)$  is a normalized expansion function equal to the test dipole current distribution in Eq. (2-33). Since a single expansion function relates to only a two-segment portion rather than the entire wire structure, these functions are commonly referred to as subsectional bases. The  $I_n$ 's in Eq. (2-35) are complex constants which represent samples of the current function  $\underline{I}(z)$ . The sinusoidal bases will resemble the triangular bases of a piecewise-linear model as illustrated in Fig. 2-2, if the wire segments are electrically short in reference to wavelength. Also illustrated in Fig. 2-2 is the current distribution  $\underline{I}(z)$  and its two-mode approximation  $\underline{I}'(z)$ .

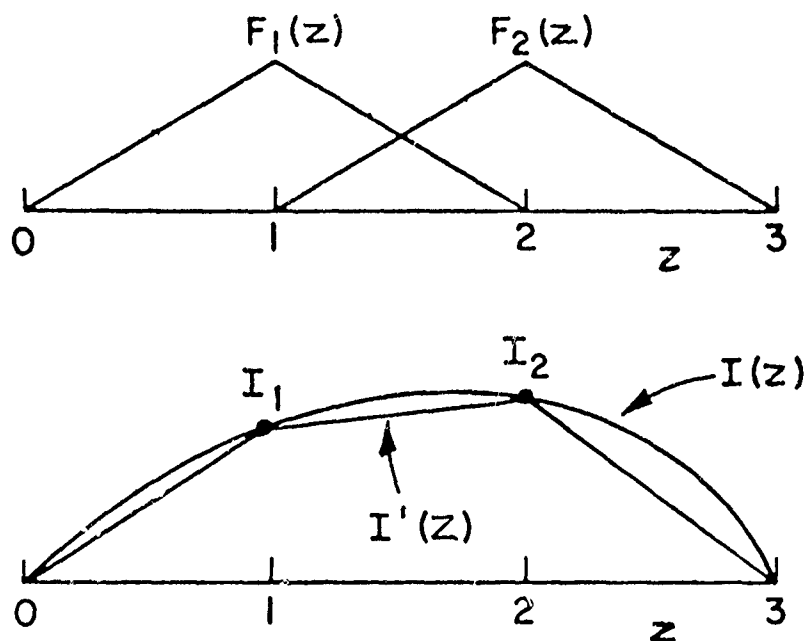


Fig. 2-2. The expansion functions  $F_1(z)$  and  $F_2(z)$ , the current distribution  $I(z)$  and the two-mode approximation  $I'(z)$ .

Notice the slope discontinuities of the piecewise-sinusoidal expansion. These discontinuities occur at the generators, lumped loads and wire corners. For all normal calculations, the calculated samples  $I_n$  will be accurate, and the corresponding piecewise-sinusoidal current distribution  $I'(z)$  will be satisfactory.

By substituting Eq. (2-35) into Eq. (2-30), the following set of simultaneous linear algebraic equations is obtained:

$$(2-36) \quad \sum_{n=1}^N I_n Z_{mn} = V_m \quad \text{where } m = 1, 2, \dots, N$$

and where

$$(2-37) \quad Z_{mn} = - \int_n F_n(z) E_z^m dz$$

The integral in Eq. (2-37) has limits which extend over the two segments in the range of expansion function  $F_n$ . For ease of computer manipulation, Eq. (2-36) may be expressed in matrix notation:

$$(2-38) \quad [Z_{mn}] (I_n) = (V_m)$$

where  $[Z_{mn}]$  is a square matrix and  $(I_n)$  and  $(V_m)$  are the column current and voltage matrices, respectively.

$[Z_{mn}]$  is the open-circuit impedance matrix for the wire-structure where the first subscript  $m$  indicates the row and the second,  $n$ , the column.  $Z_{mn}$  also represents the mutual impedance between test dipole  $m$  and expansion mode  $n$ .

## CHAPTER III

### THE GEOMETRICAL THEORY OF DIFFRACTION

#### A. Introduction

The Method of Moments is usually referred to as a low frequency technique as its use is usually applied to bodies small in terms of wavelength. The geometrical theory of diffraction (GTD), however, may be applied to bodies which are arbitrarily large in the electrical sense and is thus referred to as a high frequency technique. GTD employs rays in a systematic way to describe the field scattered by specific parts of a body, e.g., edges, tips, or corners. Only perfectly conducting bodies in an isotropic, homogeneous medium will be considered in the discussion that follows.

The basic problem in GTD is the two-dimensional case of the diffraction of an electromagnetic wave from the edge of a perfectly conducting wedge. Since this edge diffracted wave behaves like a cylindrical wave radiating from the edge, the contribution from an edge element on a three-dimensional body may be approximated by assuming the element is on the edge of a wedge extending to infinity. Wedge diffraction can, therefore, be applied to three-dimensional geometries having finite edges.

GTD was originally based on plane wave diffraction coefficients when applied to wedge diffraction. However, a different formulation for the wedge diffraction is substituted depending upon whether the incident wave is cylindrical, conical, or spherical. Rudduck [6] showed that in the treatment of antennas, it was necessary to utilize the diffraction of cylindrical waves.

#### B. Wedge Diffraction

Consider the problem of a plane wave incident upon a wedge with angle  $(2\alpha)$  equal to  $(2-n)\pi$  as shown in Fig. 3-1. At the observation point  $P(r, \phi)$  the z-component of the total field is represented by  $u(r, \phi)$

$$(3-1) \quad u(r, \phi) = V(r, \phi - \phi') \pm V(r, \phi + \phi').$$

The plus sign is used if the electric field is polarized perpendicular to the perfectly conducting edge, and the minus sign is used if the electric field is parallel to the edge.  $V(r, \phi - \phi')$  represents the incident field and  $V(r, \phi + \phi')$  represents the reflected field.

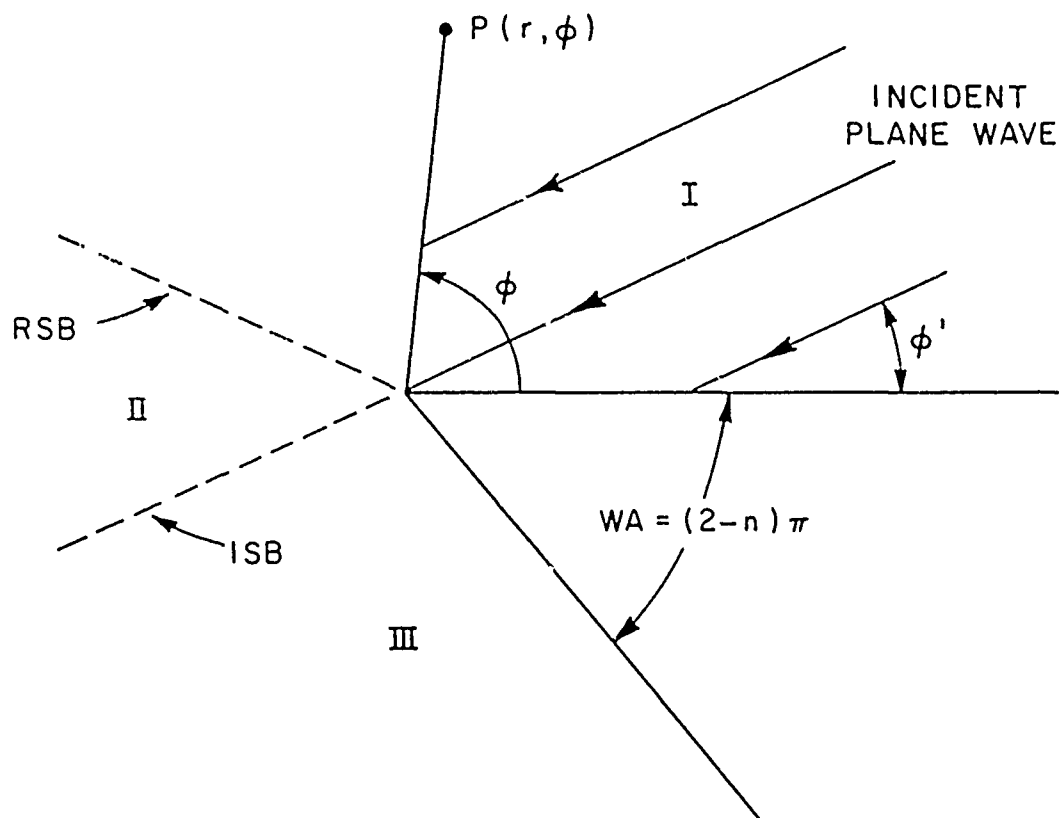


Fig. 3-1. Conducting wedge showing plane wave incidence.

These field quantities may be divided into the geometrical field  $V^*$  and the diffracted field  $V_B$ ,

$$(3-2) \quad V(r, \beta) = V^*(r, \beta) + V_B(r, \beta).$$

The geometrical field is given by

$$(3-3) \quad V^*(r, \beta) = \begin{cases} e^{jkr \cos(\beta + 2\pi n N)} & \text{if } -\pi < \beta + 2\pi n N < \pi \\ 0 & \text{otherwise} \end{cases}$$

for  $N = 0, \pm 1, \pm 2, \dots$ .

For  $\beta = \phi - \phi'$ , Eq. (3-2) gives the incident field. The incident field will be seen by any observer in regions I and II of Fig. 3-1. This region is referred to as the illumination region ( $0 < \phi < \pi + \phi'$ ) for the incident field. At  $\beta = \pi + \phi'$ , the incident shadow boundary (ISB) is encountered. Beyond this angle is the shadow region ( $\pi + \phi' < \phi < \pi$ ). Any observer in the shadow region will not see an incident field. For  $\beta = \phi + \phi'$ , Eq. (3-2) yields the reflected field. The illumination region for the reflected field is region I of Fig. 3-1 ( $0 < \phi < \pi - \phi'$ ). At  $\beta = \pi - \phi'$  is the reflection shadow boundary (RSB). Any observer beyond the RSB and outside of region I is in the shadow region for the reflected field and will not see that component of the field.

As indicated by Eq. (3-2), each geometrical field has a diffracted field  $V_B(r, \beta)$  associated with it. The diffracted field takes into account the diffraction phenomenon at the edge of the wedge and combines with the geometrical field to eliminate discontinuities on the shadow boundaries.

The diffraction problem from a conducting wedge was first solved by Sommerfeld [11]. His solution was in the form of a contour integration which proved inconvenient for computational purposes. He later derived a more practical solution, but it was only valid for large values of  $kr(1 + \cos \beta)$ . The form of this solution is

$$(3-4) \quad V_B(r, \beta) = \frac{e^{-j\left(kr + \frac{\pi}{4}\right)}}{\sqrt{2\pi kr}} \frac{\frac{1}{n} \sin \frac{\pi}{n}}{\cos \frac{\pi}{n} - \cos \frac{\beta}{n}}.$$

Pauli [12] developed a practical formula for the field diffracted by a conducting wedge which turned out to be more accurate than Sommerfeld's solution, especially in the vicinity of the shadow boundaries. His solution is:

$$(3-5) \quad V_B(r, \beta) = \frac{2 e^{j\frac{\pi}{4}}}{\sqrt{\pi}} \left( \frac{1}{n} \sin \frac{\pi}{n} \right) \frac{\left| \cos \frac{\beta}{2} \right|}{\cos \frac{\pi}{n} - \cos \frac{\beta}{n}} \\ e^{jkr \cos \beta} \frac{\int_0^\infty e^{-j\tau^2} d\tau}{\sqrt{kr(1 + \cos \beta)}} + [\text{Higher Order Terms}]$$

The higher order terms may be neglected for large values of  $kr$ .

A diffraction coefficient  $D(\beta)$  designated by Keller [13] may be related to the  $V_B$  function by

$$(3-6) \quad V_B(r, \beta) = D(\beta) \frac{e^{-jkr}}{\sqrt{r}}.$$

In 1967 a formulation introduced by Hutchins and Kouyoumjian [14] yielded far better accuracy, particularly near the shadow boundaries and for  $r < \lambda$  than that obtained from the Pauli formulation (Eq. (3-5)). Hutchins' and Kouyoumjian's formulation is given by,

$$(3-7) \quad V_B(L, \beta, n) = I_{-\pi}(L, \beta, n) + I_{+\pi}(L, \beta, n),$$

where

$$(3-8) \quad I_{\pm\pi}(L, \beta, n) = \frac{e^{-j(kL + \frac{\pi}{4})}}{j n \sqrt{2\pi}} \sqrt{a} \cot\left(\frac{\pi \pm \beta}{2n}\right)$$

$$e^{jkLa} \int_{\sqrt{kLa}}^{\infty} e^{-j\tau^2} d\tau + [\text{Higher Order Terms}]$$

where

$$(3-9) \quad a = 1 + \cos(\beta - 2n\pi N).$$

$N$  is a positive or negative integer or zero, whichever best satisfies the equations,

$$(3-10) \quad 2n\pi N - \beta = -\pi, \quad \text{for } I_{-\pi}$$

and

$$(3-11) \quad 2n\pi N - \beta = +\pi, \quad \text{for } I_{+\pi}$$

$L$  is a distance parameter to be defined later.



Consider a source field  $\underline{E}^i(s')$  located at  $s'(\rho', \phi')$  as depicted in Fig. 3-2. The source may be either electric or magnetic and may generate an incident wave on the edge of the wedge which is either plane, cylindrical, conical, or spherical. The diffracted vector field at the point  $s(\rho, \phi)$  may be represented in terms of a dyadic diffraction coefficient. The diffracted fields may be represented in a more compact form if they are expressed in terms of a ray-fixed coordinate system centered at the point or points of diffraction  $Q_E$  as suggested by Kouyoumjian and Pathak [15].

The diffracted field may be written as

$$(3-12) \quad \underline{E}^d(s) = \underline{E}^i(Q_E) \cdot D_E(\hat{s}, \hat{i}) A(s) e^{-jks}.$$

The relationships between the orthogonal unit vectors is shown in Fig. 3-2. Writing the diffracted field in a more convenient form involving the  $V_B$  function,

$$(3-13) \quad \begin{bmatrix} E_{||}^d(s) \\ E_{\perp}^d(s) \end{bmatrix} \sim \begin{bmatrix} -V_B^- & 0 \\ 0 & -V_B^+ \end{bmatrix} \begin{bmatrix} E_{||}^i(Q_E) \\ E_{\perp}^i(Q_E) \end{bmatrix} \frac{\sqrt{L} e^{jkl}}{\sin \beta_0} A(s) e^{-jks}$$

where

$$(3-14) \quad V_B^{\pm} = V_B(L, \beta^{\pm}, n) \mp V_B(L, \beta^{\pm}, n).$$

The minus sign is used for an electric field polarized parallel to the edge (soft boundary condition), and the positive sign is used for the electric field polarized perpendicular to the edge (hard boundary condition).  $\beta^{\pm} = \phi \mp \phi'$  where the minus sign is used for the incident field and the positive for the reflected field. The ray divergence factor or spatial attenuation factor  $A(s)$  is defined as

$$(3-15) \quad A(s) = \begin{cases} \frac{1}{\sqrt{s}} & \text{for plane, cylindrical and conical wave incidence} \\ \left( \frac{s'}{s(s'+s)} \right)^{1/2} & \text{for spherical wave incidence} \end{cases}$$



The distance L parameter is defined as

$$(3-16) \quad L = \begin{cases} s \sin^2 \theta_0 & \text{for plane wave incidence} \\ \frac{\rho' \rho}{\rho + \rho'} & \text{for cylindrical wave incidence} \\ \frac{s' s \sin^2 \theta_0}{s + s'} & \text{for conical and spherical wave incidence} \end{cases}$$

Through the introduction of L by Pathak and Kouyoumjian, it is possible to use the diffraction formulation of Eq. (3-13) for near-zone cases. Experience has shown that accurate results may be obtained for  $kL > 1$ . This formulation will prove useful in Chapter IV when we consider a source near a conducting wedge.

# CHAPTER IV A HYBRID TECHNIQUE COMBINING THE METHOD OF MOMENTS AND THE GEOMETRICAL THEORY OF DIFFRACTION

## A. Introduction

Consider the problem of a monopole near the edge of a perfectly conducting wedge as shown in Fig. 4-1a. To determine the current distribution on the monopole, it is necessary to change Eq. (2-38) to include the effect of the edge. This modified equation for the impedance matrix is given as [1,2]

$$(4-1) \quad [Z'_{mn}] (I'_n) = (V_m)$$

where  $[Z'_{mn}]$  is the new impedance matrix.  $(I'_n)$  is the modified column current matrix due to the effect of the edge. An element of  $[Z'_{mn}]$  may be expressed as

$$(4-2) \quad Z'_{mn} = Z_{mn} + \Delta Z_{mn}$$

$Z_{mn}$  is the original impedance matrix from Eq. (2-37) and  $\Delta Z_{mn}$  is the additional term due to the effect of the edge.

To gain some physical insight into the problem, consider Fig. 4-1b. The monopole is segmented, and on each segment the current is assumed to be constant.  $Z_{mn}$  is interpreted physically to be due to the z component of the electric field at segment m from the unit current passing through segment n.  $\Delta Z_{mn}$  is defined as the reaction between a field diffracted from the edge of the wedge due to a unit current flowing in segment n,  $E^d_{n(\perp)}$ , and the current density in segment m  $J_m$  as follows:

$$(4-3) \quad \Delta Z_{mn} = \langle J_m, E^d_{n(\perp)} \rangle$$

The geometry of the situation is shown in Fig. 4-1c.  $E^d_{n(\perp)}$  is found by applying geometrical theory of diffraction techniques. To calculate  $\Delta Z_{mn}$ , the near-field incident upon the edge due to segment n is found using the method of moments. The component of this field

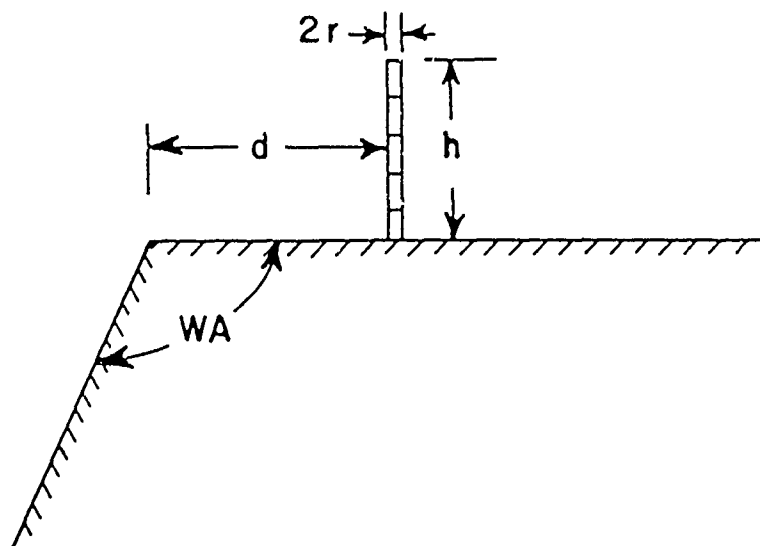


Fig. 4-1a. Monopole on a conducting wedge.

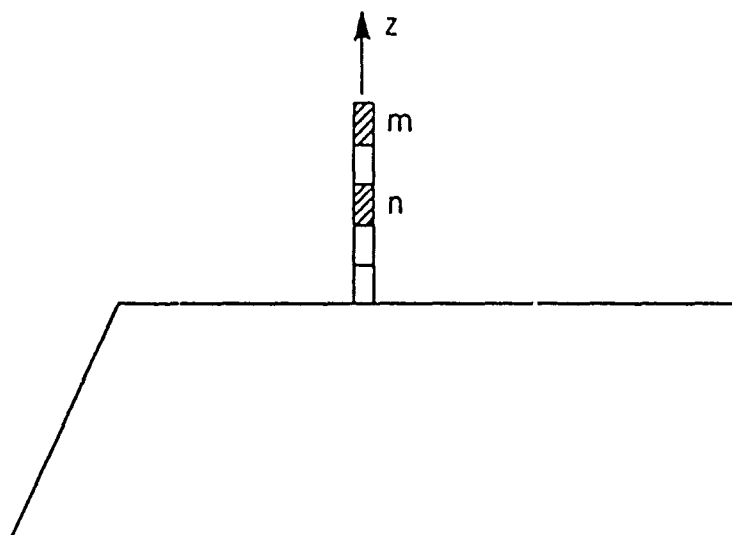


Fig. 4-1b. Monopole on a conducting wedge with segment  $m$  receiving radiation from source segment  $n$ .

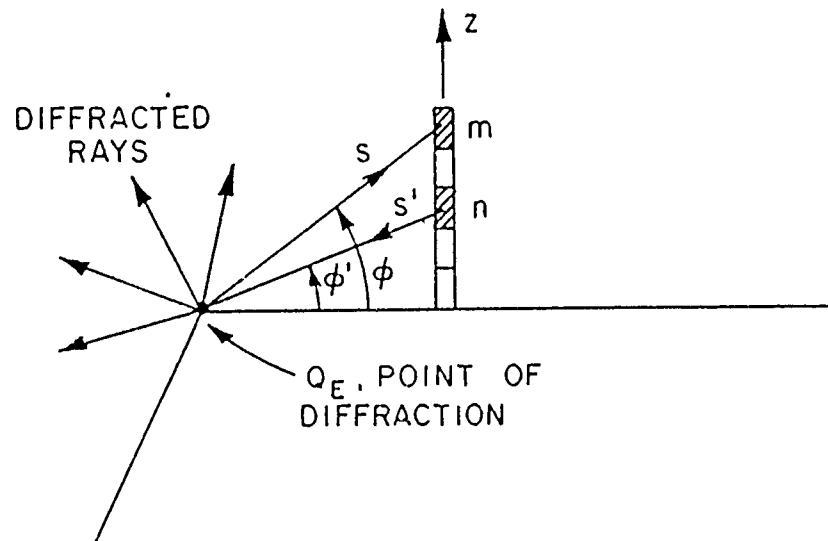


Fig. 4-1c. Monopole on a conducting wedge with segment m receiving diffracted radiation from source segment n.

which is perpendicular to the edge and to the direction of propagation is the term  $E_{\perp}^i(Q_E)$  in Eq. (3-13). This component is found from the total field by:

$$(4-4) \quad E_{\perp}^i(Q_E) = E_{\rho}^i \sin \phi' + E_z^i \cos \phi' .$$

$E_{\rho}^i$  and  $E_z^i$  are the  $\rho$  and  $z$  circular cylindrical coordinate components of the electric near field due to the current on segment n of the monopole. The field diffracted from the edge is now calculated by applying Eq. (3-13):

$$(4-5) \quad E_{\perp}^d(s) = -V_B^+ E_{\perp}^i(Q_E) \frac{\sqrt{L} e^{j k L}}{\sin \beta_0} A(s) e^{-j k s} .$$

$\beta_0 = 90^\circ$ , therefore,  $\sin \beta_0 = 1$ . For spherical wave incidence

$$A(s) = \left( \frac{s'}{s(s' + s)} \right)^{1/2} \text{ and } L = \frac{s' s}{s + s'} . \text{ Equation (4-5) may now be}$$

written as

$$(4-6) \quad E_{\perp}^d(s) = -V_B^+ E_{\perp}^i(Q_E) \left[ \frac{s' s}{s' + s} \right]^{1/2} \left[ \frac{s'}{s(s' + s')} \right]^{1/2} e^{jk \left[ \frac{s' s}{s' + s} \right]} e^{-jks}$$

Simplifying,

$$(4-7) \quad E_{\perp}^d(s) = -V_B^+ E_{\perp}^i(Q_E) \frac{s'}{s' + s} e^{jk \left[ \frac{ss'}{s' + s} - s \right]}$$

Equation (4-7) is then substituted for  $E_{n(\perp)}^d$  in Eq. (4-3), and the reaction integral is carried out:

$$(4-8) \quad \Delta Z_{mn} = \int J_m \cdot E_{\perp}^d(s) \cos \phi \, d\ell_m$$

where the integral is over the length of segment m.

For each of the impedance elements,  $Z_{mn}$ , of Eq. (2-38), the modified impedance element  $Z_{mn}'$  is determined by summing  $Z_{mn}$  with the corresponding  $\Delta Z_{mn}$ .  $Z_{mn}'$  is then substituted for  $Z_{mn}$  in Eq. (2-38) which, when solved, will result in a new current ( $I'$ ).

#### B. Far-Zone Field Pattern Calculation

The far-zone field patterns are determined by using the hybrid technique and a two-point diffraction method as illustrated in Fig. 4-2a to approximate the true physical situation depicted in Fig. 4-2b. The two-point diffraction method assumes that the ground plane extends to infinity in the x direction, allowing us to ignore the contribution of the diffracted fields from those edges and the corners. The true physical situation will have diffracted field contributions from all four sides and corners, but the contributions from points 1 and 2 in the  $\theta$ -plane will dominate. The sum of  $X_1$  and  $X_2$  in Figs. 4-2a and b equals 28 inches.

The patterns are calculated by summing the direct electric field due to the new current ( $I'$ ) on segment n with the incident near field from segment n diffracted from points 1 and 2 into the far zone,

$$(4-9) \quad \underline{E}^T = \underline{E}^n + \underline{E}_1^D + \underline{E}_2^D$$

where  $E^n$  is the direct field from segment  $n$ ,  $E_1^D$  and  $E_2^D$  are the fields diffracted from points 1 and 2, respectively, and  $E^T$  is the total far-zone field due to segment  $n$ . The geometry is depicted in Fig. 4-2c. At a given angle of  $\theta$ , the total fields for each of the monopole's segments are summed to give the particular far-zone field at that angle.

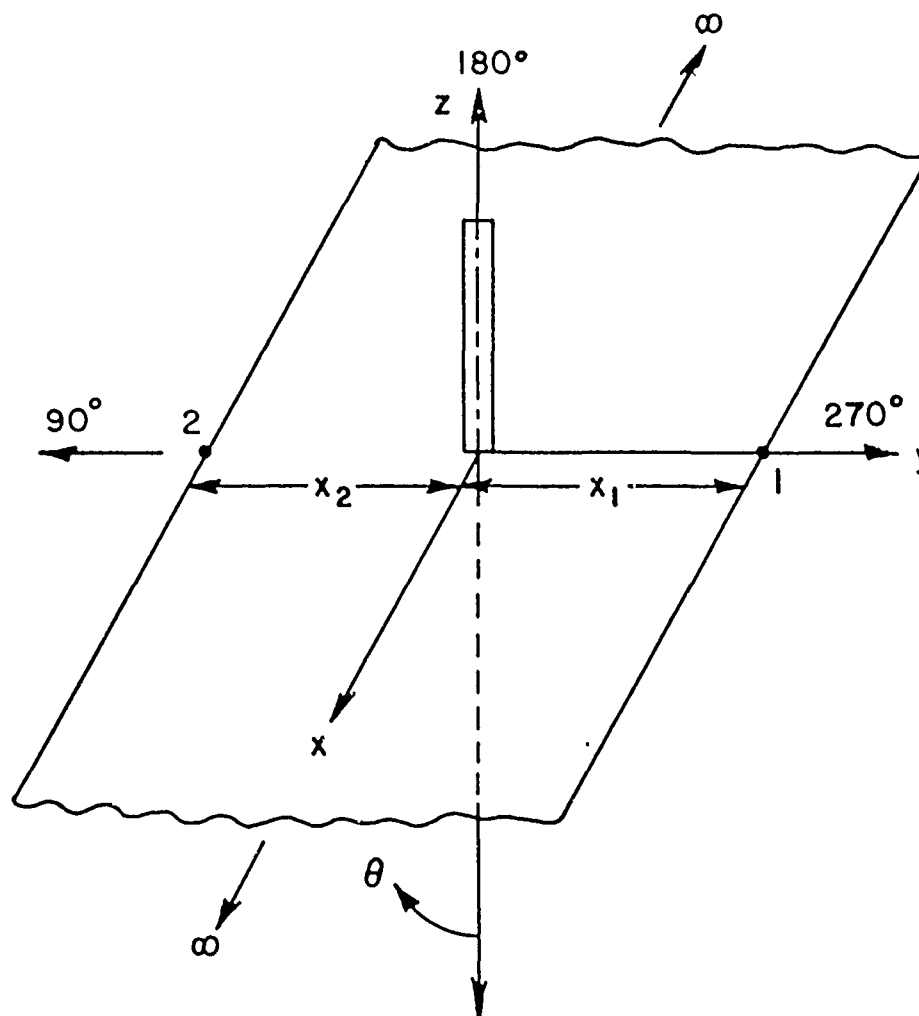


Fig. 4-2a. Two-point diffraction approximation for determining far-field patterns for a single monopole on a ground plane.  $x_1 + x_2 = 28$ ".



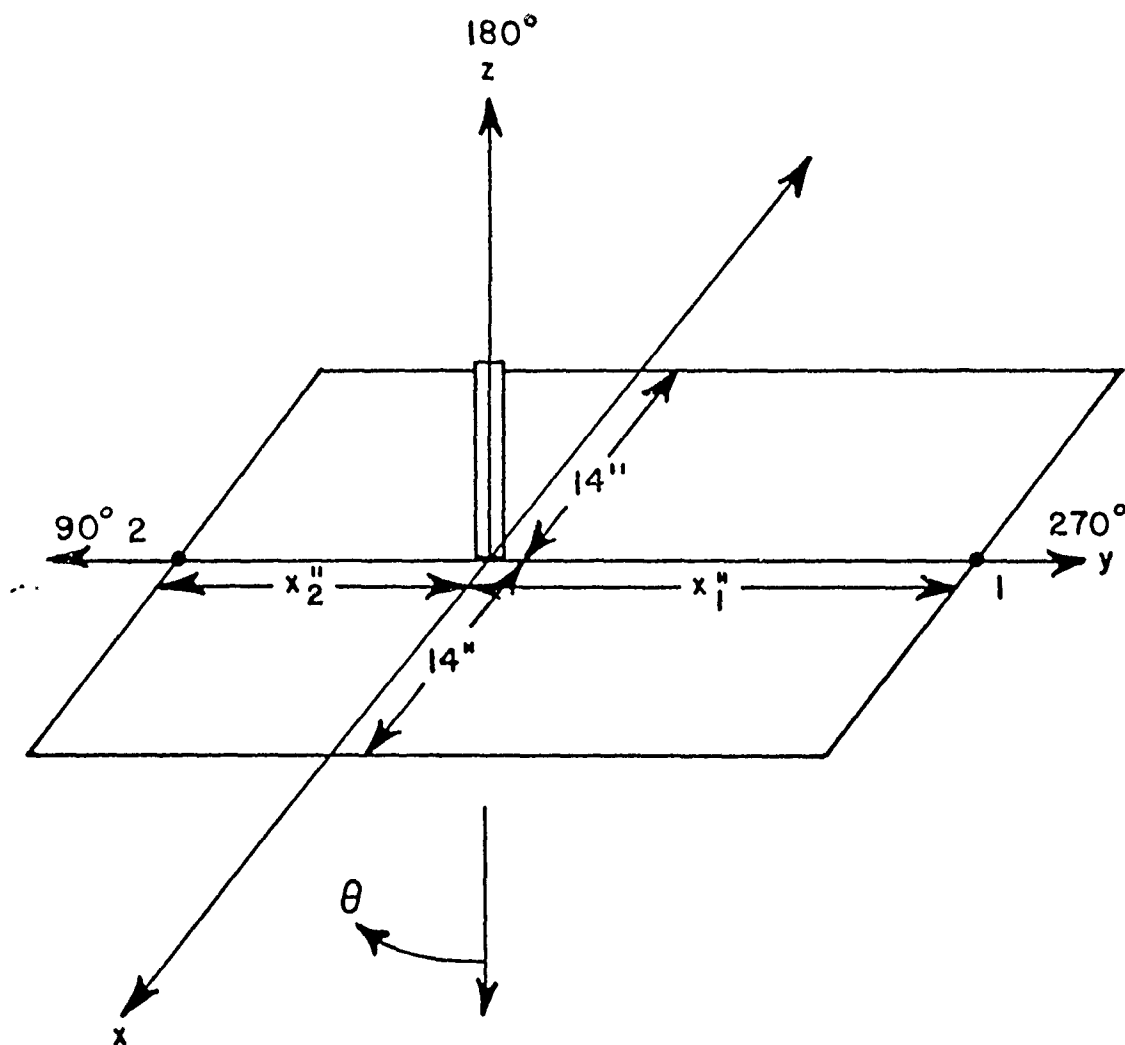


Fig. 4-2b. True physical situation.  $x_1 + x_2 = 28''$ .

The direct electric field from segment  $n$  is calculated via the Method of Moments, while the diffracted fields from the edges are found using the Geometrical Theory of Diffraction. The same procedure applied before in this chapter to find the modified impedance matrix is used here. However, instead of finding the edge diffracted field at another segment  $m$  on the monopole due to a segment  $n$ , the edge diffracted field in the far zone is desired. Applying Eq. (3-13), we find the perpendicular component of the diffracted field to be,

$$(4-10) \quad E_1^d(s) = -V_B^+ E_1^i(Q_E) \frac{s'}{s + s'} e^{jk \left[ \frac{s' s}{s + s'} \right]} e^{-jks} e^{jkx \sin \theta} ,$$

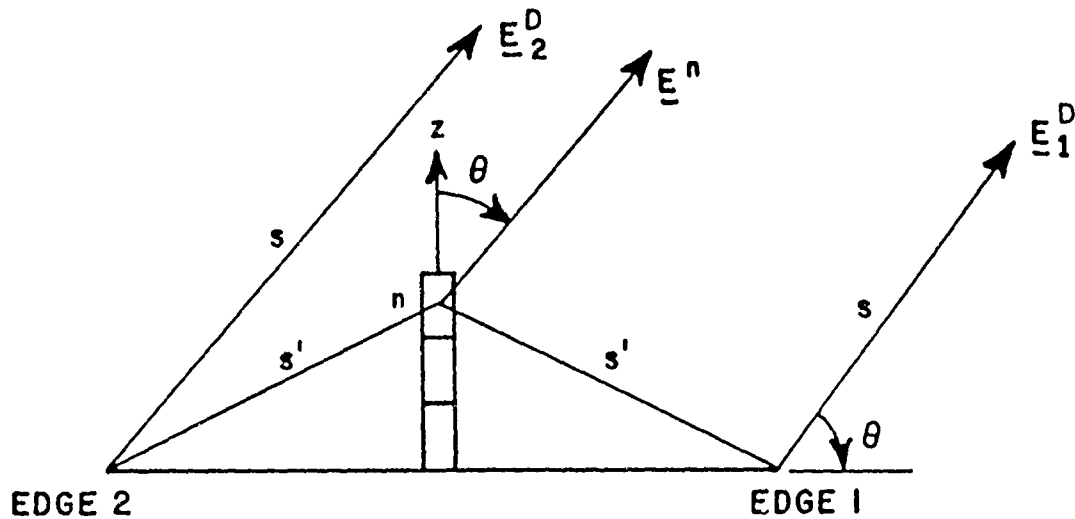


Fig. 4-2c. Contributions to the far-zone field include the direct field  $\underline{E}^n$  and the diffracted fields  $\underline{E}_1^D$  and  $\underline{E}_2^D$ .

where  $x$  is the distance from the edge to the point where the phase is referenced, and the term  $e^{jkx \sin \theta}$  puts the diffracted field in the proper phase with the direct field. In the far zone  $s$  is much much greater than  $s'$ ; therefore, Eq. (4-10) becomes

$$(4-11) \quad E_{\perp}^d(s) = -V_B^{\pm} E_{\perp}^i(Q_E) s' e^{jks'} e^{jkx \sin \theta} \frac{e^{jks}}{s}$$

The term  $\frac{e^{-jks}}{s}$  is suppressed in the far zone reducing Eq. (4-11) to

$$(4-12) \quad E_{\perp}^d(s) = -V_B^{\pm} E_{\perp}^i(Q_E) s' e^{jks'} e^{jkx \sin \theta}$$

Since the electric field is polarized perpendicular to the edge of the ground plane  $V_B^+$  is used. The significance of the + and - signs was discussed in Chapter III.

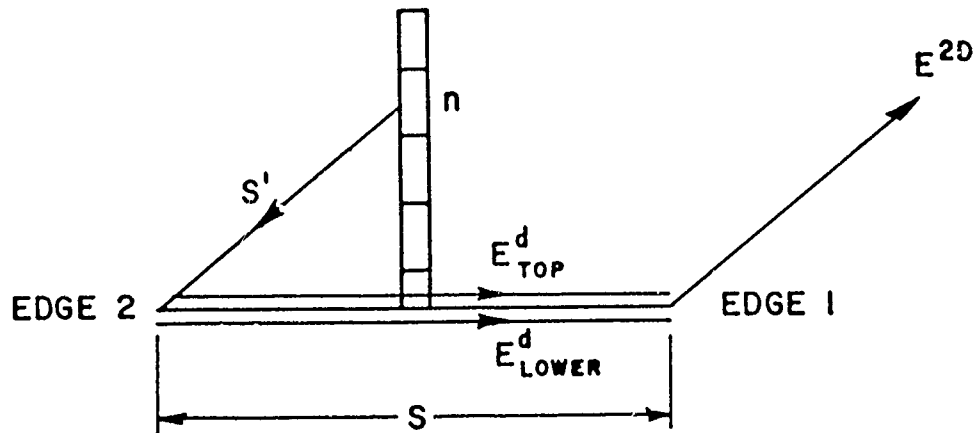


Fig. 4-2d. Geometry for the second order diffracted fields.

To take care of discontinuities occurring in the patterns at the edges of the ground plane, it was necessary to include the second order diffracted fields from edges 1 and 2. The second order diffracted field is an edge diffracted field whose incident field is the diffracted field from the opposite edge due to a particular monopole segment  $n$ . The geometry is shown in Fig. 4-2d. There are two steps in finding the contribution of the second order diffracted fields in the far zone. First, the near-field diffraction from one edge and incident upon the opposite is calculated. For this, a form like Eq. (4-7) is used,

$$(4-13) \quad E_{\perp}^d(s) = -V_B^{\pm} E_{\perp}^i(Q_E) \frac{s'}{s + s'} e^{jk \left[ \frac{s s'}{s + s'} - s \right]}$$

Two fields must be calculated using Eq. (4-13). One field travels across the top of the ground plane ( $E_{\text{top}}^d$ ) and the other travels along the underside ( $E_{\text{lower}}^d$ ) as shown in Fig. 4-2d. Since each of these fields are grazing incident fields (direction of propagation parallel with ground plane), they are each divided by a factor of two and substituted into Eq. (4-12) for  $E_{\perp}^i(Q_E)$ . The two results are summed to yield the second order diffracted field in the far zone. The second order diffracted fields are calculated for both edges ( $E_1^{2D}$  and  $E_2^{2D}$ ) and then summed in Eq. (4-9) to yield a new expression for the total far-zone field as follows,

$$(4-14) \quad \underline{E}^T = \underline{E}^n + \underline{E}_1^D + \underline{E}_2^D + \underline{E}_1^{2D} + \underline{E}_2^{2D}$$

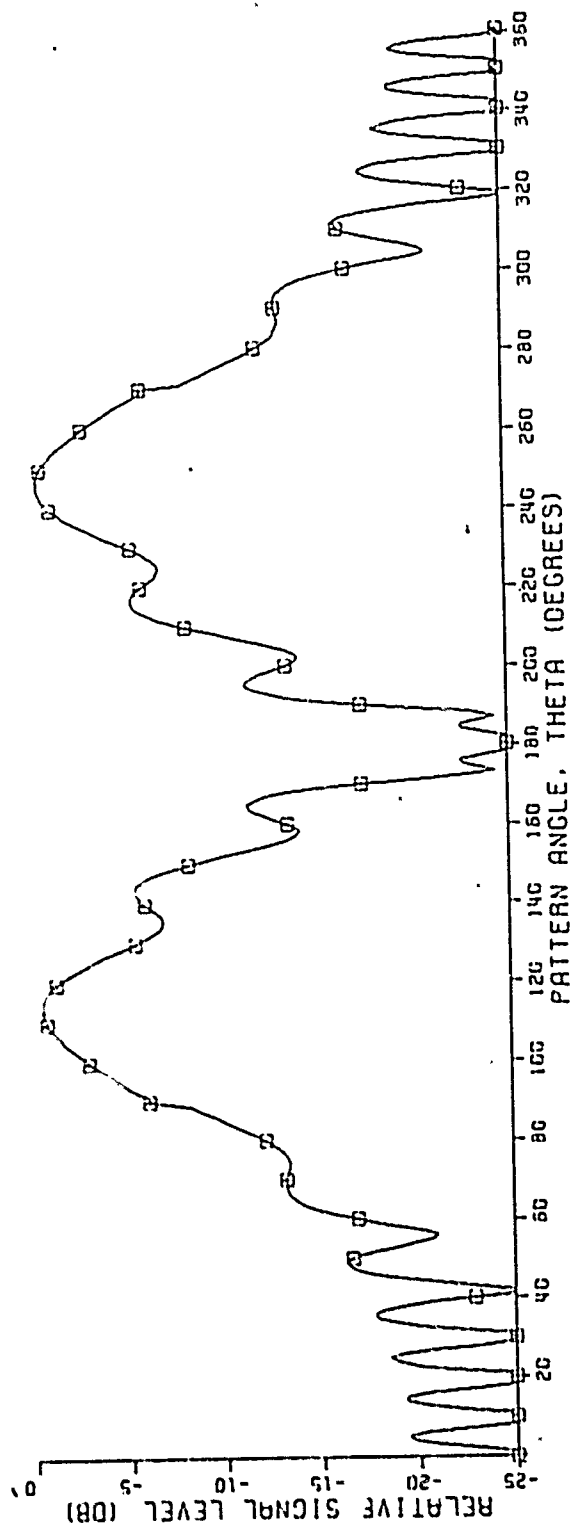
With these expressions, the far-zone field patterns of one monopole or two monopoles on a ground plane are accurately approximated.

### C. Single Monopole on a Ground Plane

The far-field pattern of a quarter wavelength monopole calculated using the two-point diffraction approximation is shown in Fig. 4-3a. The  $X_1$  and  $X_2$  values in Fig. 4-2a are each three wavelengths as indicated by the computer drawn sketch in Fig. 4-3a. This pattern is compared with the measured pattern of the actual situation and the calculated pattern of Lopez [16] in Fig. 4-3b. Lopez's patterns are those of a stub on a circular ground plane with a three-wavelength radius. Lopez also used a two-point diffraction approximation. His two-point diffraction method is valid everywhere except near the caustic which exists in his problem. By studying the measured and calculated patterns in Fig. 4-3b, it is evident that this is indeed the case. From 0 to about 10 degrees in Fig. 4-3b, the shapes of the calculated and measured patterns differ. It is seen from Figs. 4-3a and b that the two-point diffraction method is a reasonable approximation for the true physical situation as the two points are the dominate diffraction mechanisms, and the only other contributor to the far-field pattern is the monopole.

In Figs. 4-4a through 4-6a the far-field patterns are calculated using the hybrid technique and two-point diffraction at 14 inches to either side of the  $1/4\lambda$  monopole. The a parts of Figs. 4-4 through 4-6 are to be compared with the b parts which are far-field patterns of a stub on a four-sided ground plane calculated by Burnside's GTD computer program [17]. The reason for making the comparison with the pure GTD program is to provide an independent check on the validity of our computer program.

Burnside's program uses infinitesimally short current sources which have amplitudes and locations so as to simulate a quarter wavelength monopole with a sinusoidal current distribution. His program also takes into account the diffraction from the four corners and all four sides. However, in this comparison, the two opposite sides are set at distances much greater than the other two so as to approximate Fig. 4-2a and so that the points on the two closer sides will dominate the diffracted field contribution.



180  
90  
270  
3λ

MONOPOLE LENGTH=0.25 WAVELENGTHS

FREQUENCY=300.0 MHZ

□ FIELD INCLUDING EDGE DIFFRACTION

Fig. 4-3a.

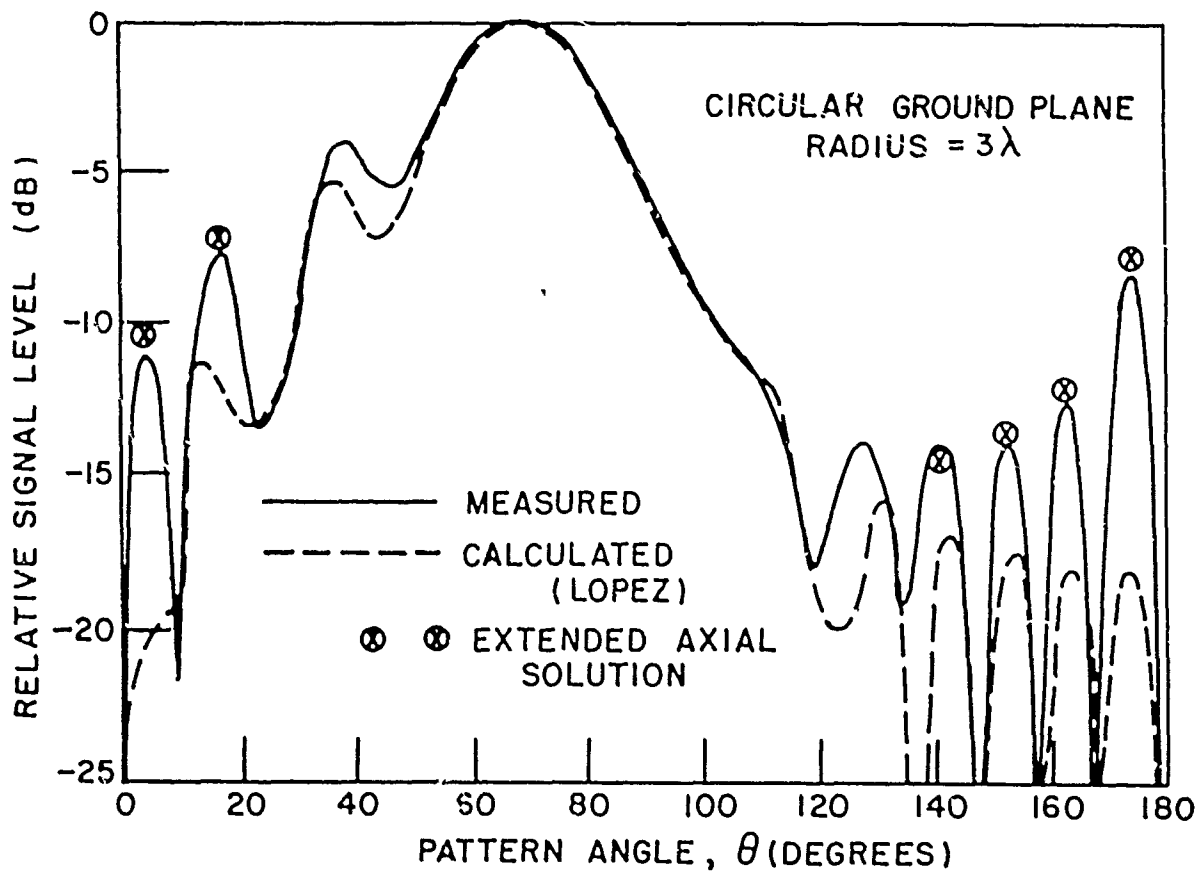
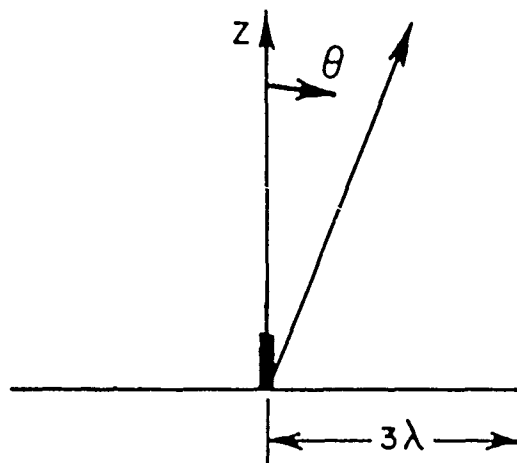
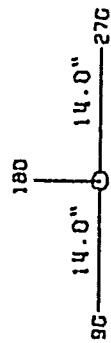
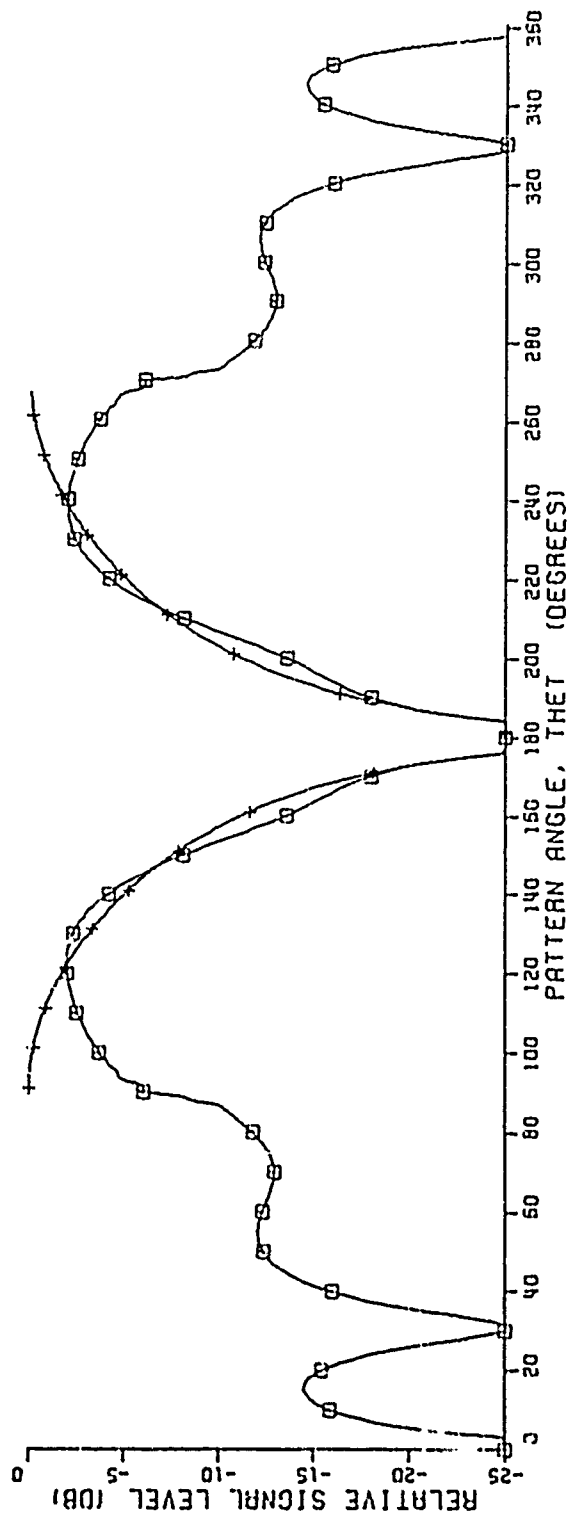


Fig. 4-3b. Radiation pattern of a stub on a circular ground plane.



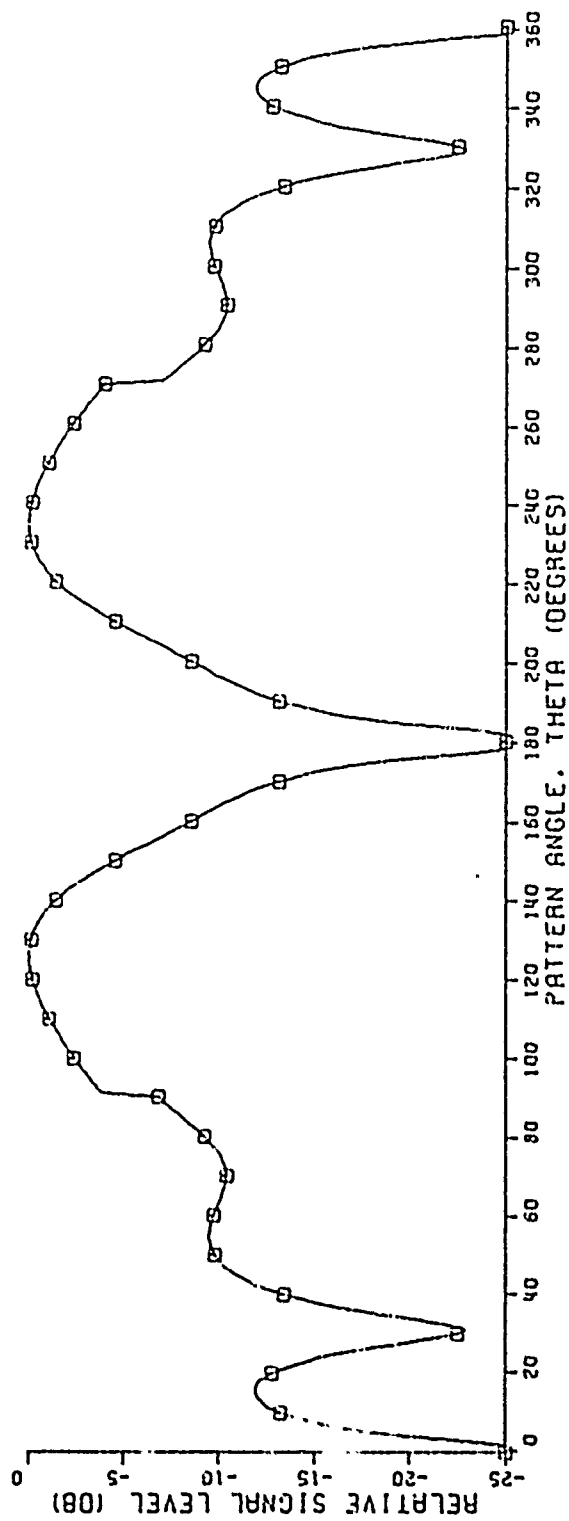
MONOPOLE LENGTH=0.25 WAVELENGTHS

FREQUENCY=300.0 MHZ

○ FIELD INCLUDING EDGE DIFFRACTION

+ FIELD FROM ANT. ON INFINITE GROUND PLANE

Fig. 4-4a.



190  
14.0" 14.0" 270

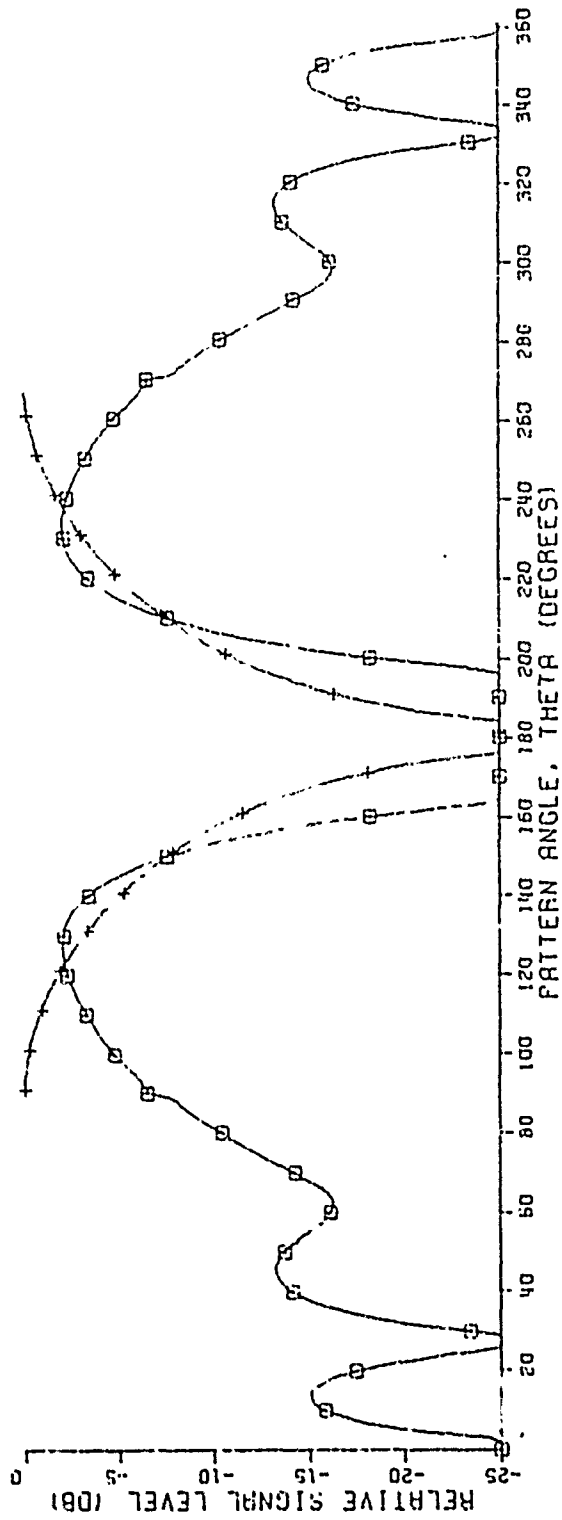
MONOPOLE LENGTH=0.25 WAVELENGTHS

FREQUENCY=800.0 MHZ

FIELD INCLUDING EDGE DIFFRACTION

Fig. 4-4b. Calculated by Burnside's method.

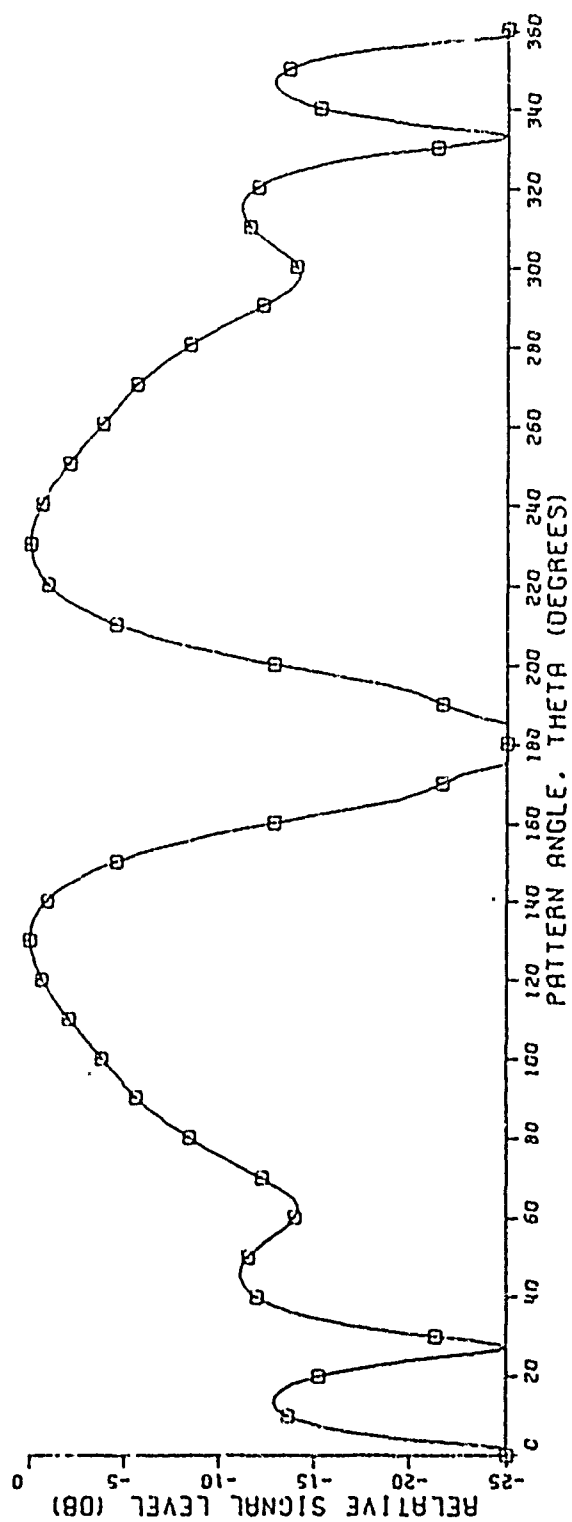




MONOPOLE LENGTH=0.25 WAVELENGTHS  
 FREQUENCY=900.0 MHZ

□ FIELD INCLUDING EDGE DIFFRACTION  
 + FIELD FROM ANT. ON INFINITE GROUND PLANE

Fig. 4-5a.



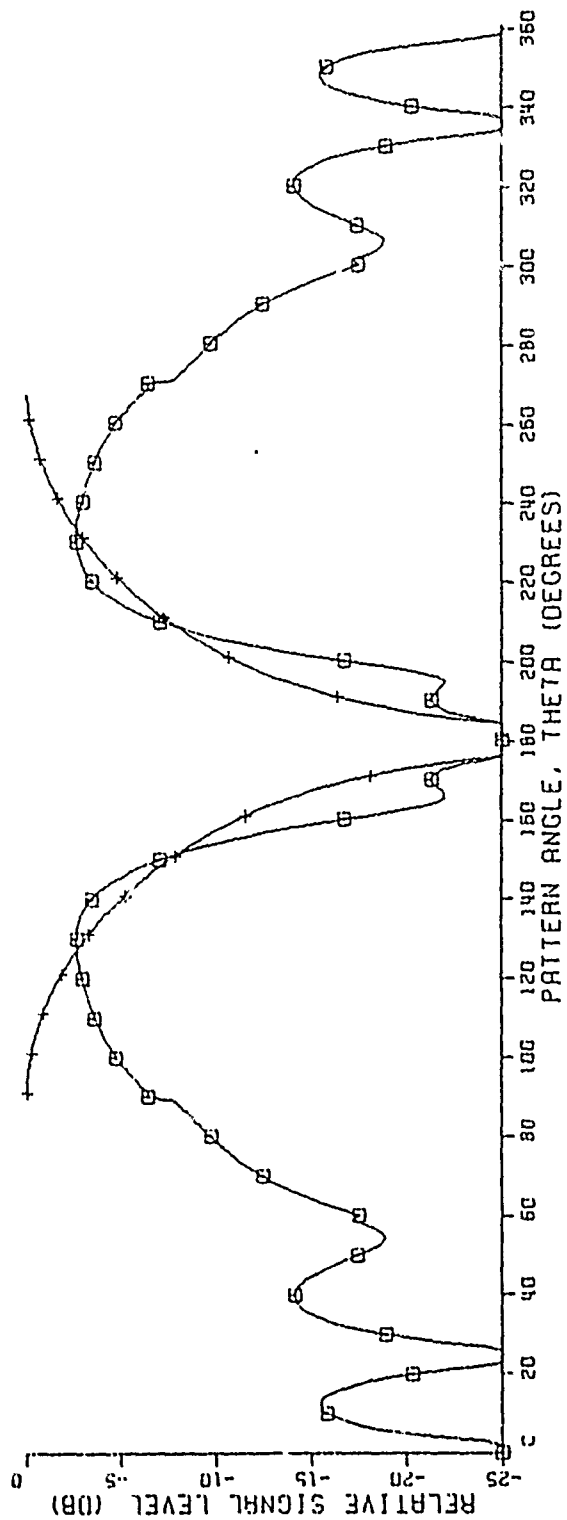
180  
14.0" 14.0" 270

MONOPOLE LENGTH=0.25 WAVELENGTHS

FREQUENCY=900.0 MHZ

FIELD INCLUDING EDGE DIFFRACTION

Fig. 4-5b. Calculated by Burnside's method.



180.  
14.0" 14.0" 270

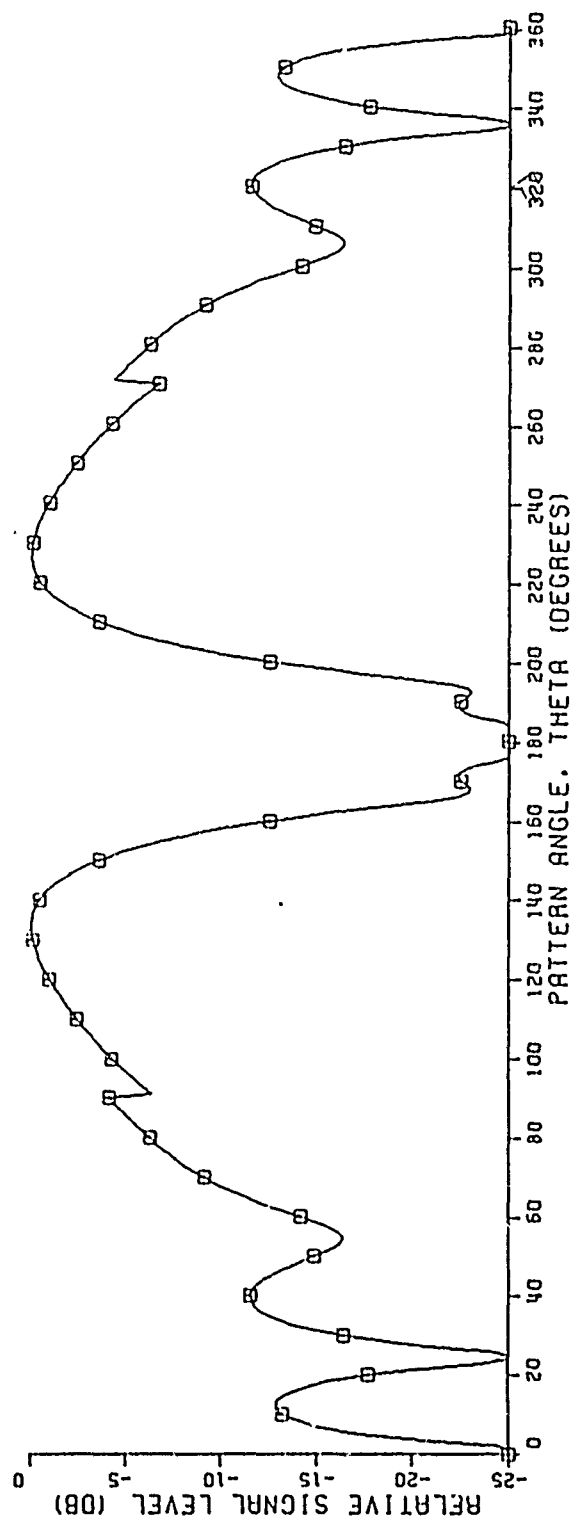
MONOPOLE LENGTH=0.25 WAVELENGTHS

FREQUENCY=1000.0 MHZ

W FIELD INCLUDING EDGE DIFFRACTION

+ FIELD FROM ANT. ON INFINITE GROUND PLANE

Fig. 4-6a.



180  
 14.0" 14.0" 270  
 90

MONOPOLE LENGTH=0.25 WAVELENGTHS

FREQUENCY=1000.0 MHZ

FIELD INCLUDING EDGE DIFFRACTION

Fig. 4-6b. Calculated by Burnside's method.

Also contained in Figs. 4-4a, 4-5a, and 4-6a are the far-field patterns of the monopole as if it were on an infinite ground plane with no diffracted field contributions. This pattern is indicated by the + symbol on the curve and the pattern with the edge diffraction by the  $\square$  symbol. By comparing these two patterns, the effect of the edge diffraction is quite noticeable. The level differences of the patterns between the a and b parts of Figs. 4-4, 4-5, and 4-6 is because the pattern including diffraction is normalized with the pattern from the monopole on an infinite ground plane. Nonetheless, the similarity between the patterns calculated by the two different methods is apparent. Also, Fig. 4-6b has discontinuities at  $90^\circ$  and  $270^\circ$ , which are similar to those encountered with the hybrid technique before the second order edge diffraction was included.

#### D. Two Monopoles on a Ground Plane

Computer-drawn sketches in each of the figures in this section describe the geometry for that particular pattern. An explanation of these sketches is illustrated with an example. Fig. 4-7 is a representation of the computer sketch in Fig. 4-8a. Fourteen inches is the corresponding dimension between the center of the two monopole array and the edge of the ground plane, while 0.2 inch is the spacing between the tips of the monopoles. The relative size of the monopoles in the computer sketch is not to scale, and the inclination angle of the monopoles to the ground plane indicated by the sketch does not necessarily represent the actual angle used. The angle of the monopoles or elements with respect to the ground plane is indicated to the right of the computer sketch ( $20^\circ$ , in this case). All patterns in this section begin ( $0^\circ$ ) on the underside of the ground plane so that endfire for the array occurs at  $180^\circ$  as indicated in Fig. 4-7 and the computer sketches.

Just as with the single monopole cases, the pattern from the antenna without the edge diffracted fields is indicated by the + symbol in the figures to follow and the total field with diffraction by the  $\square$  symbol. By comparing these two patterns, the effects of the edge diffraction in all cases can be studied.

In the first group of patterns, Figs. 4-8, 4-9, 4-10, three random cases are chosen and compared with Burnside's GTD computer program for the same geometry.

The signal levels between the hybrid method and Burnside's GTD program differ because the field including diffraction is normalized with the field containing no diffraction for comparison purposes in Figs. 4-3a, 4-9a, 4-10a. The discontinuities occurring in some of the patterns around  $90$  and  $270$  degrees are due to the noninclusion

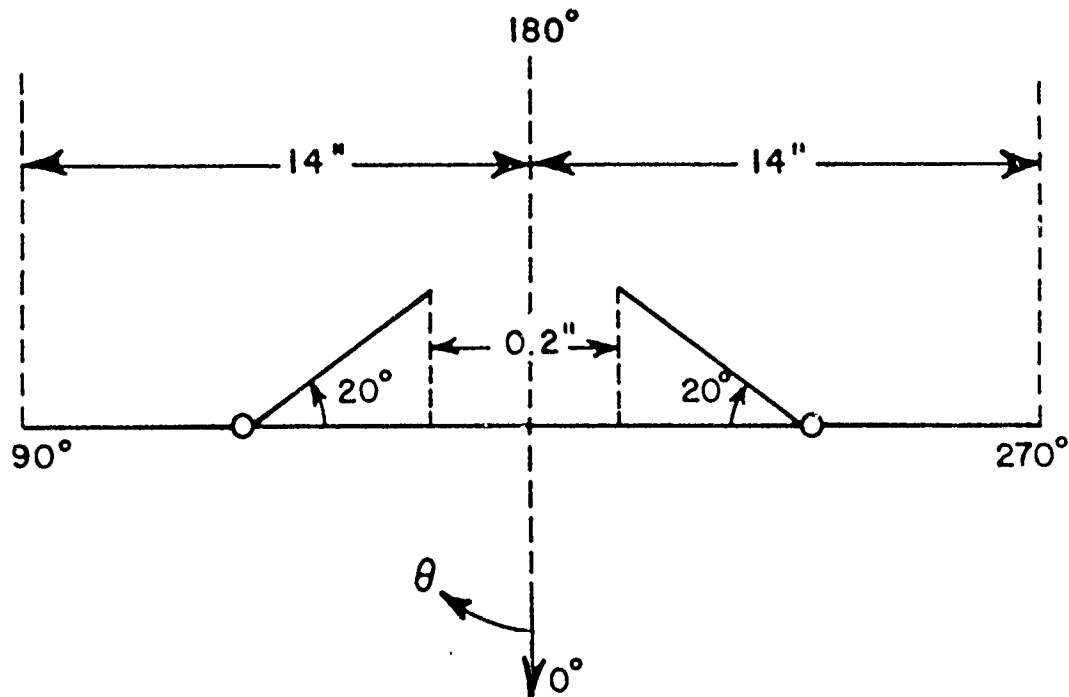


Fig. 4-7. Representation of the computer drawing below the patterns in this section.

of higher order diffraction. It is not worth the added computational efforts for our purposes to include higher order diffraction around the edges of the ground plane. The two programs calculate the patterns by different methods but display a great deal of similarity.

Figures 4-11a, b, c are the patterns of the monopoles located symmetrically on the ground plane for 800, 900, and 1000 MHz. The desired pattern shape appears to be obtainable at the higher frequencies. At 800 MHz, the null at 180° is intolerable.

Figures 4-12a, b, c and Figs. 4-13a, b, c demonstrate the effects on the pattern by locating the monopoles asymmetrically on the ground plane. The monopole or element spacing and angle with respect to the ground plane are the same as in Figs. 4-11a, b, c. As with the symmetric cases, the pattern evolves more to the desired pattern as the frequency increases to 1000 MHz. As the frequency increases, the levels of the nulls in the region of main concern from 120° to 240° grow shallower.

Figures 4-14a-f display the effects of the far-field patterns due to changes in the separation between the two monopoles or elements. As the spacing is increased, the pattern shape becomes less desirable due to the deepening of the center null. The

smaller spacings are, therefore, more useful in achieving the desired pattern. Thus, 0.3 inch was chosen as a reasonable spacing for the remaining patterns in the section.

Figures 4-15, 4-16, and 4-17 illustrate the effects on the pattern due to changes in the angle of the monopoles with respect to the ground plane.

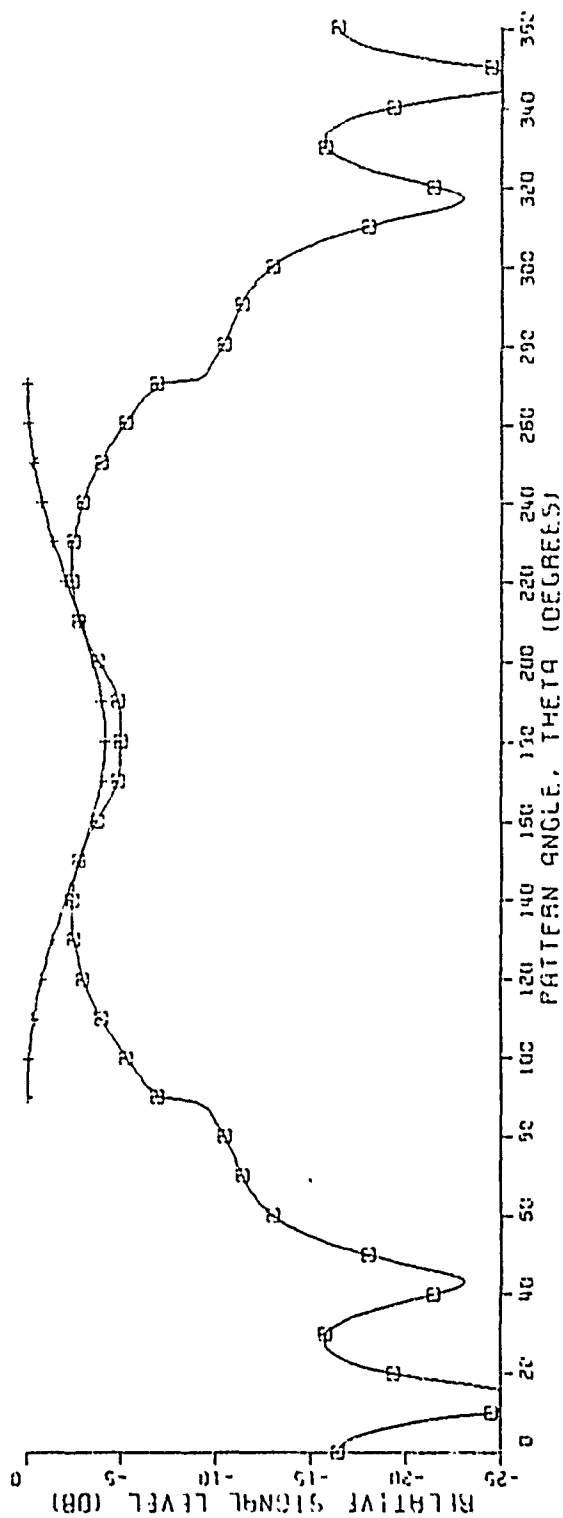
Angles less than 30 degrees were excluded because the close proximity of the monopoles to the ground plane in the true physical situation could result in inadequate input impedances over the range of frequency. Angles greater than 45 degrees were also tested but resulted in nondesirable pattern shapes.

A monopole angle of 30 degrees with a tip spacing of 0.3 inch seems to yield the optimum results. In Figs. 4-18 through 4-22 these geometrical values are used to test for the two monopole array at different locations on the ground plane.

In Figs. 4-18a, b, c the discontinuities around 70 to 110 degrees are due to the close proximity of the edge to the monopole array. Even still, the general pattern shape is valid. From studying Figs. 4-18 through 4-22 a more desirable pattern shape is obtained as the monopole array is moved closer to the edge. As the array is shifted toward the center, deep nulls, particularly at the low end of the frequency range (800 MHz), develop.

Additional patterns are contained in Appendices I and II. Appendix I contains patterns with the center of the monopole array located at 12 inches from one ground plane edge and 16 inches from the other edge with the monopoles angles set at 30 and 45 degrees for various element spacings.

Appendix II has patterns with the center of the monopole array located eight inches from one edge and 20 inches from the other. The monopoles angles are set at 30 degrees, and different element spacings are tested.



155

14 0" 0.2' 14.0' 270 ANGLE OF ELEMENTS=20.0 DEGREES

MONOPOLE LENGTH=0.25 WAVELENGTHS

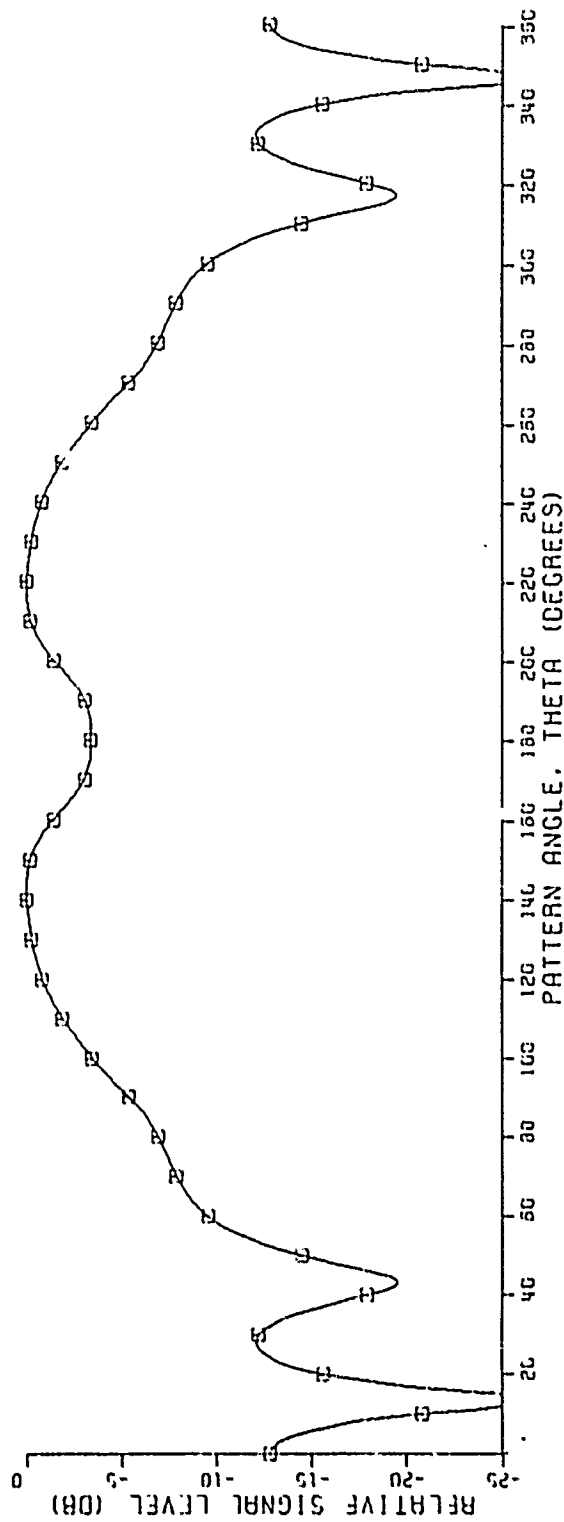
FREQUENCY=900.0 MHZ

± FIELD INCLUDING EDGE DIFFRACTION

+ FIELD FROM ANT. ON INFINITE GROUND PLANE

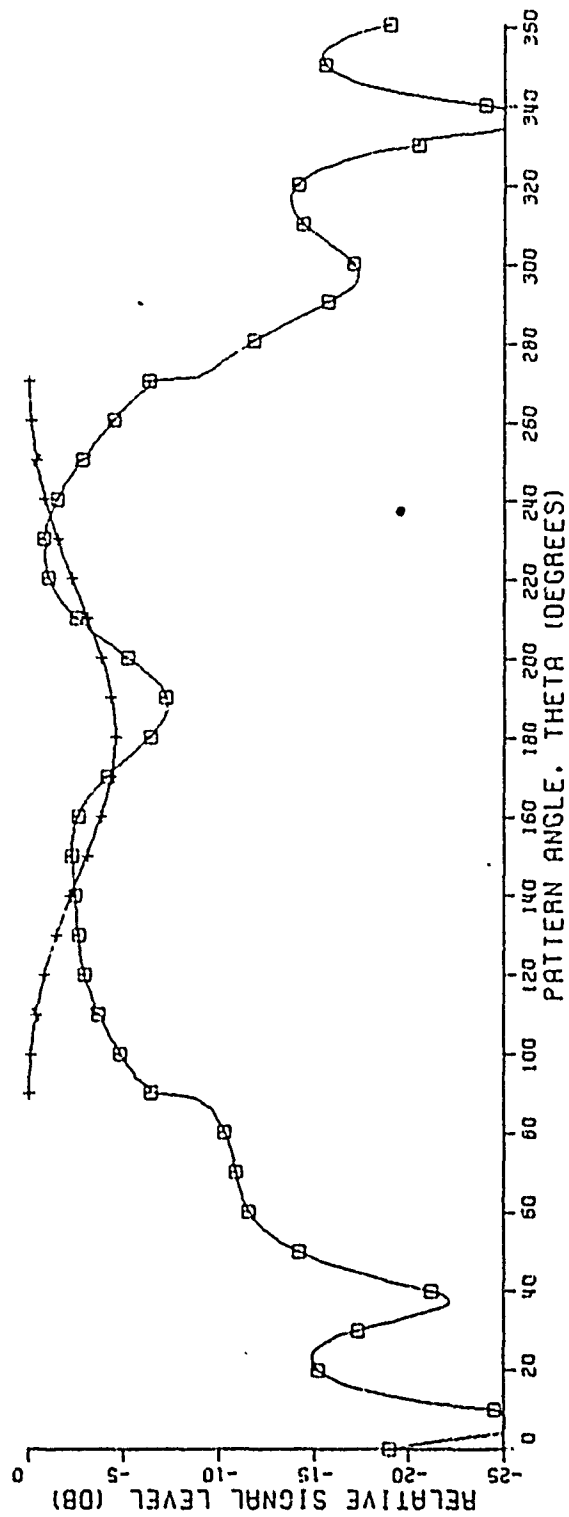
Fig. 4-8a.





90° 14.0" 0.2" 14.0" 270° 180°  
 MONOPOLE LENGTH=0.25 WAVELENGTHS  
 FREQUENCY=900.0 MHZ  
 E FIELD INCLUDING EDGE DIFFRACTION

Fig. 4-8b. Calculated by Burnside's GTD computer program.



180

90 12.0" 0.2" 16.0" 270

ANGLE OF ELEMENTS=20.0 DEGREES

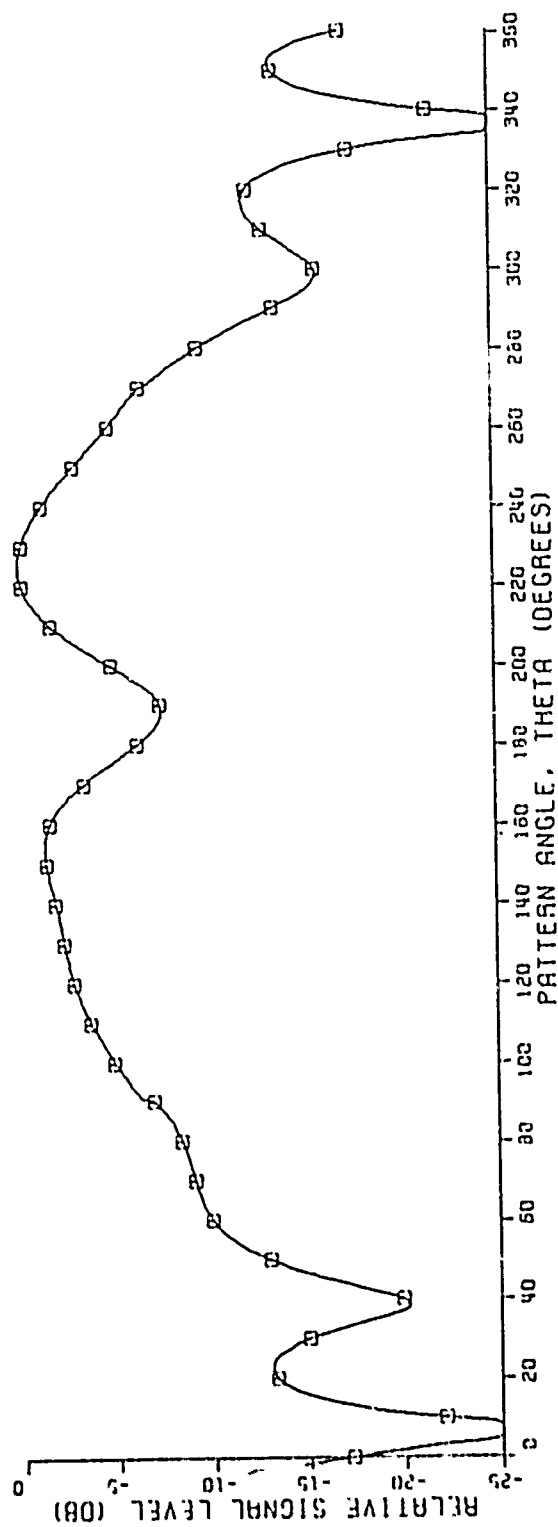
MONOPOLE LENGTH=0.22 WAVELENGTHS

FREQUENCY=800.0 MHZ

○ FIELD INCLUDING EDGE DIFFRACTION

+ FIELD FROM ANT. ON INFINITE GROUND PLANE

Fig. 4-9a.



180

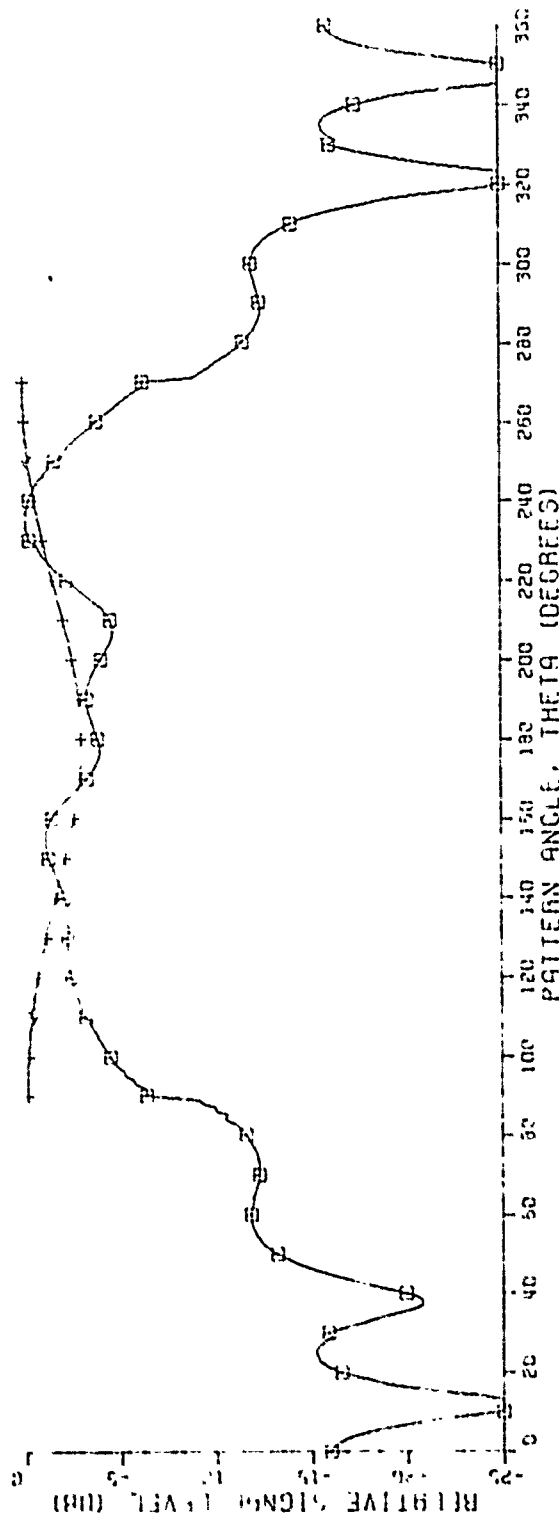
90 12 0" 16.0" 270 ANGLE OF ELEMENTS = 20.0 DEGREES

MONOPOLE LENGTH = 0.25 WAVELENGTHS

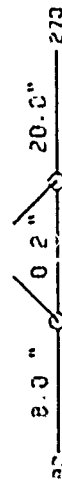
FREQUENCY = 800.0 MHZ

W FIELD INCLUDING EDGE DIFFRACTION

Fig. 4-9b. Calculated by Burnside's computer program.



180



ANGLE OF ELEMENTS=20.0 DEGREES

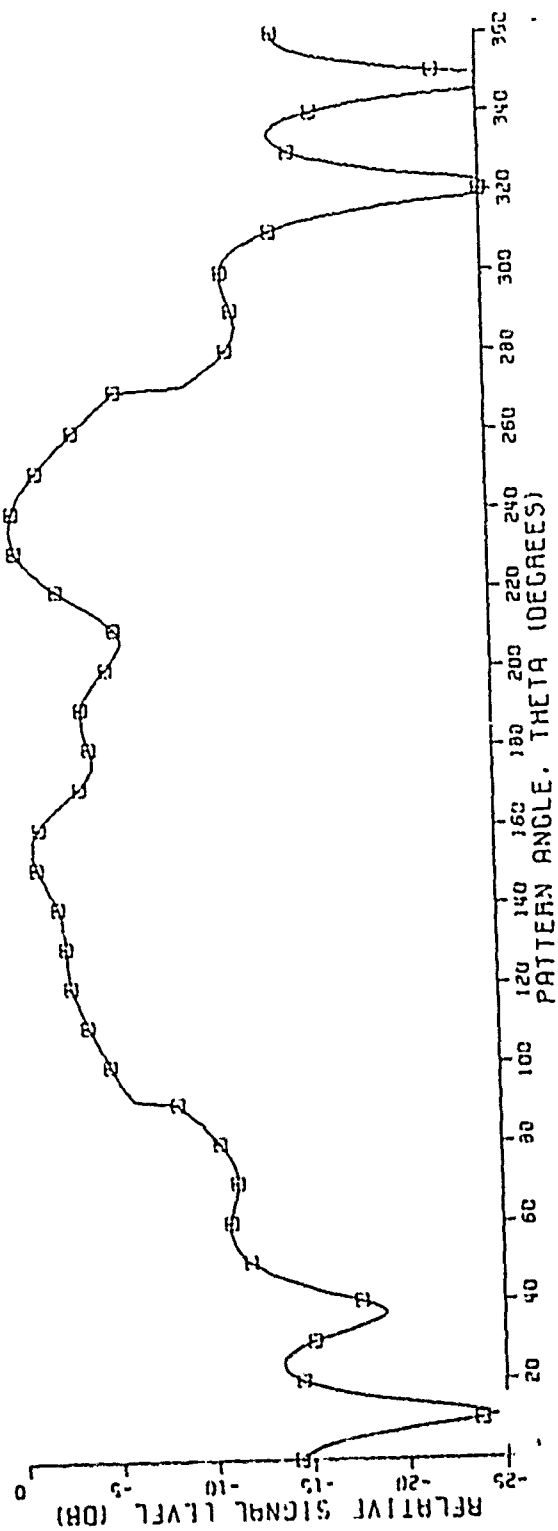
WAVELENGTH=0.28

FREQUENCY=1000.0 MHZ

FIELD INCLUDING FOG DIFFRACTION

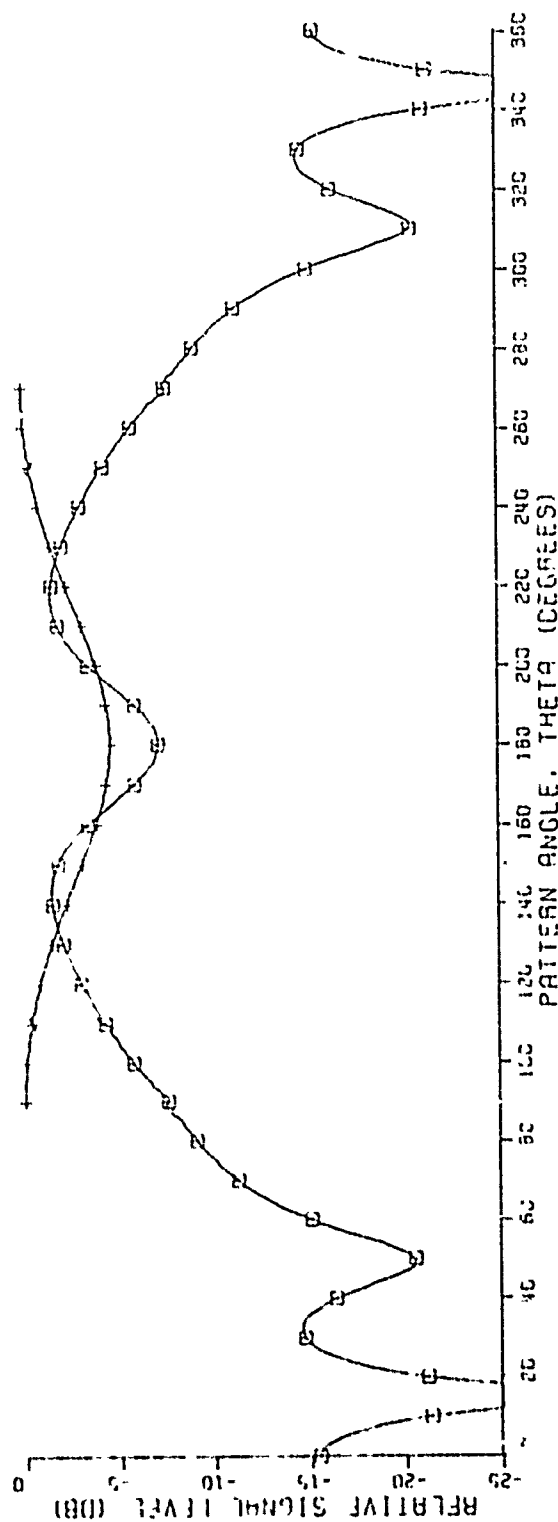
+ FIELD FROM ANT. ON INFINITE GROUND PLANE

Fig. 4-10a.



MONOPOLE LENGTH=0.25 WAVELENGTHS  
 FREQUENCY=1000.0 MHZ  
 FIELD INCLUDING EDGE DIFFRACTION

Fig. 4-10b. Calculated by Burnside's computer program.



180

90 — 14.0" — 0.2" — 14.0" — 270 ANGLE OF ELEMENTS=20.0 DEGREES

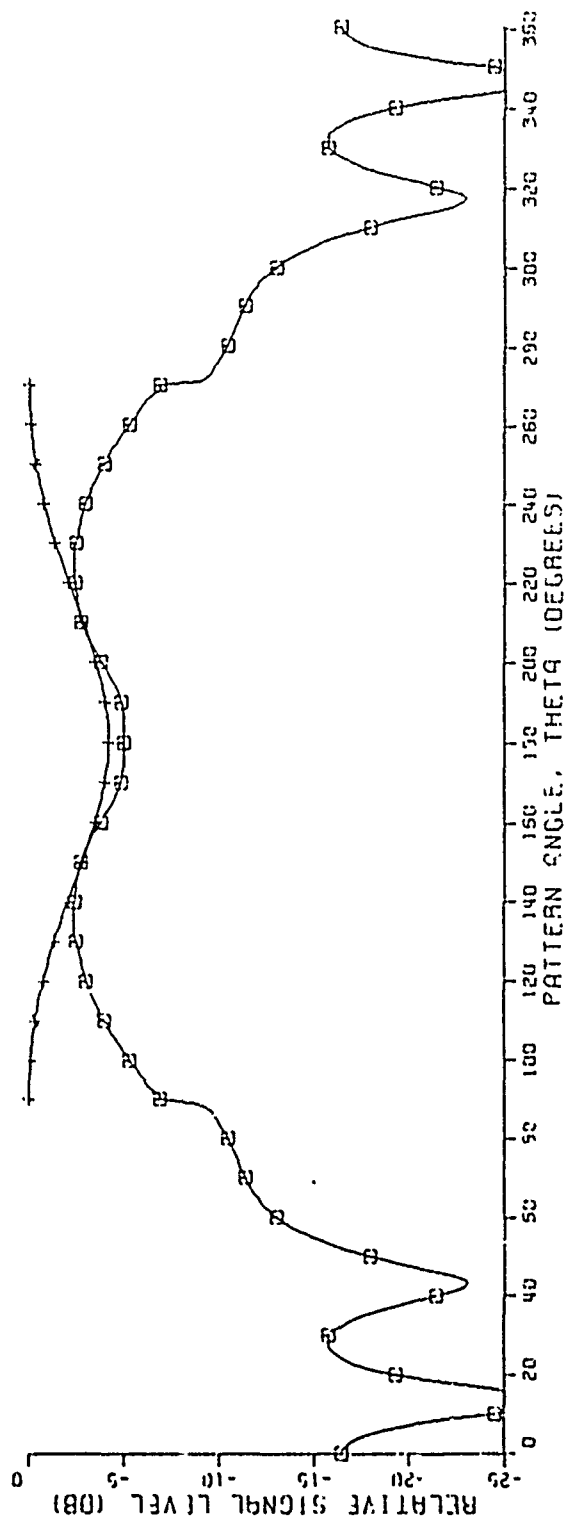
WAVELENGTH=0.22 WAVELENGTHS

FREQUENCY=800.0 MHZ

E FIELD INCLUDING EDGE DIFFRACTION

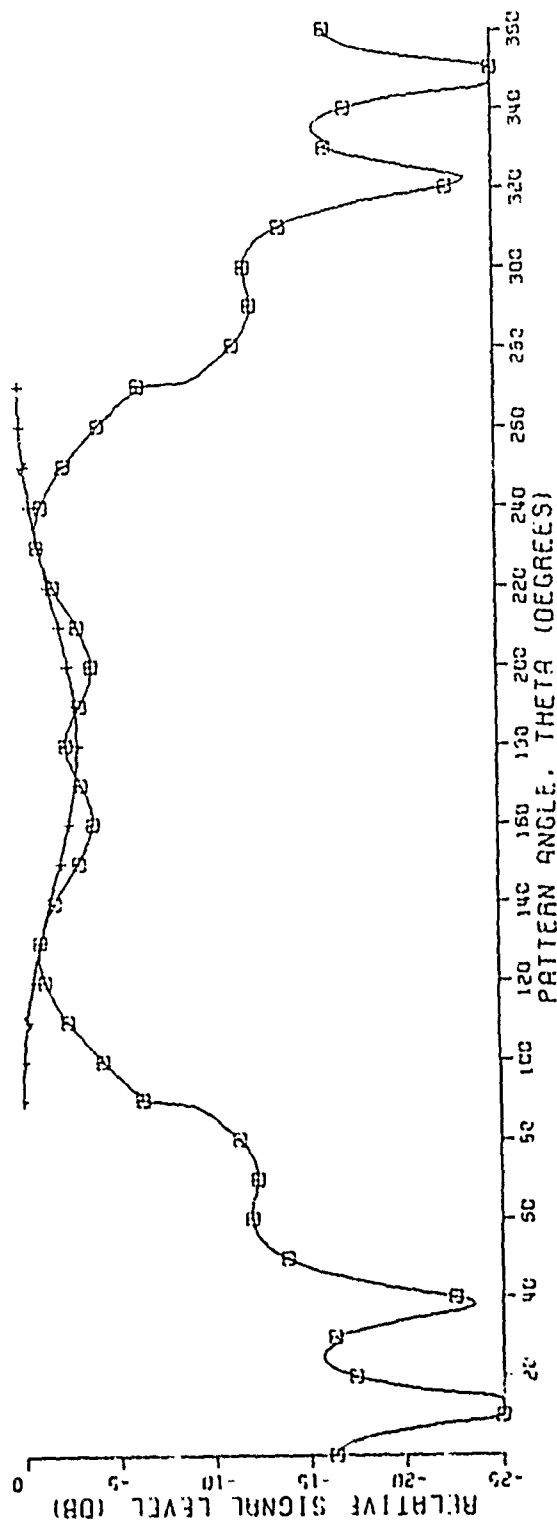
+ FIELD FROM ANT. ON INFINITE GROUND PLANE

Fig. 4-11a.



190  
 90° 14.0" 0.2" 14.0" 270° ANGLE OF ELEMENTS=20.0 DEGREES  
 MONOPOLE LENGTH=0.25 WAVELENGTHS  
 FREQUENCY=900.0 MHZ  
 + FIELD INCLUDING EDGE DIFFRACTION  
 + FIELD FROM ANT. ON INFINITE GROUND PLANE

Fig. 4-11b.



150  
 90 14 0" 0.2" 14.0" 270  
 ANGLE OF ELEMENTS=20.0 DEGREES

WAVELENGTH=0.20 WAVELENGTHS

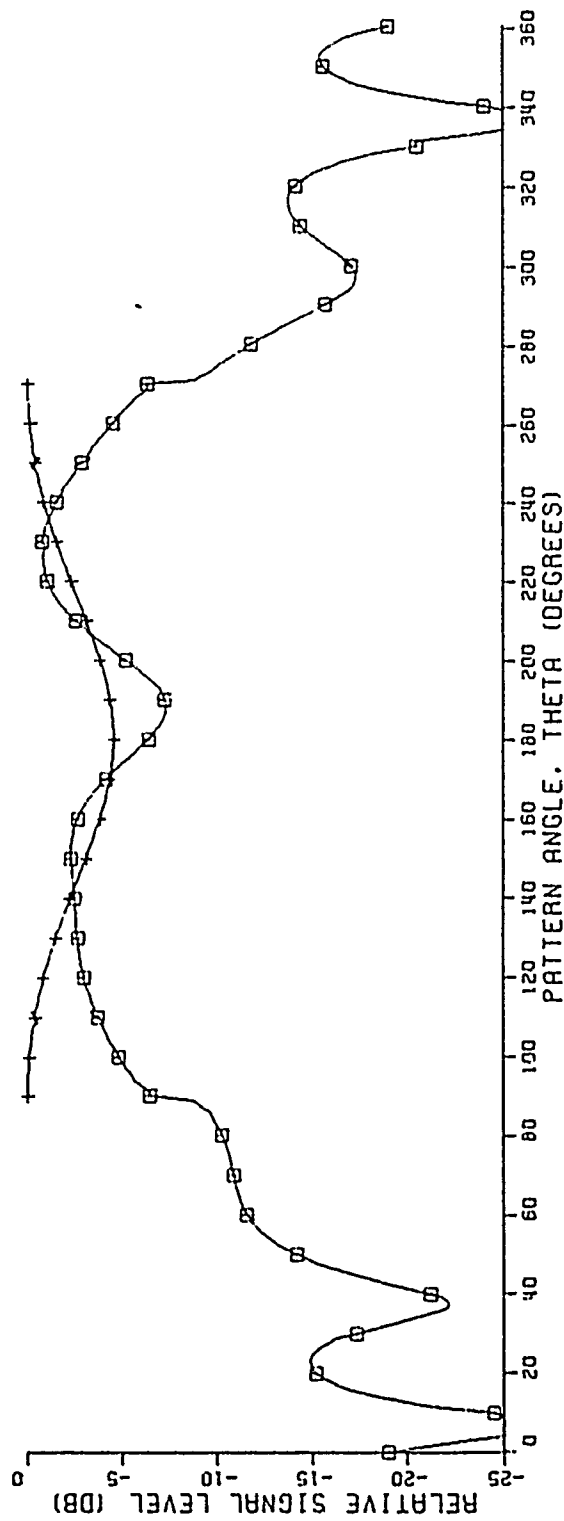
FREQUENCY=1000.0 MHZ

□ FIELD INCLUDING EDGE DIFFRACTION

+ FIELD FROM ANT. ON INFINITE GROUND PLANE

Fig. 4-11c.





180

90 12.0" 0.2" 16.0" 270

ANGLE OF ELEMENTS=20.0 DEGREES

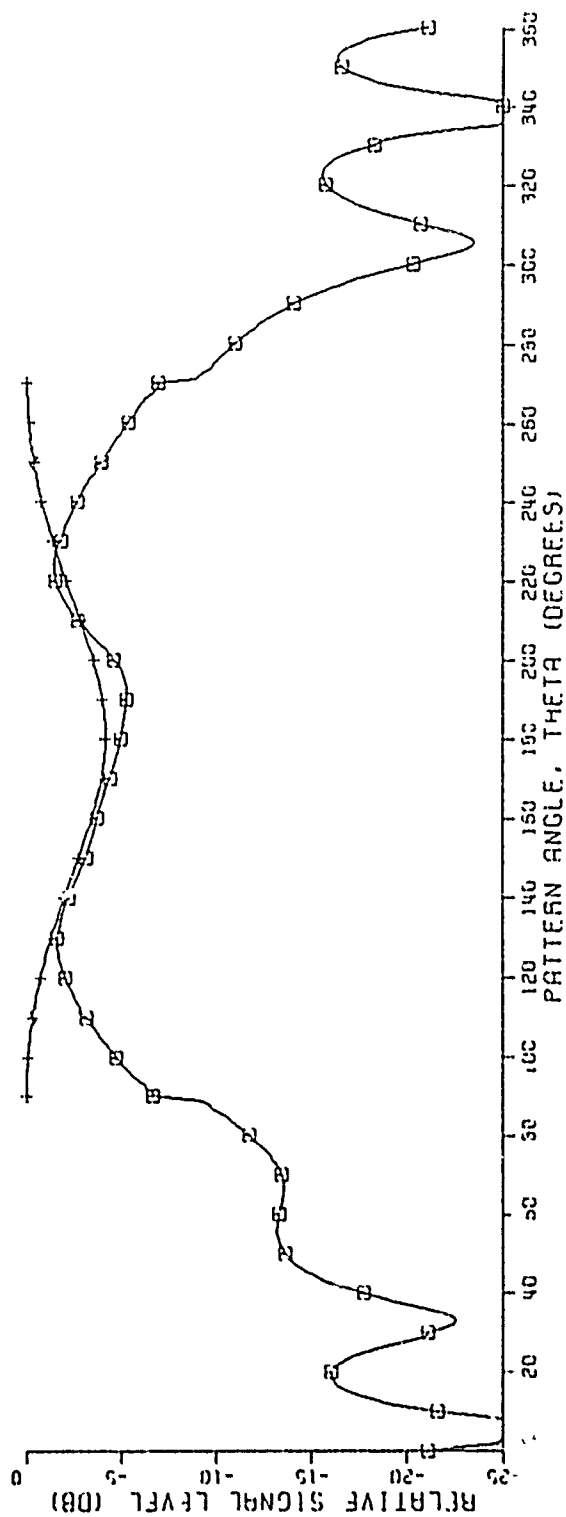
HORNPØLE LENGTH=0.22 WAVELENGTHS

FREQUENCY=800.0 MHZ

□ FIELD INCLUDING EDGE DIFFRACTION

+ FIELD FROM ANT. ON INFINITE GROUND PLANE

Fig. 4-12a.



192

90 12 0" 0 2' 15.0" 270

ANGLE OF ELEMENTS=20.0 DEGREES

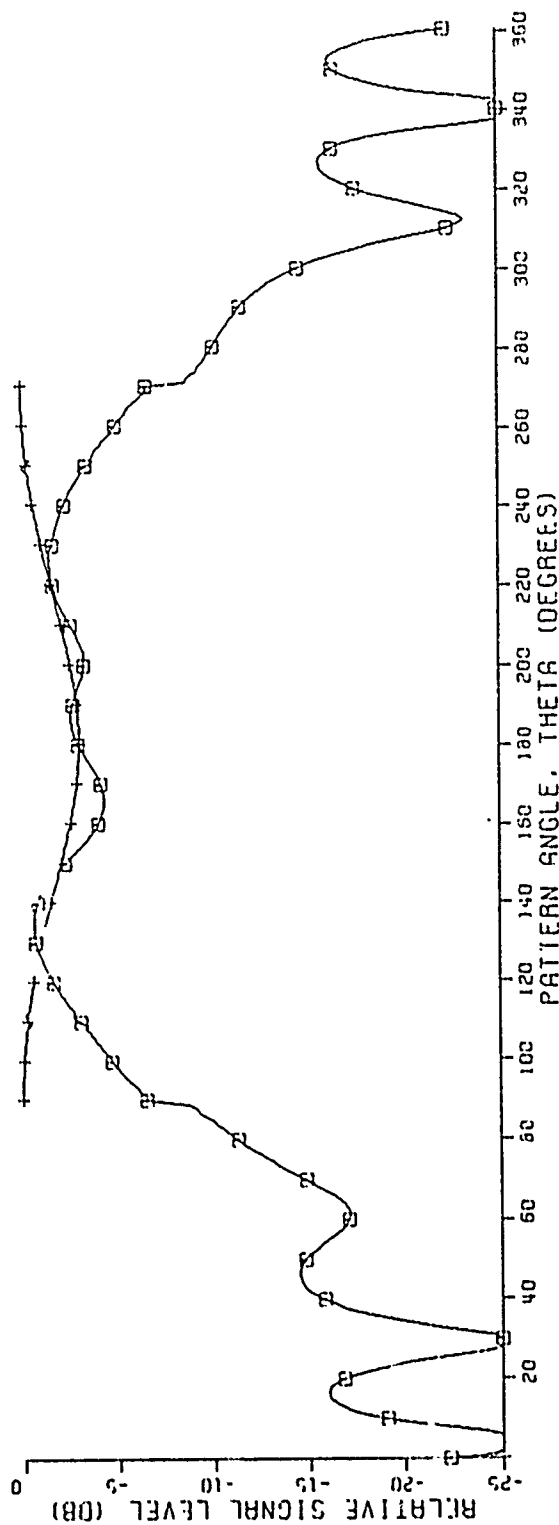
MONOPOLE LENGTH=0.25 WAVELENGTHS

FREQUENCY=900.0 MHZ

□ FIELD INCLUDING EDGE DIFFRACTION

+ FIELD FROM ANT. ON INFINITE GROUND PLANE

Fig. 4-12b.



150

90 12 0" 0.2 16.0" 270 ANGLE OF ELEMENTS=20.0 DEGREES

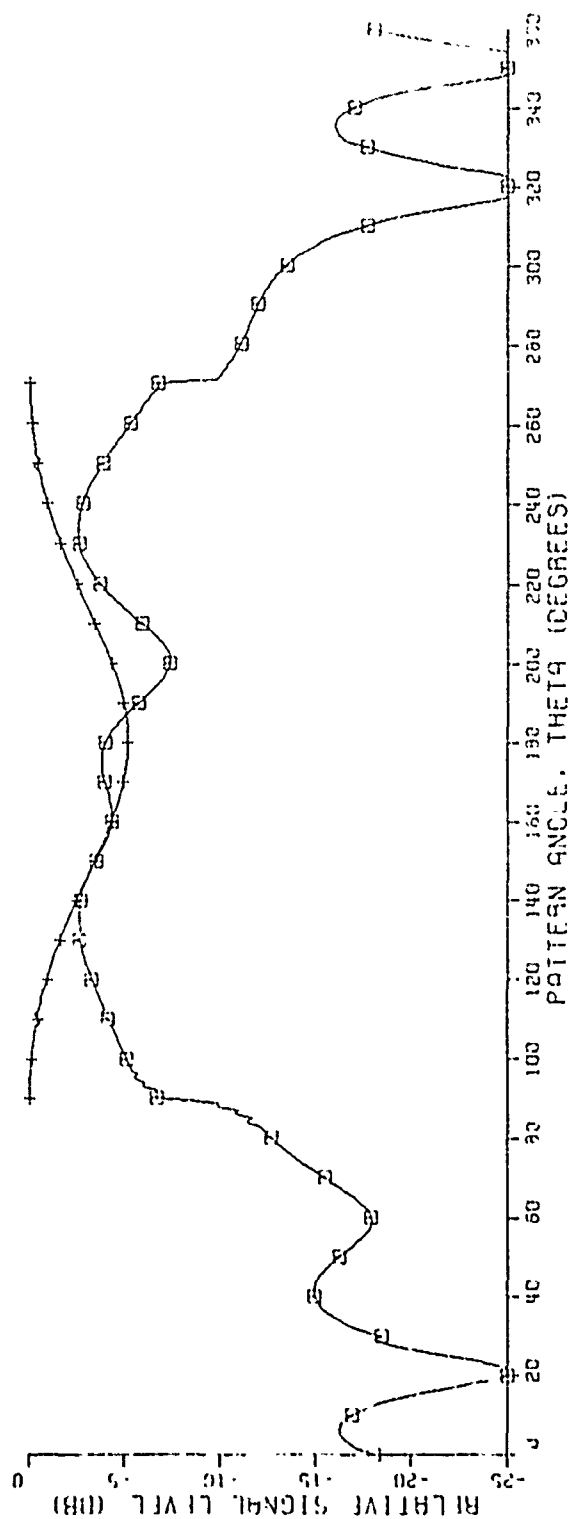
MONOPOLE LENGTH=0.28 WAVELENGTH

FREQUENCY=1000.0 MHZ

Ø FIELD INCLUDING EDGE DIFFRACTION

+ FIELD FROM ANT. ON INFINITE GROUND PLANE

Fig. 4-12c.



180

37 8 0 " 0 2' 20.0" 270

MONOPOLE LENGTH=0.22 WAVELENGTHS

FREQUENCY=800.0 MHZ

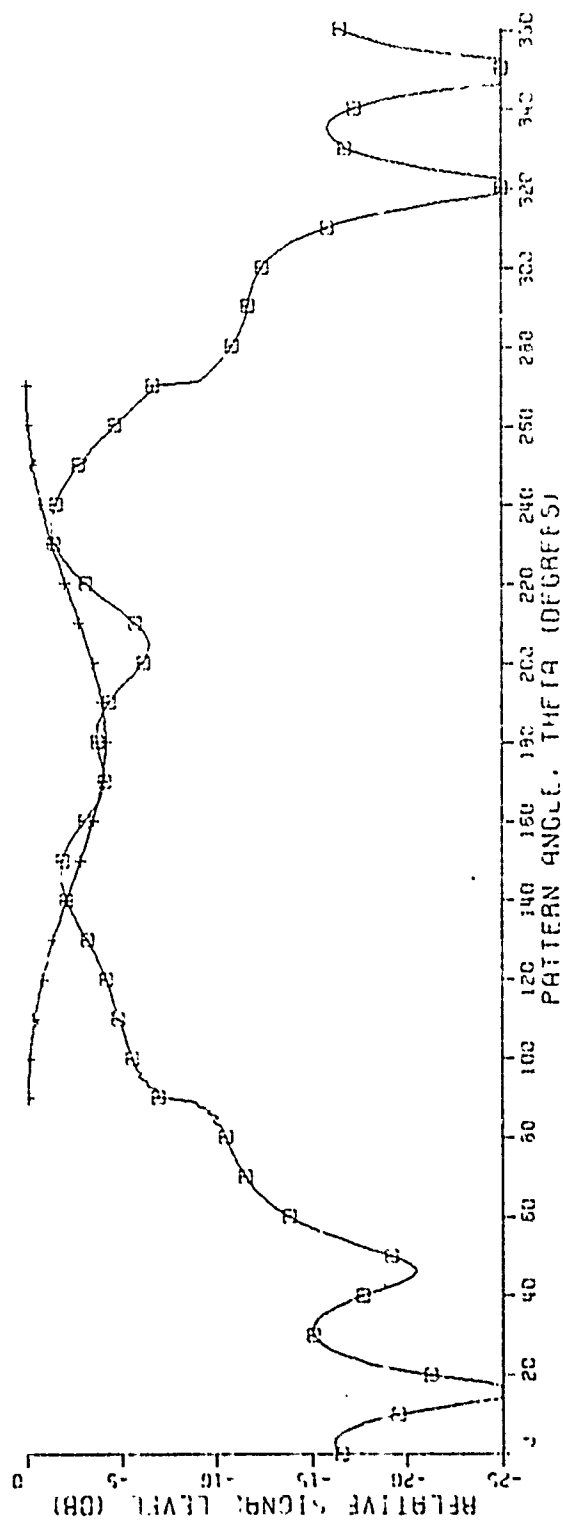
E FIELD INCLUDING EDGE DIFFRACTION

+ FIELD FROM ANT. ON INFINITE GROUND PLANE

ANGLE OF ELEMENTS=20.0 DEGREES

PATTERN ANGLE, THETA (DEGREES)

Fig. 4-13a.



180

90 8.0" 0.2" 20.0" 270

ANGLE OF ELEMENTS-20.0 DEGREES

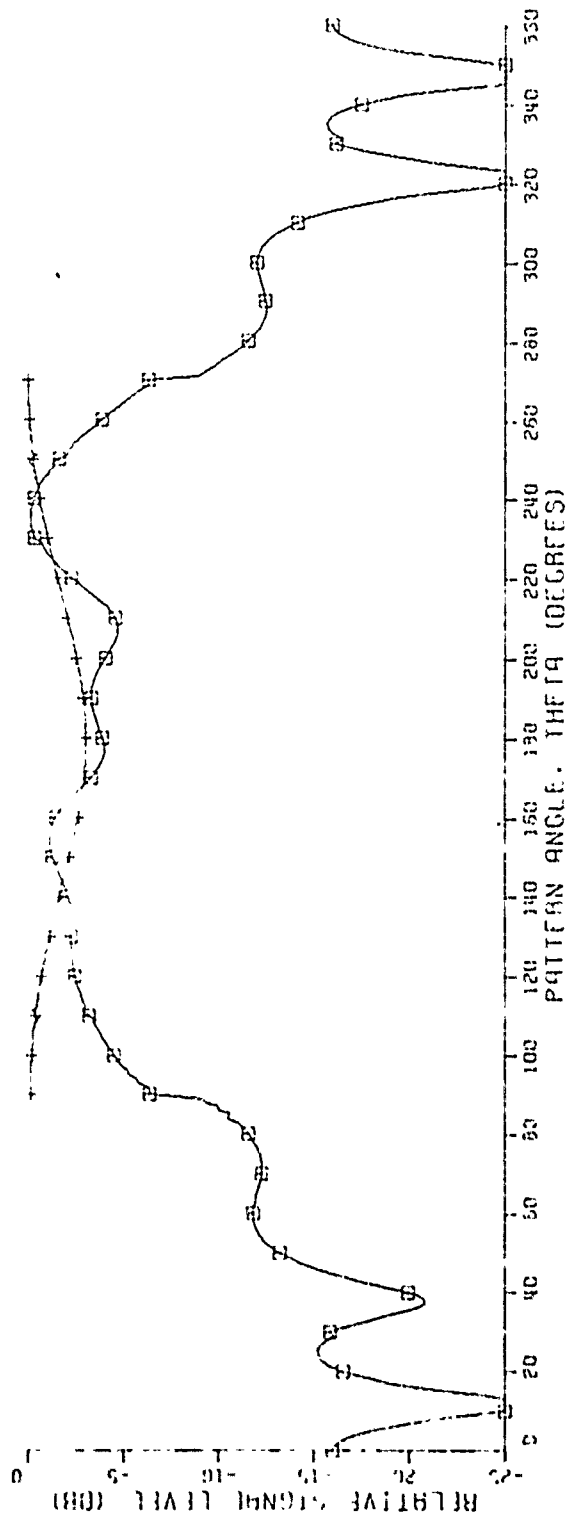
MONOPOLE LENGTH=0.25 WAVELENGTHS

FREQUENCY=900.0 MHz

WFIELD INCLUDING EDGE DIFFRACTION

+ FIELD FROM ANT. ON INFINITE GROUND PLANE

Fig. 4-13b.



130

80" 0.2" 20.0" 270 ANGLE OF ELEMENTS=20.0 DEGREES

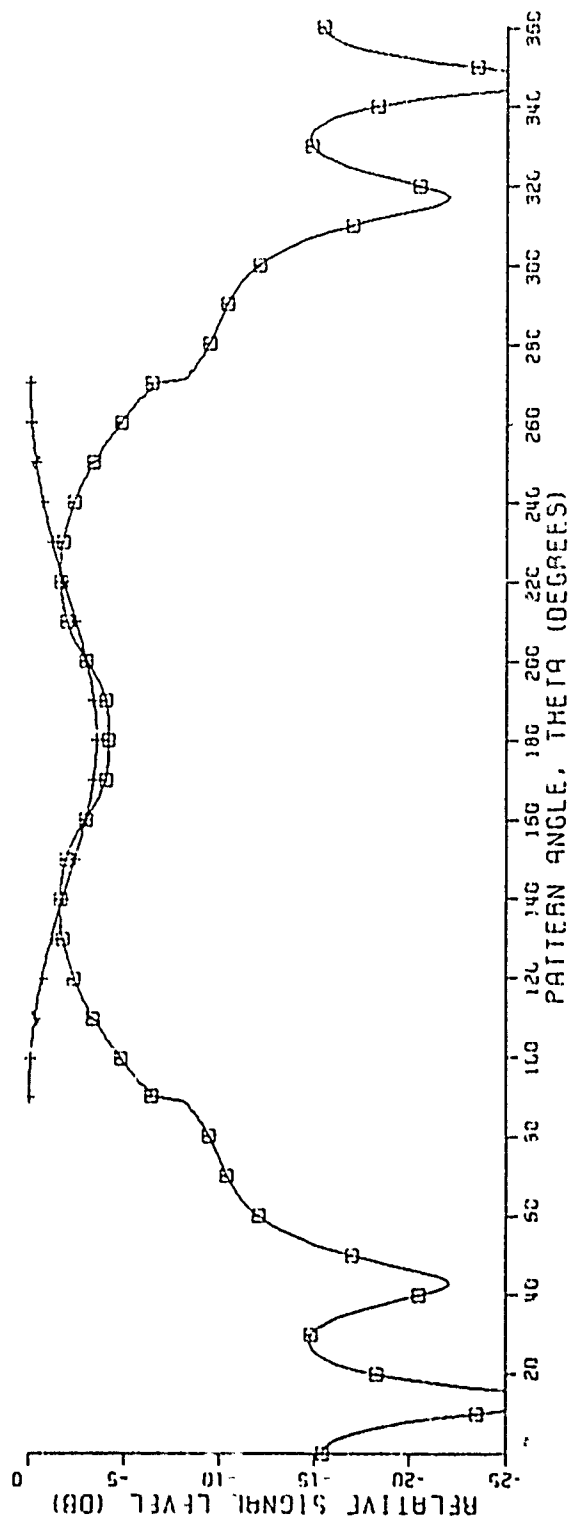
MONOPOL LENGTH=0.28 WAVELENGTHS

FREQUENCY=1000.0 MHZ

W FIELD INCLUDING EDGE DIFFRACTION

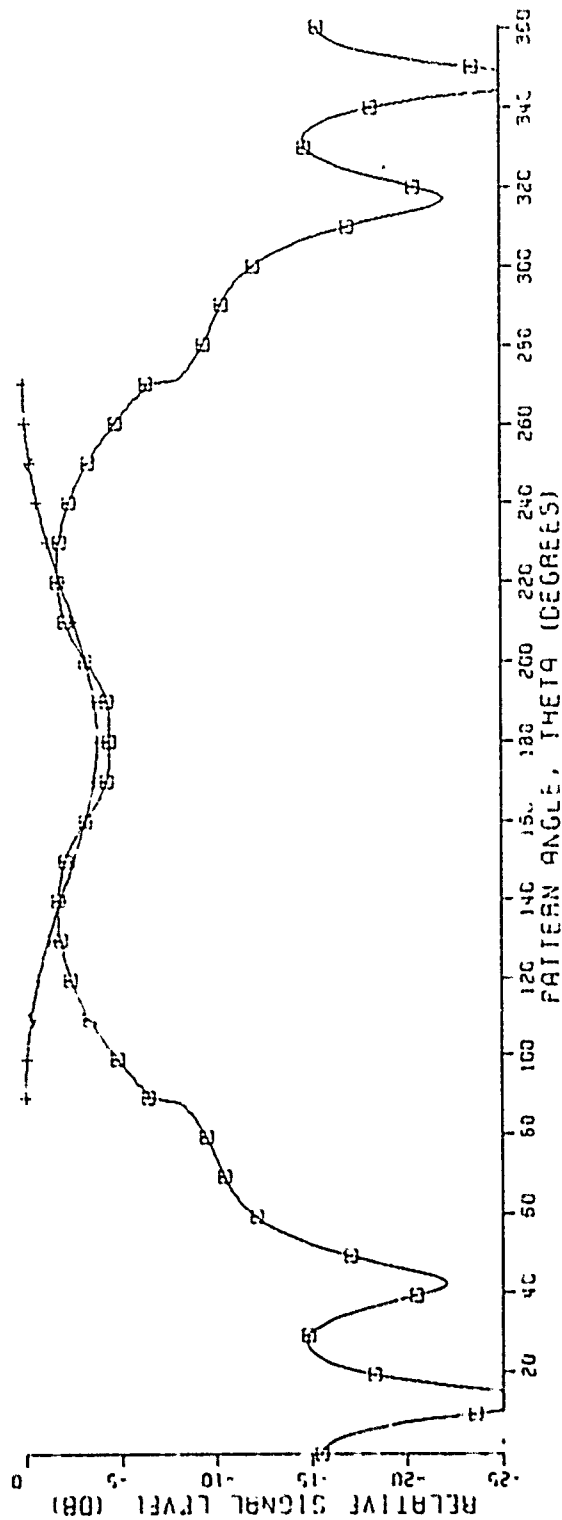
+ FIELD FROM ANT. ON INFINITE GROUND PLANE

Fig. 4-13c.



180  
 90 14 0" 0.2" 14.0" 270  
 MONOPOLE LENGTH=0.25 WAVELENGTHS  
 FREQUENCY=900.0 MHZ  
 FIELD INCLUDING EDGE DIFFRACTION  
 + FIELD FROM ANT. ON INFINITE GROUND PLANE

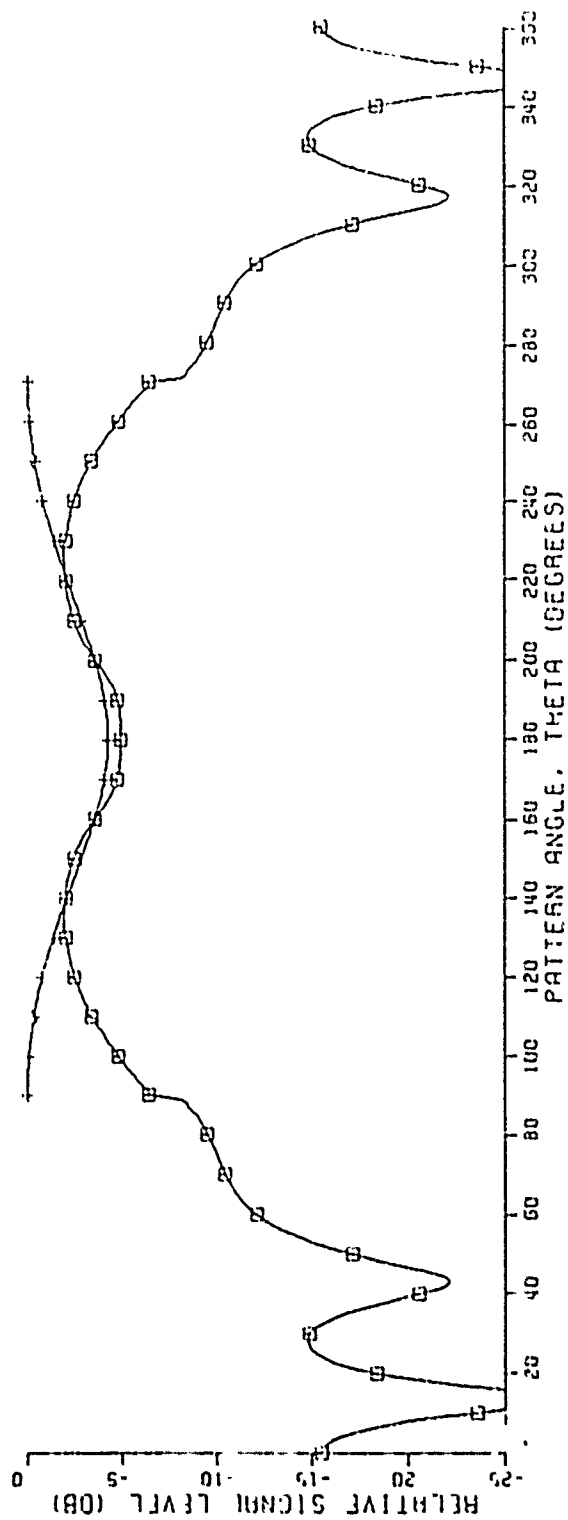
Fig. 4-14a.



180  
 90 14 0" 0 3" 14 0" 270  
 ANGLE OF ELEMENTS=20.0 DEGREES  
 MONOPOLE LENGTH=0.25 WAVELENGTHS  
 FREQUENCY=900.0 MHZ  
 E FIELD INCLUDING EDGE DIFFRACTION  
 + FIELD FROM ANT. ON INFINITE GROUND PLANE

Fig. 4-14b.





180

90 14.0" 0.5" 270 ANGLE OF ELEMENTS=20.0 DEGREES

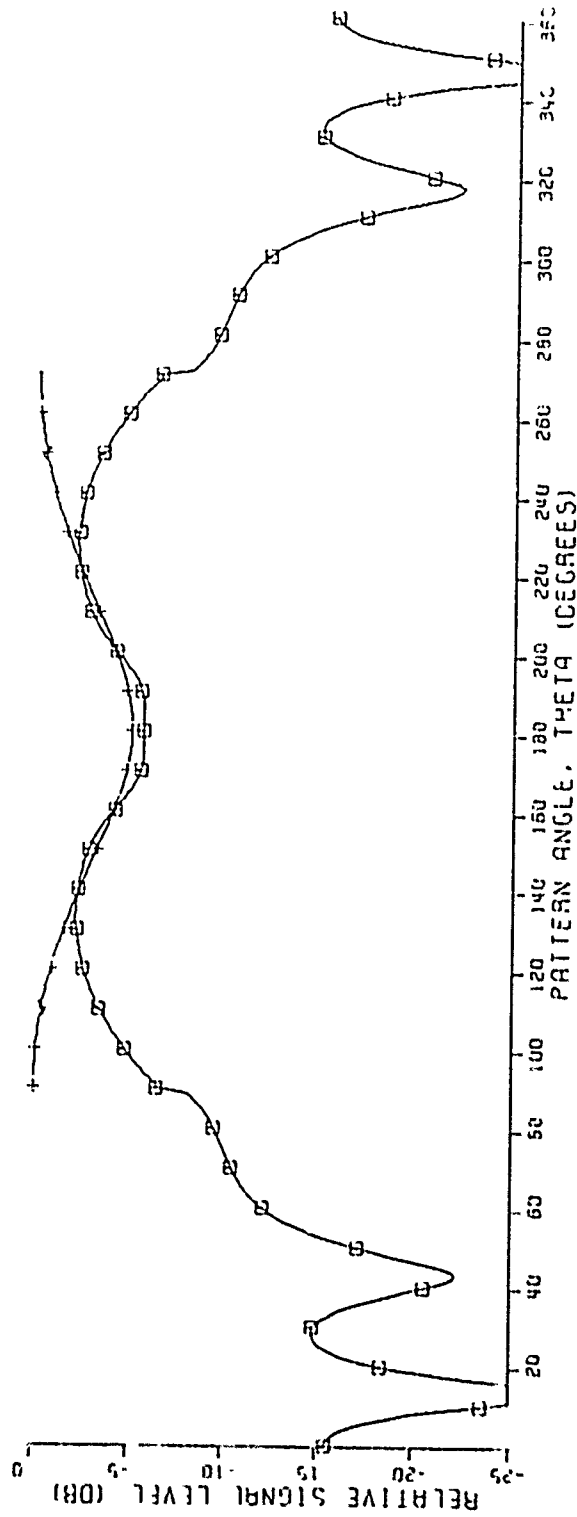
WAVELENGTH=0.25

FREQUENCY=900.0 MHZ

FIELD INCLUDING EDGE DIFFRACTION

+ FIELD FROM ANT. ON INFINITE GROUND PLANE

Fig. 4-14c.



180

90 14 0" 1 C" 14 0" 270 ANGLE OF ELEMENTS=20.0 DEGREES

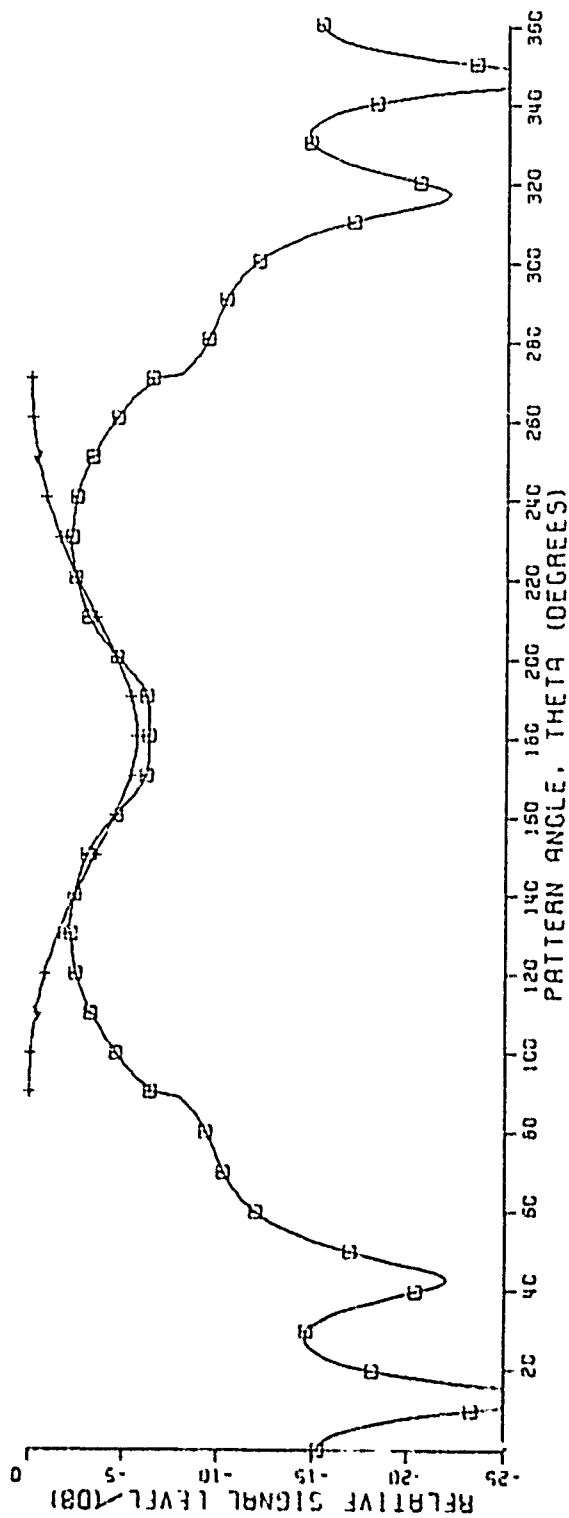
MONOPOLE LENGTH=0.25 WAVELENGTHS

FREQUENCY=900.0 MHZ

+ FIELD INCLUDING EDGE DIFFRACTION

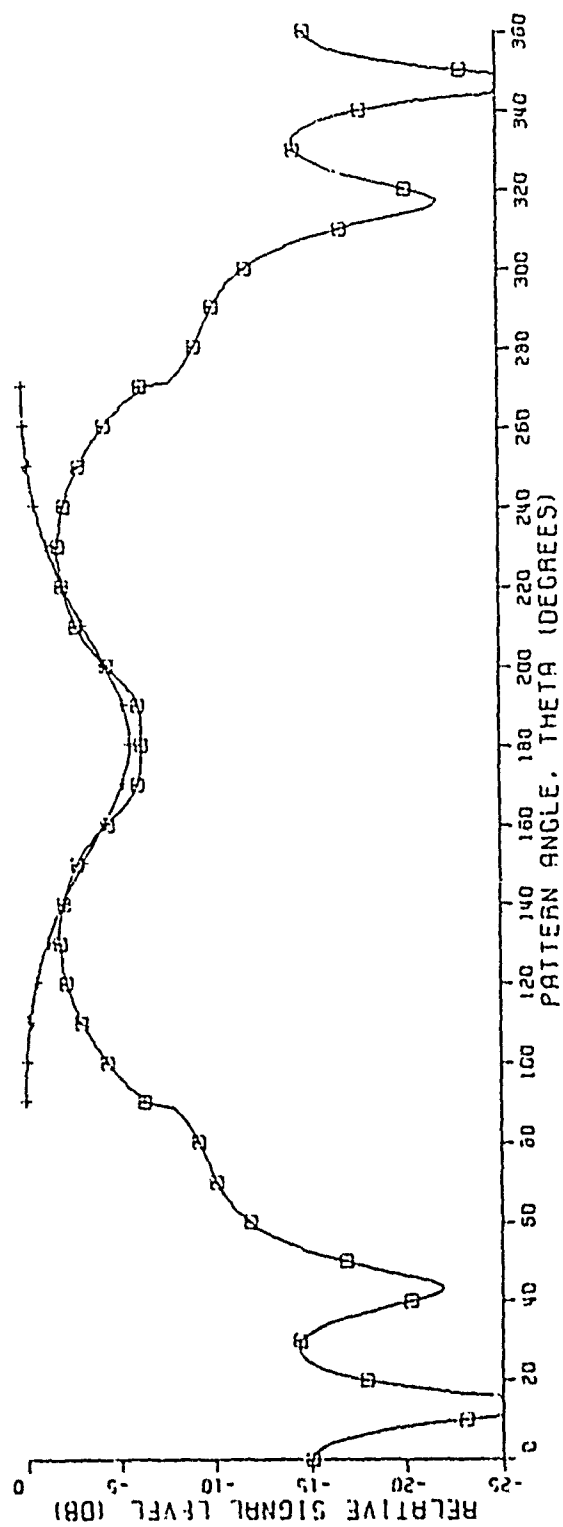
+ FIELD FROM ANT. ON INFINITE GROUND PLANE

Fig. 4-14d.



180  
 90 — 14.0" — 20.0" — 14.0" — 270  
 ANGLE OF ELEMENTS = 20.0 DEGREES  
 MONOPOLE LENGTH = 0.25 WAVELENGTHS  
 FREQUENCY = 900.0 MHZ  
 + FIELD INCLUDING EDGE DIFFRACTION  
 + FIELD FROM ANT. ON INFINITE GROUND PLANE

Fig. 4-14e.



180

90 14 0" 3.3" 14.0" 270

ANGLE OF ELEMENTS=20.0 DEGREES

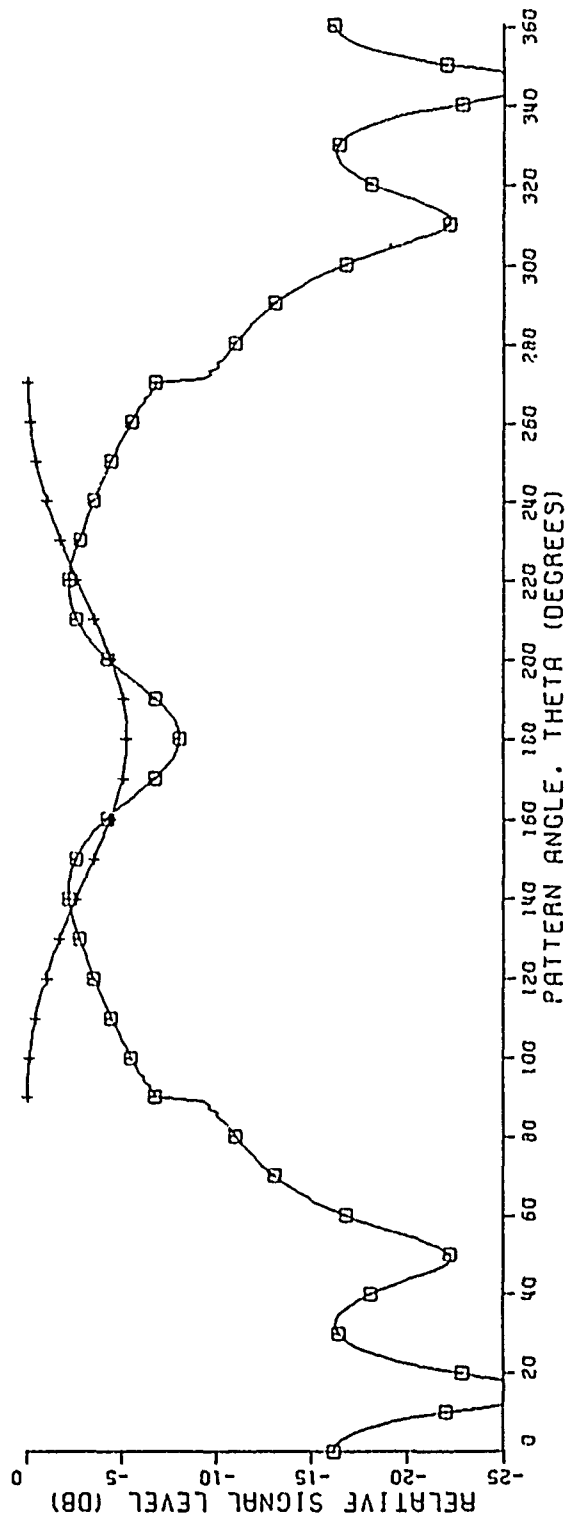
MENOPOL LENGTH=0.25 WAVELENGTHS

FREQUENCY=900.0 MHZ

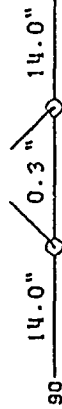
FIELD INCLUDING EDGE DIFFRACTION

+ FIELD FROM ANT. ON INFINITE GROUND PLANE

Fig. 4-14f.



180



ANGLE OF ELEMENTS=30.0 DEGREES

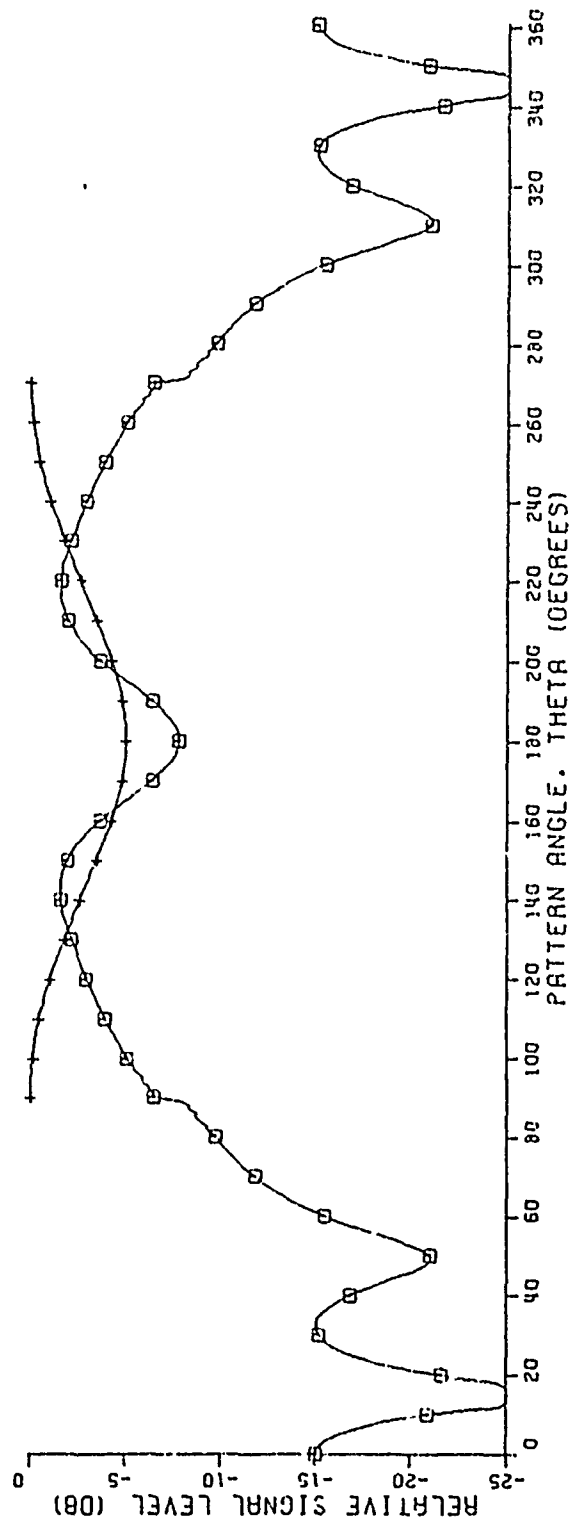
MONOPOLE LENGTH=0.22 WAVELENGTHS

FREQUENCY=800.0 MHZ

○ FIELD INCLUDING EDGE DIFFRACTION

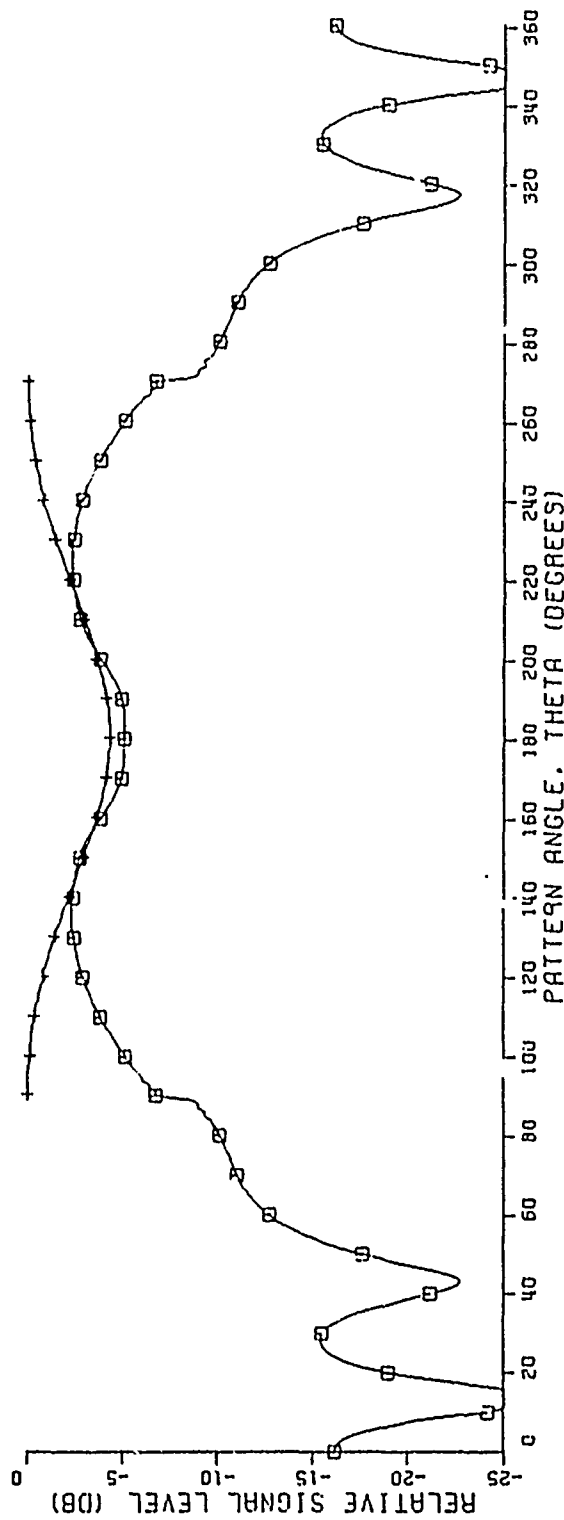
+ FIELD FROM ANT. ON INFINITE GROUND PLANE

Fig. 4-15a.



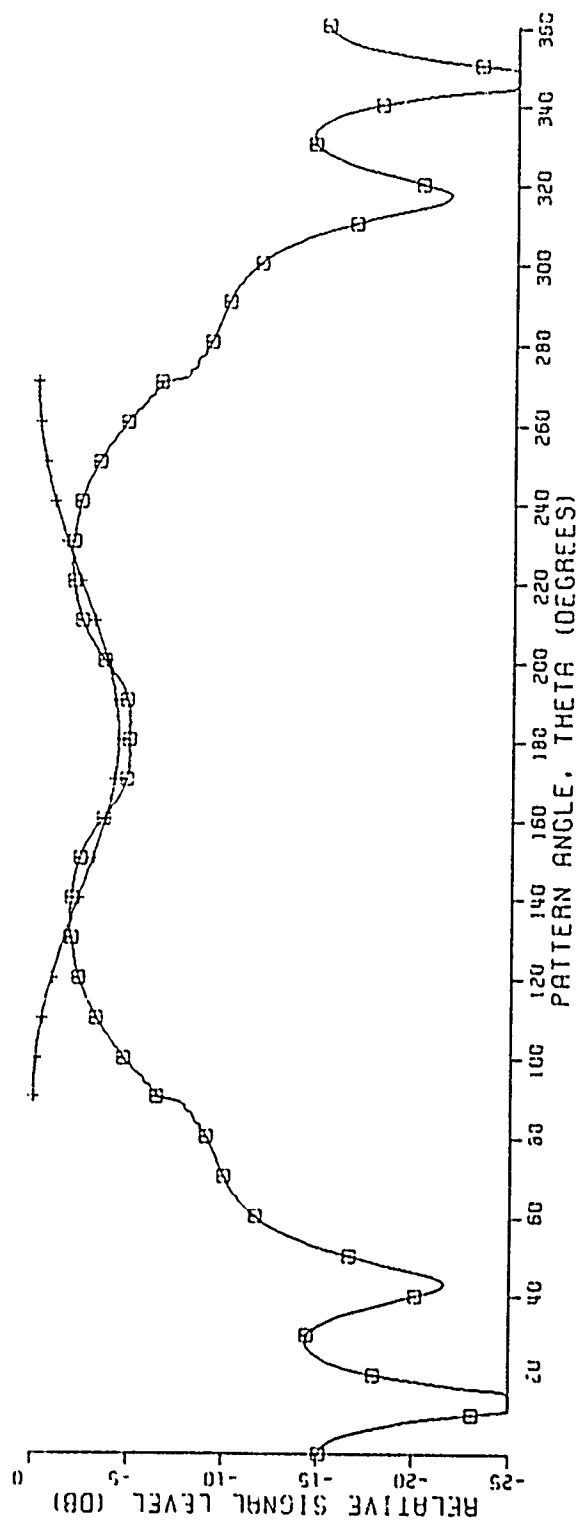
180  
 90  
 14.0" 0.3" 14.0" 270  
 ANGLE OF ELEMENTS=45.0 DEGREES  
 MONOPOLE LENGTH=0.22 WAVELENGTHS  
 FREQUENCY=800.0 MHZ  
 O FIELD INCLUDING EDGE DIFFRACTION  
 + FIELD FROM ANT. ON INFINITE GROUND PLANE

Fig. 4-15b.



180  
 90 — 14.0" — 0.5" — 14.0" — 270 ANGLE OF ELEMENTS = 30.0 DEGREES  
 MONOPULE LENGTH = 0.25 WAVELENGTHS  
 FREQUENCY = 900.0 MHZ  
 □ FIELD INCLUDING EDGE DIFFRACTION  
 + FIELD FROM ANT. ON INFINITE GROUND PLANE

Fig. 4-16a.



MONOPOLE LENGTH=0.25 WAVELENGTHS  
 FREQUENCY=900.0 MHZ  
 ANGLE OF ELEMENTS=45.0 DEGREES

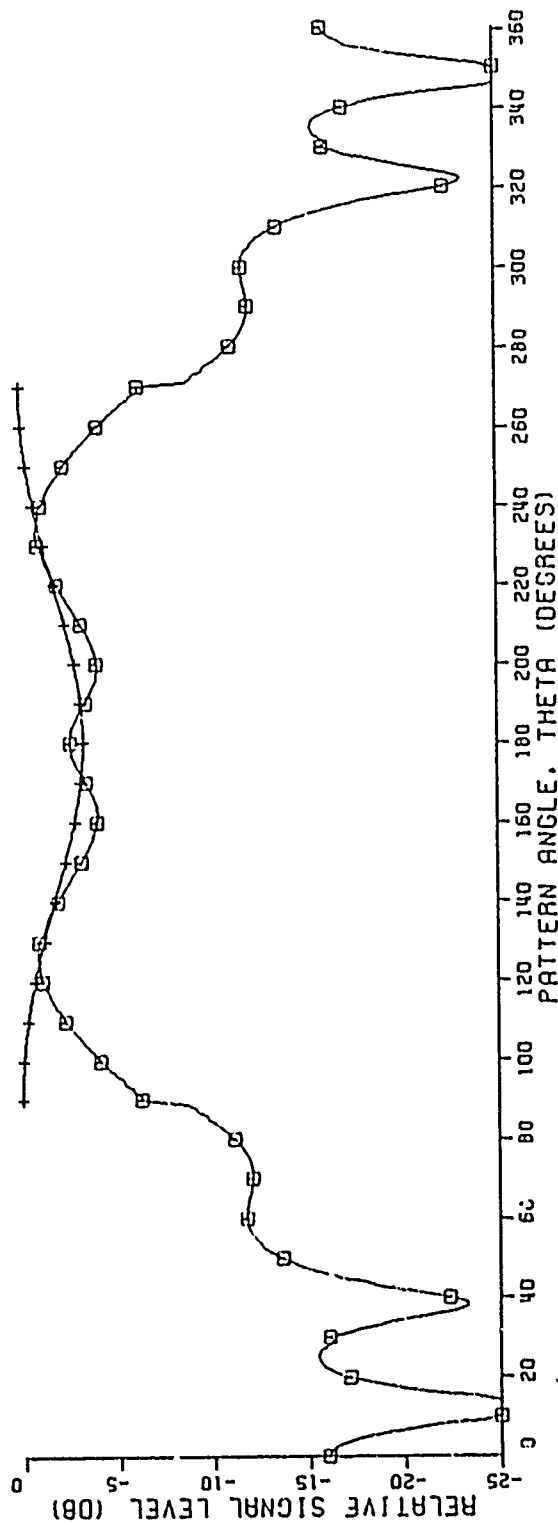


± FIELD INCLUDING EDGE DIFFRACTION

+ FIELD FROM ANT. ON INFINITE GROUND PLANE

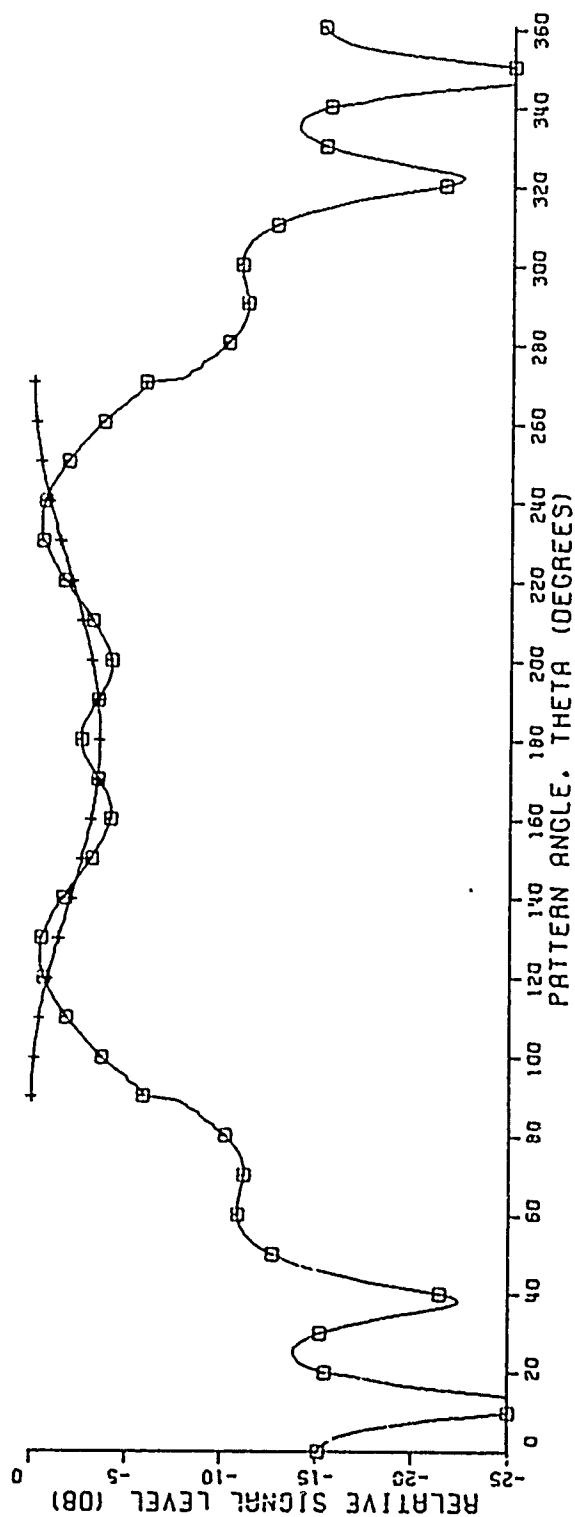
Fig. 4-16b.





180  
 90 14.0" 0.3" 14.0" 270  
 ANGLE OF ELEMENTS=30.0 DEGREES  
 MONOPOLE LENGTH=0.28 WAVELENGTHS  
 FREQUENCY=1000.0 MHZ  
 □ FIELD INCLUDING EDGE DIFFRACTION  
 + FIELD FROM ANT. ON INFINITE GROUND PLANE

Fig. 4-17a.



180

90 14.0" 0.3" 14.0" 270 ANGLE OF ELEMENTS=45.0 DEGREES

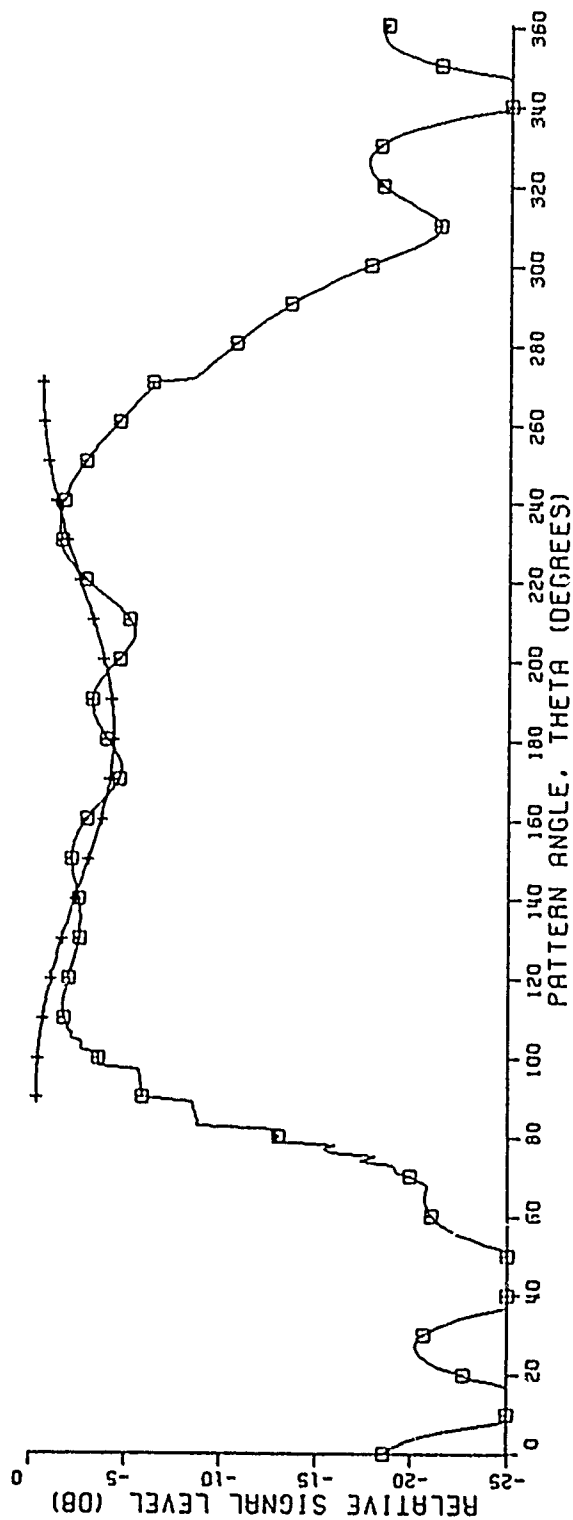
MONOPOLE LENGTH=0.28 WAVELENGTHS

FREQUENCY=1000.0 MHZ

□ FIELD INCLUDING EDGE DIFFRACTION

+ FIELD FROM ANT. ON INFINITE GROUND PLANE

Fig. 4-17b.



180

90 4.0" 0.3" 24.0" 270

ANGLE OF ELEMENTS=30.0 DEGREES

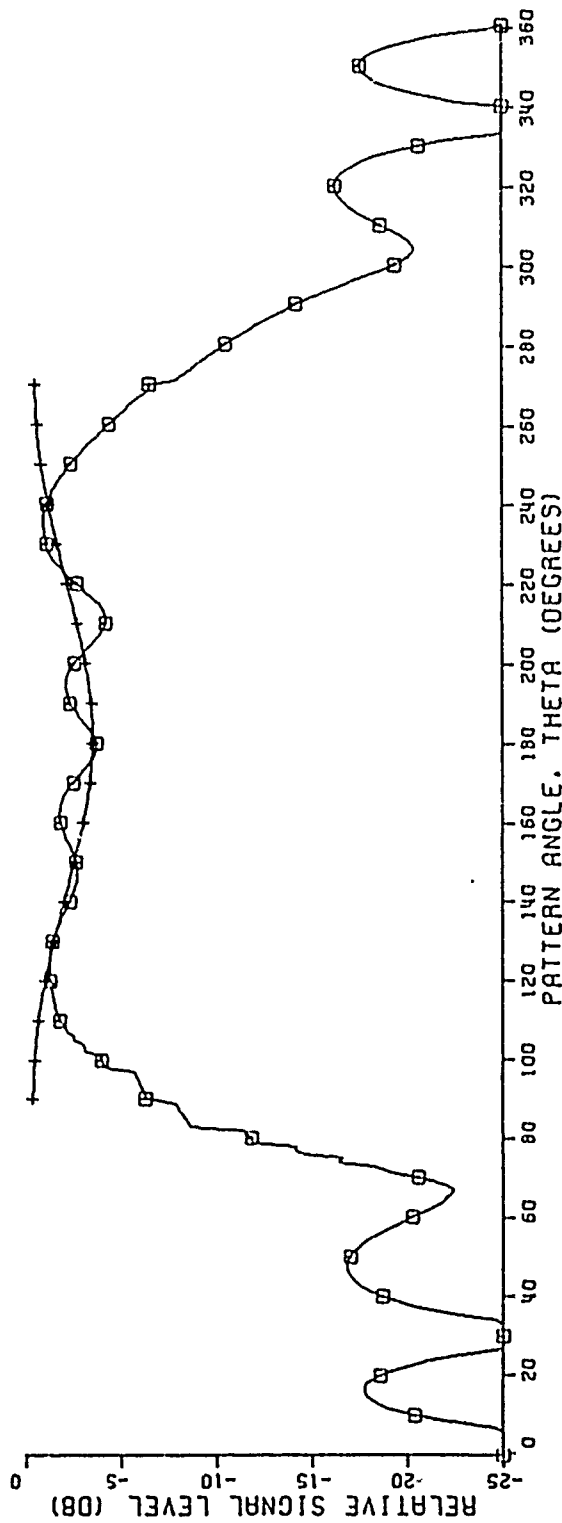
MONOPOLE LENGTH=0.22 WAVELENGTHS

FREQUENCY=800.0 MHZ

○ FIELD INCLUDING EDGE DIFFRACTION

+ FIELD FROM ANT. ON INFINITE GROUND PLANE

Fig. 4-18a. Ground plane location effects.



180

90 4.0" 0.3" 24.0" 270

ANGLE OF ELEMENTS=30.0 DEGREES

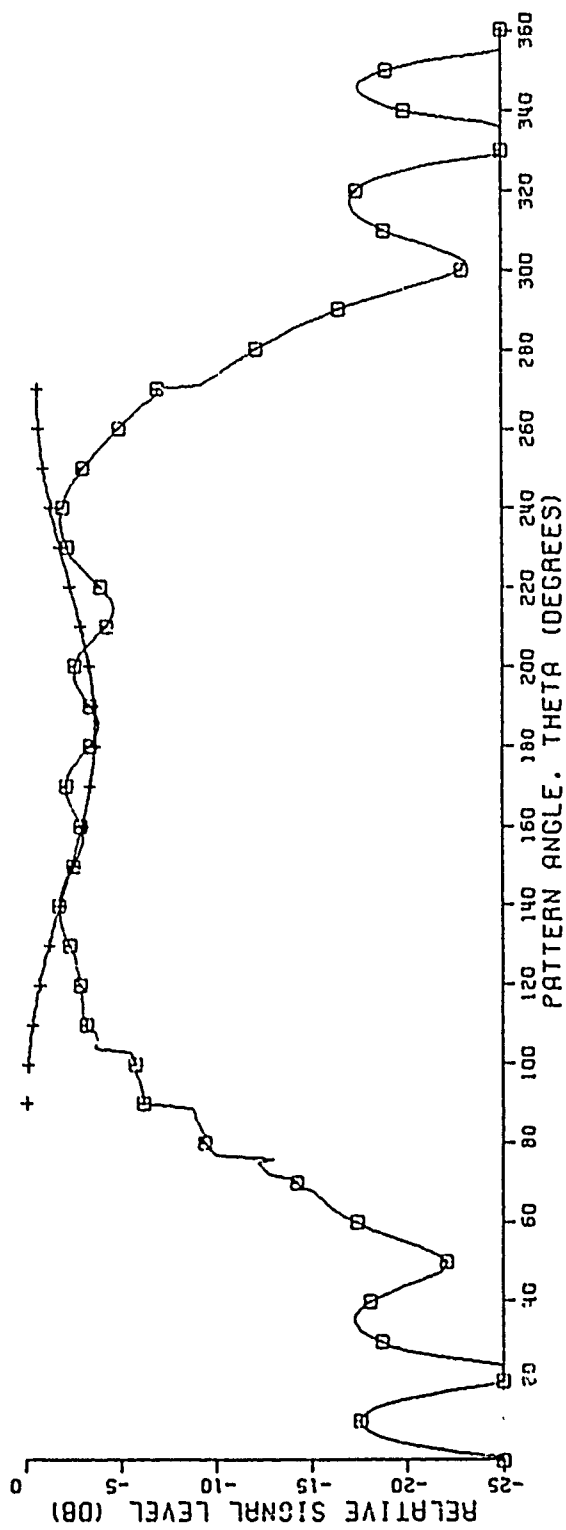
MONOPOLE LENGTH=0.25 WAVELENGTHS

FREQUENCY=900.0 MHZ

□ FIELD INCLUDING EDGE DIFFRACTION

+ FIELD FROM ANT. ON INFINITE GROUND PLANE

Fig. 4-18b.



180

90 4.0" 0.3" 24.0" 270

ANGLE OF ELEMENTS=30.0 DEGREES

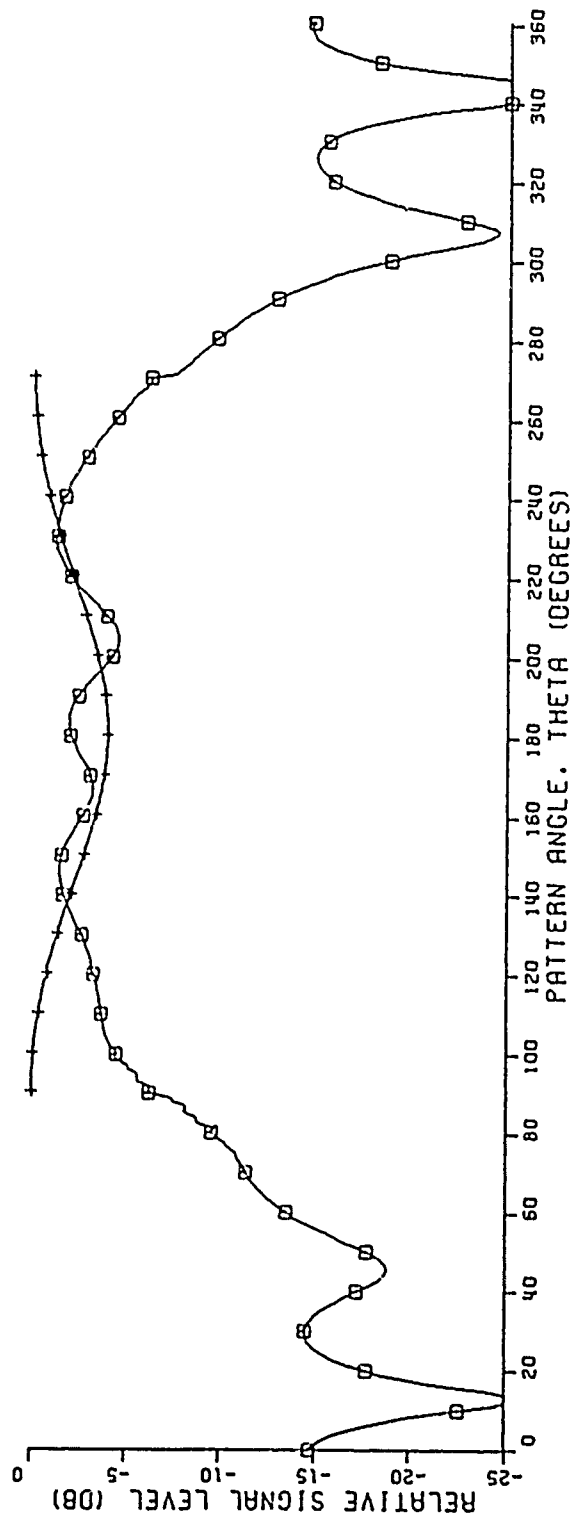
MONOPOLE LENGTH=0.28 WAVELENGTHS

FREQUENCY=1000.0 MHZ

□ FIELD INCLUDING EDGE DIFFRACTION

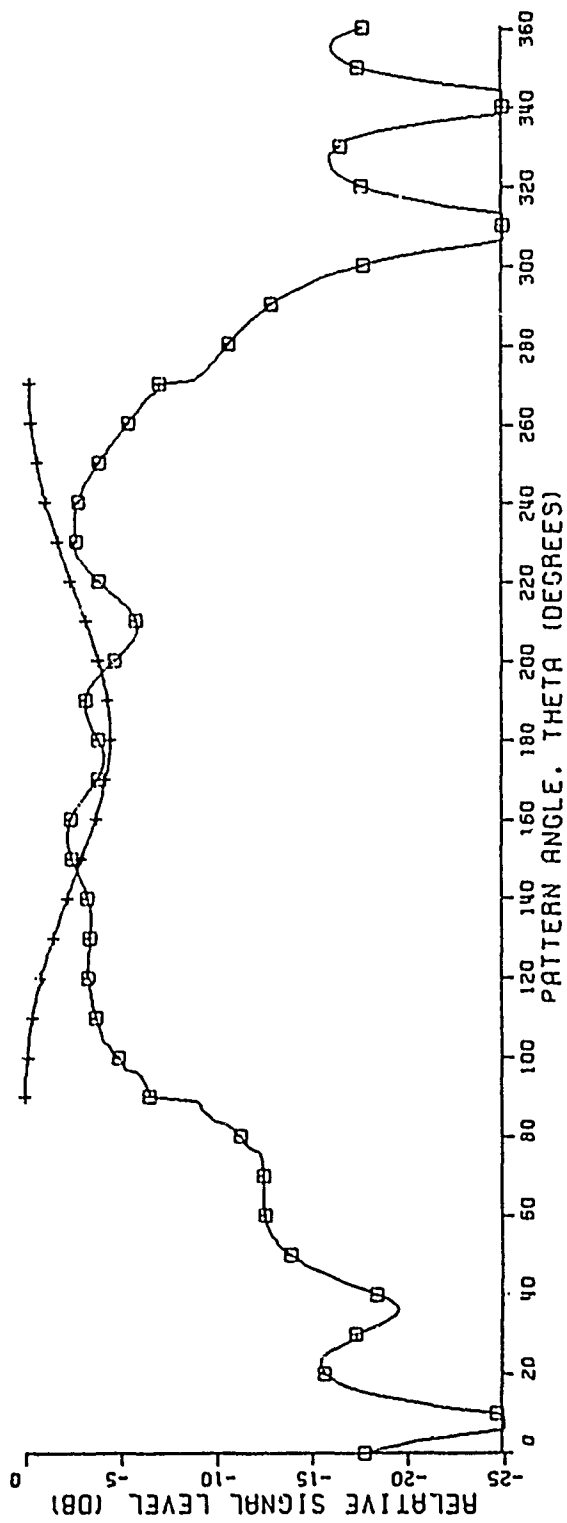
+ FIELD FROM ANT. ON INFINITE GROUND PLANE

Fig. 4-18c.



180  
 90 6.0" 0.3" 22.0" 270 ANGLE OF ELEMENTS=30.0 DEGREES  
 MONOPOLE LENGTH=0.22 WAVELENGTHS  
 FREQUENCY=800.0 MHZ  
 O FIELD INCLUDING EDGE DIFFRACTION  
 + FIELD FROM ANT. ON INFINITE GROUND PLANE

Fig. 4-19a.



180

90 6.0" 0.3" 22.0" 270

ANGLE OF ELEMENTS=30.0 DEGREES

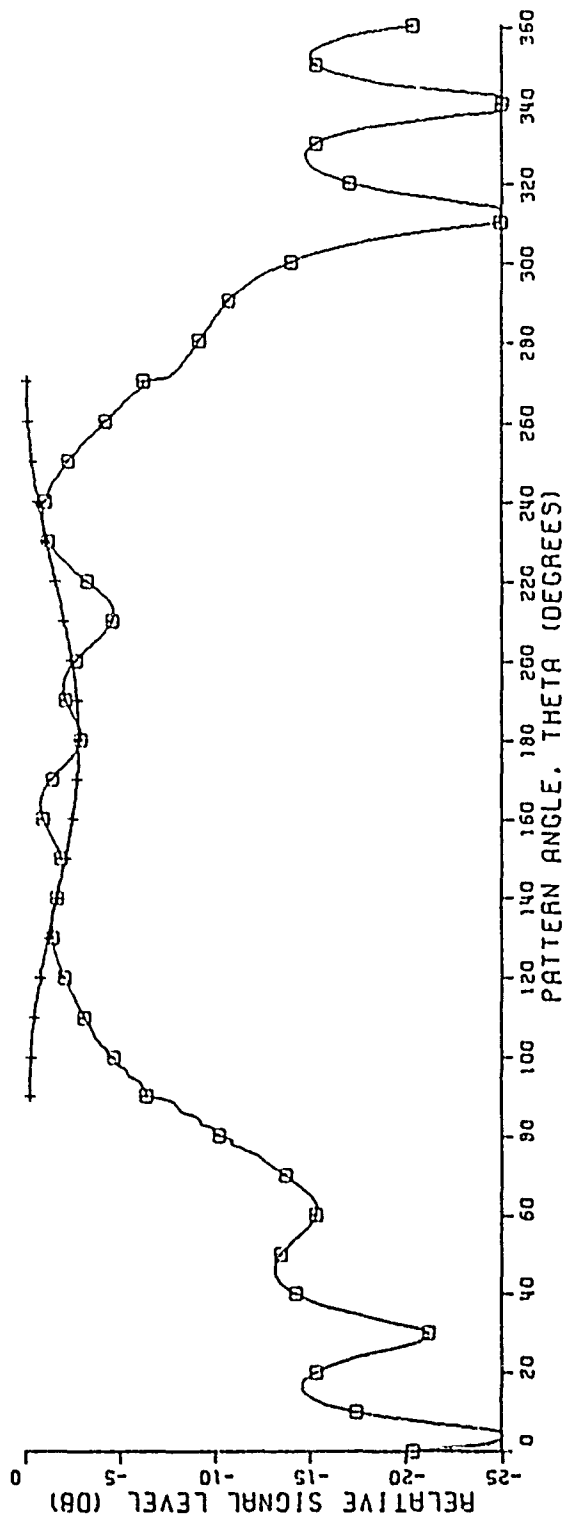
MONOPOLE LENGTH=0.25 WAVELENGTHS

FREQUENCY=900.0 MHZ

□ FIELD INCLUDING EDGE DIFFRACTION

+ FIELD FROM ANT. ON INFINITE GROUND PLANE

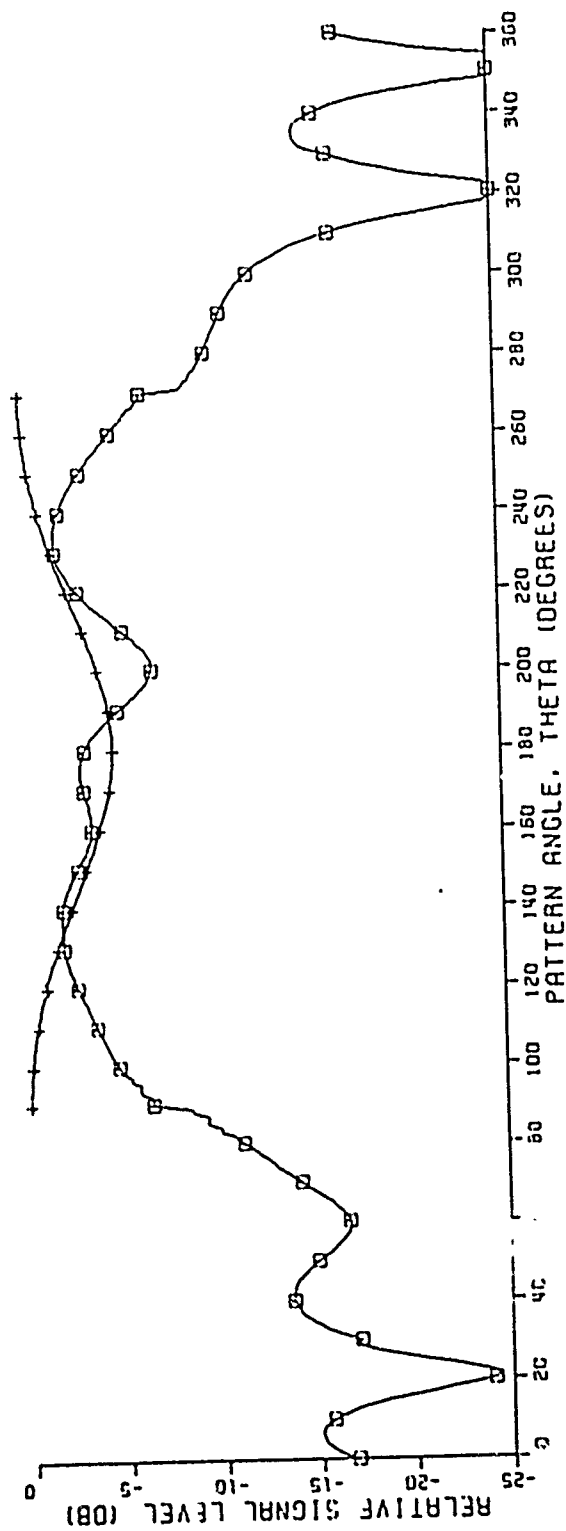
Fig. 4-19b.



180  
 90 — 6.0" — 0.3" — 22.0" — 270  
 MONOPOLE LENGTH=0.28 WAVELENGTHS  
 FREQUENCY=1000.0 MHZ  
 ○ FIELD INCLUDING EDGE DIFFRACTION  
 + FIELD FROM ANT. ON INFINITE GROUND PLANE

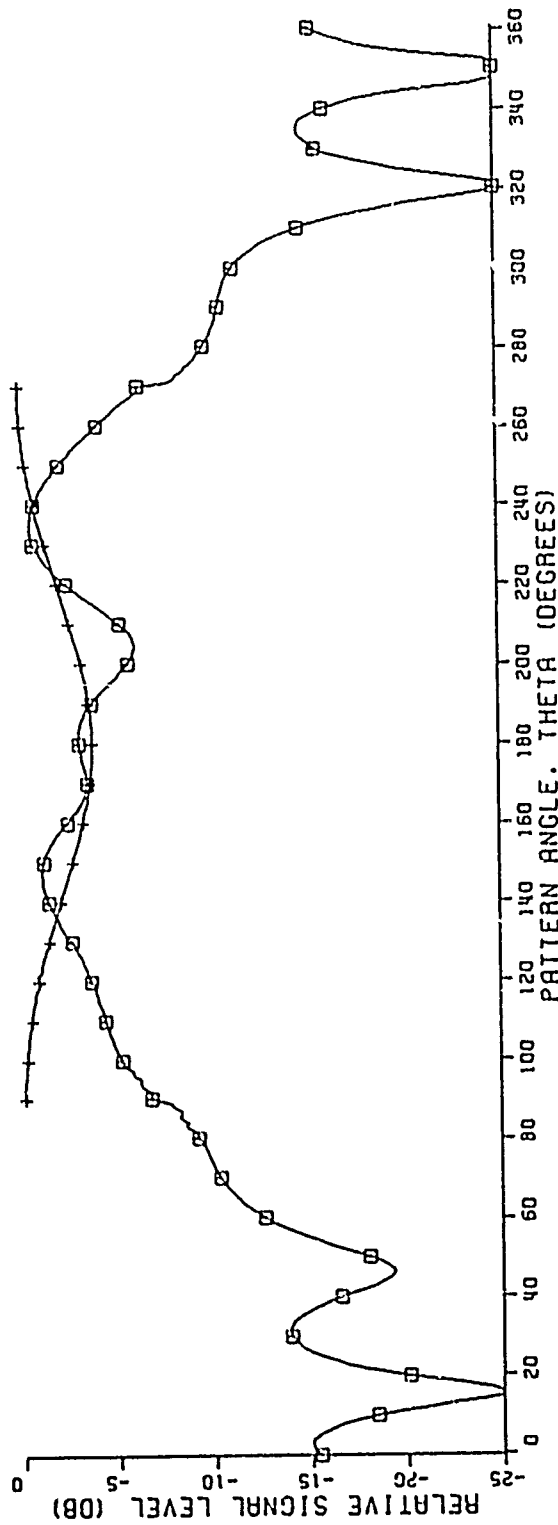
Fig. 4-19c.





180  
 90 — 8.0" — 0.3" — 20.0" — 270  
 ANGLE OF ELEMENTS = 30.0 DEGREES  
 MONOPOLE LENGTH = 0.22 WAVELENGTHS  
 FREQUENCY = 800.0 MHZ  
 □ FIELD INCLUDING EDGE DIFFRACTION  
 + FIELD FROM ANT. ON INFINITE GROUND PLANE

Fig. 4-20a.



180

90 8.0" 0.3" 20.0" 270

ANGLE OF ELEMENTS=30.0 DEGREES

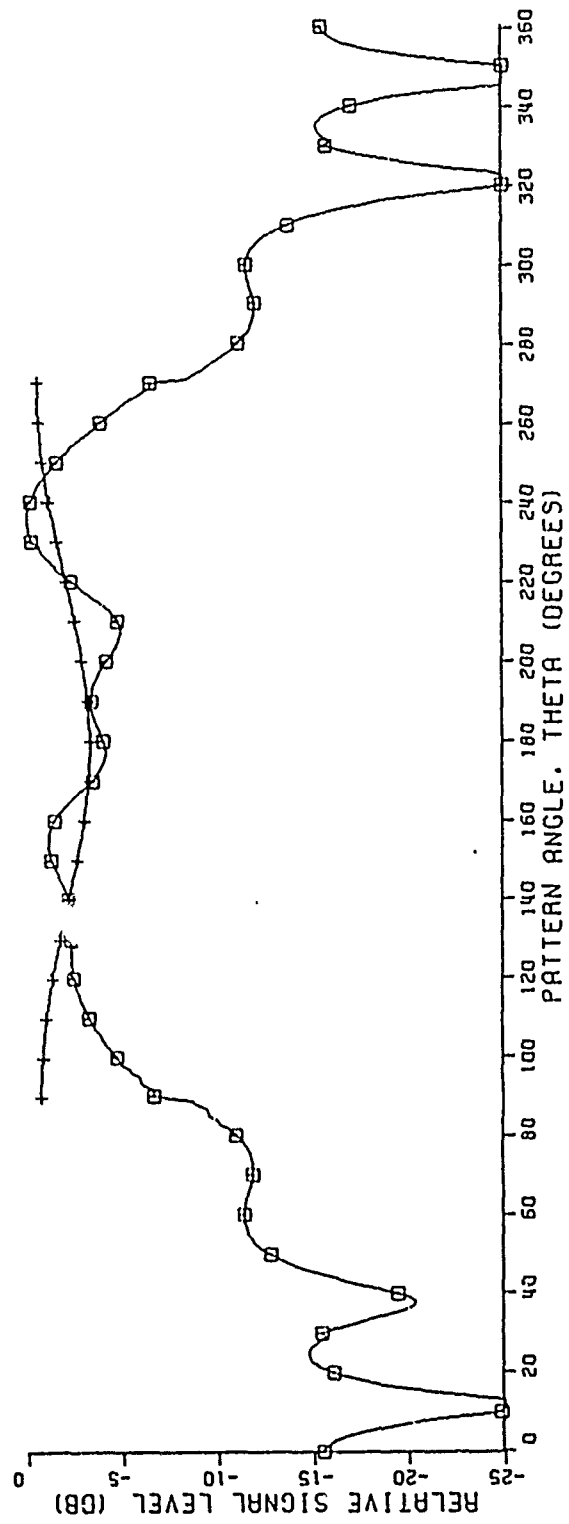
MONOPOLE LENGTH=0.25 WAVELENGTHS

FREQUENCY=900.0 MHZ

□ FIELD INCLUDING EDGE DIFFRACTION

+ FIELD FROM ANT. ON INFINITE GROUND PLANE

Fig. 4-20b.



180

90 8.0" 0.3" 20.0" 270

ANGLE OF ELEMENTS=30.0 DEGREES

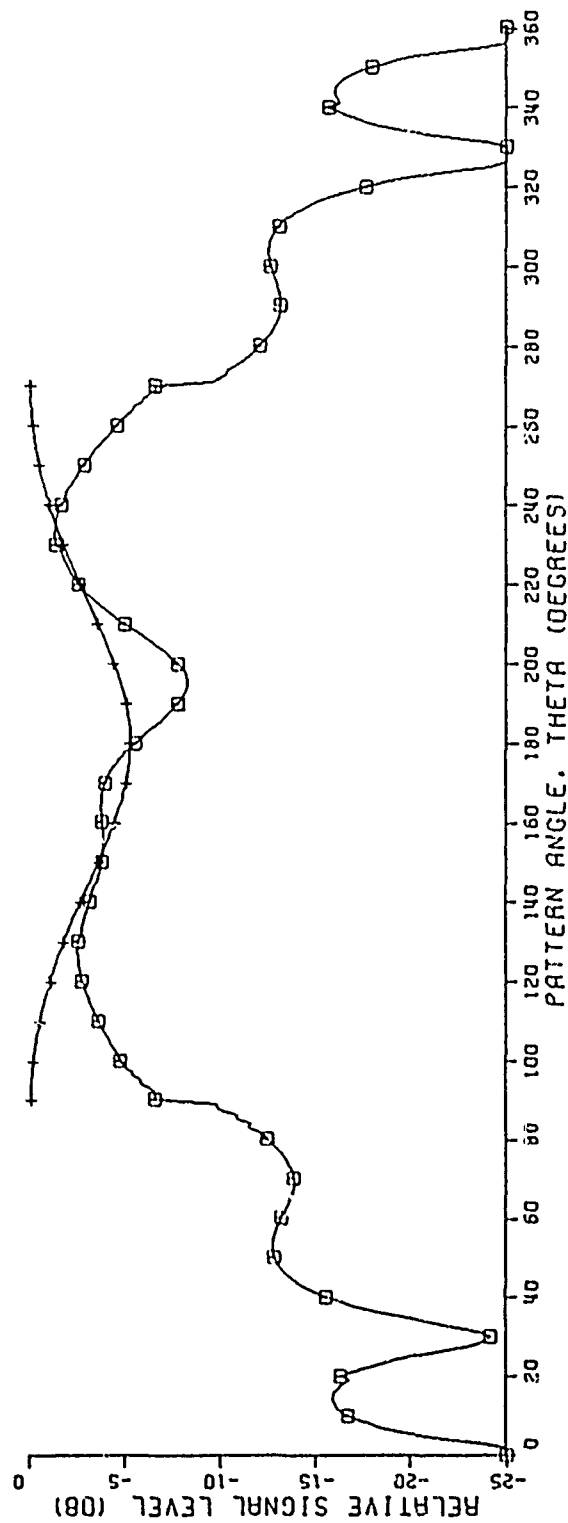
MONOPOLE LENGTH=0.28 WAVELENGTHS

FREQUENCY=1000.0 MHZ

○ FIELD INCLUDING EDGE DIFFRACTION

+ FIELD FROM ANT. ON INFINITE GROUND PLANE

Fig. 4-20c.



180

90 10.0" 0.3" 18.0" 270

ANGLE OF ELEMENTS=30.0 DEGREES

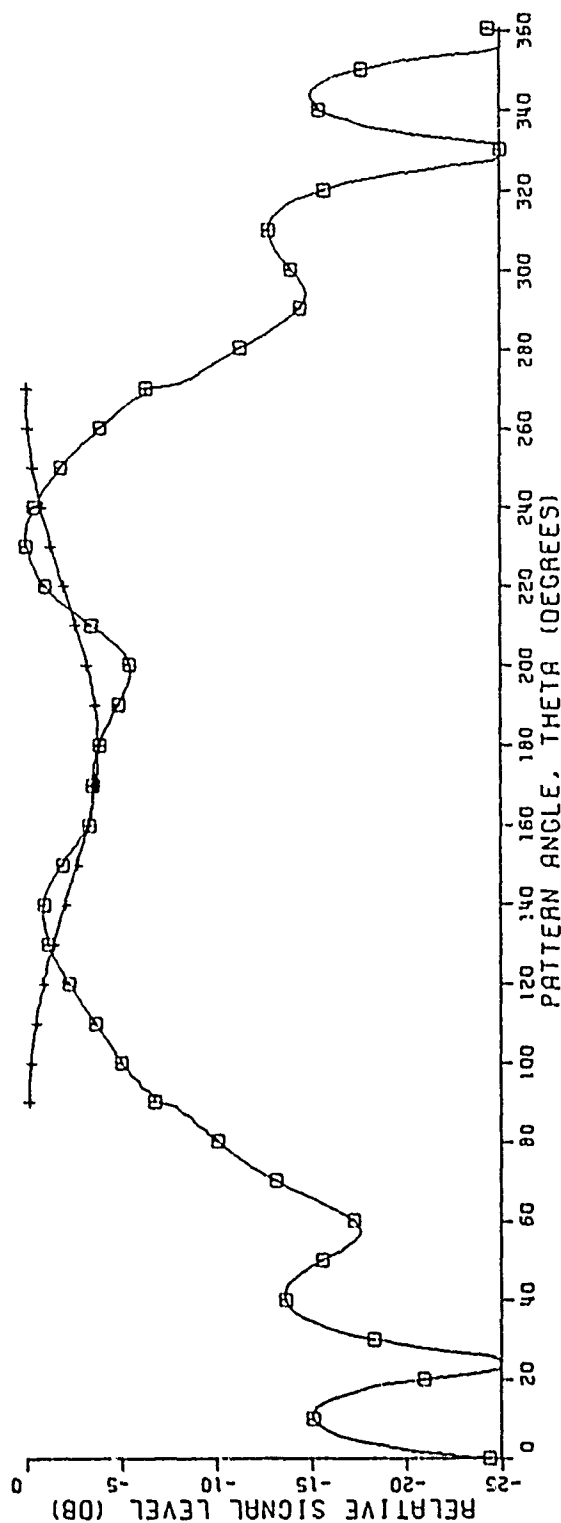
MONOPOLE LENGTH=0.22 WAVELENGTHS

FREQUENCY=800.0 MHZ

□ FIELD INCLUDING EDGE DIFFRACTION

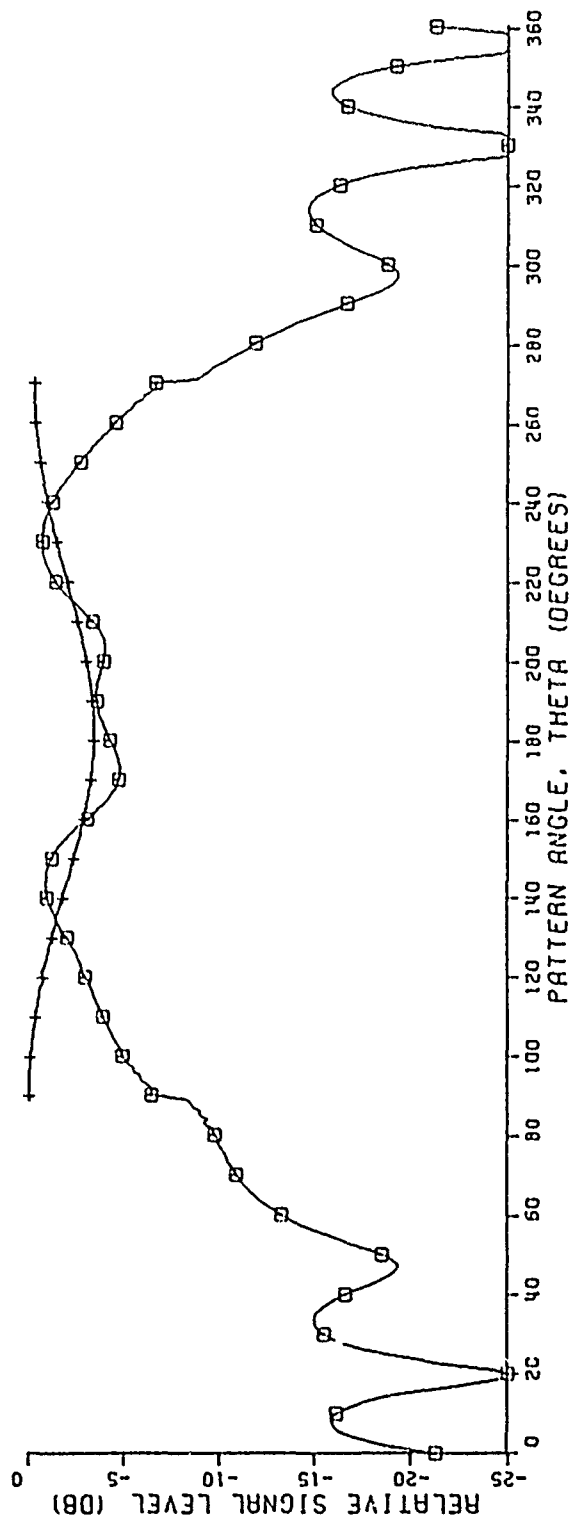
+ FIELD FROM ANT. ON INFINITE GROUND PLANE

Fig. 4-21a.



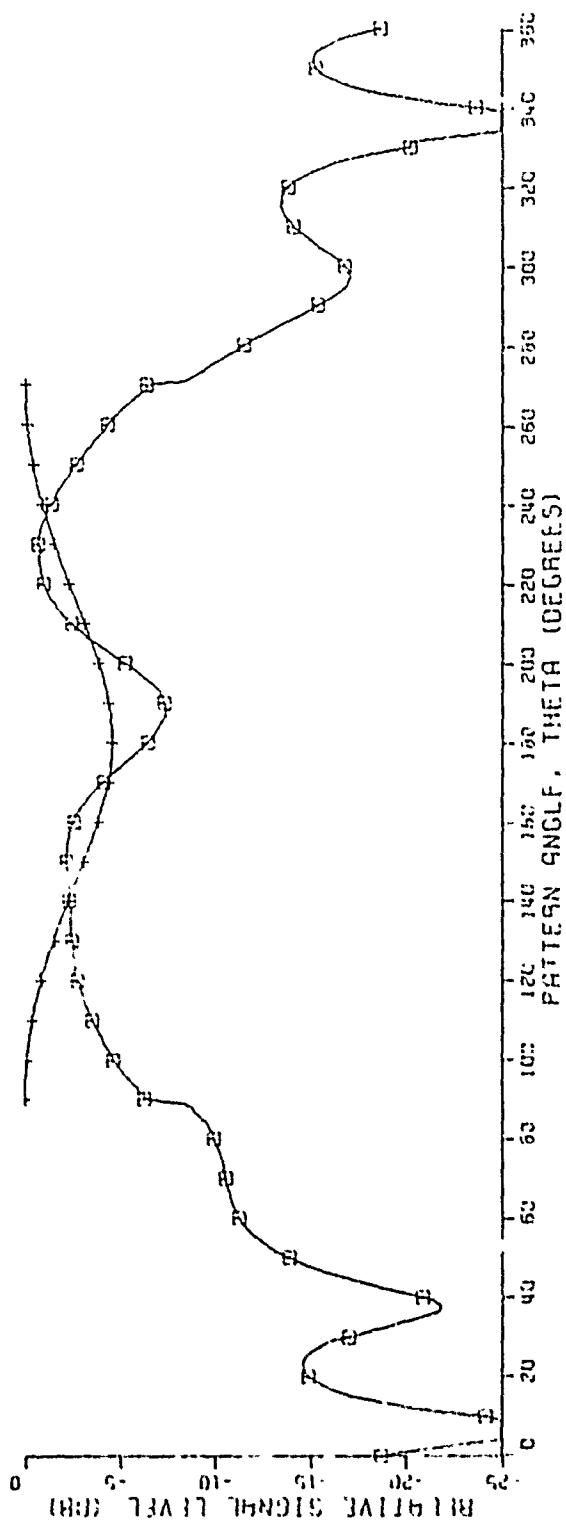
180  
 90 10.0" 0.3" 18.0" 270  
 ANGLE OF ELEMENTS=30.0 DEGREES  
 MONOPOLE LENGTH=0.25 WAVELENGTHS  
 FREQUENCY=900.0 MHZ  
 O FIELD INCLUDING EDGE DIFFRACTION  
 + FIELD FROM ANT. ON INFINITE GROUND PLANE

Fig. 4-21b.



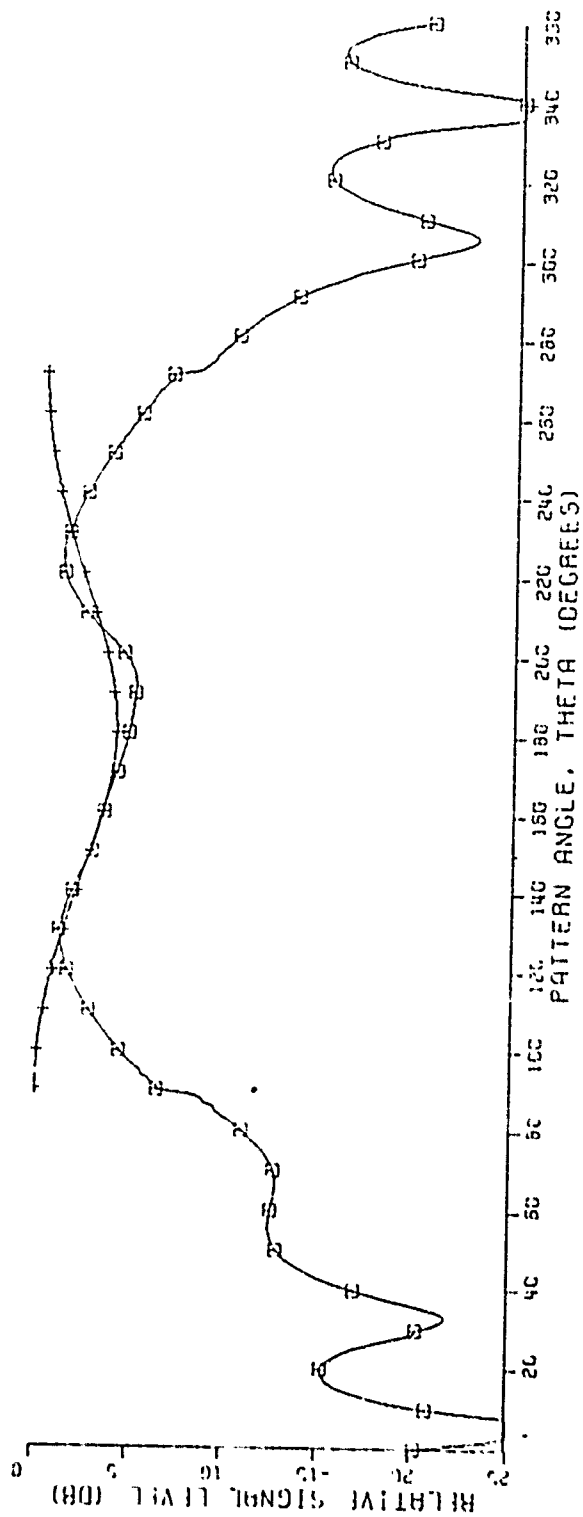
180  
 10.0" 0.3" 18.0" 270  
 ANGLE OF ELEMENTS=30.0 DEGREES  
 MONOPOLE LENGTH=0.28 WAVELENGTHS  
 FREQUENCY=1000.0 MHZ  
 □ FIELD INCLUDING EDGE DIFFRACTION  
 + FIELD FROM ANT. ON INFINITE GROUND PLANE

Fig. 4-21c.



180  
 90° 12 0" 0.3" 15.0" 270  
 MONOPOLE LENGTH=0.22 WAVELENGTHS  
 FREQUENCY=900.0 MHZ  
 - FIELD INCLUDING EDGE DIFFRACTION  
 + FIELD FROM ANT. ON INFINITE GROUND PLANE

Fig. 4-22a.



150

90 12 0" 0.5 15 0" 270 ANGLE OF ELEMENTS=30.0 DEGREES

MONOPOLE LENGTH=0.25 WAVELENGTHS

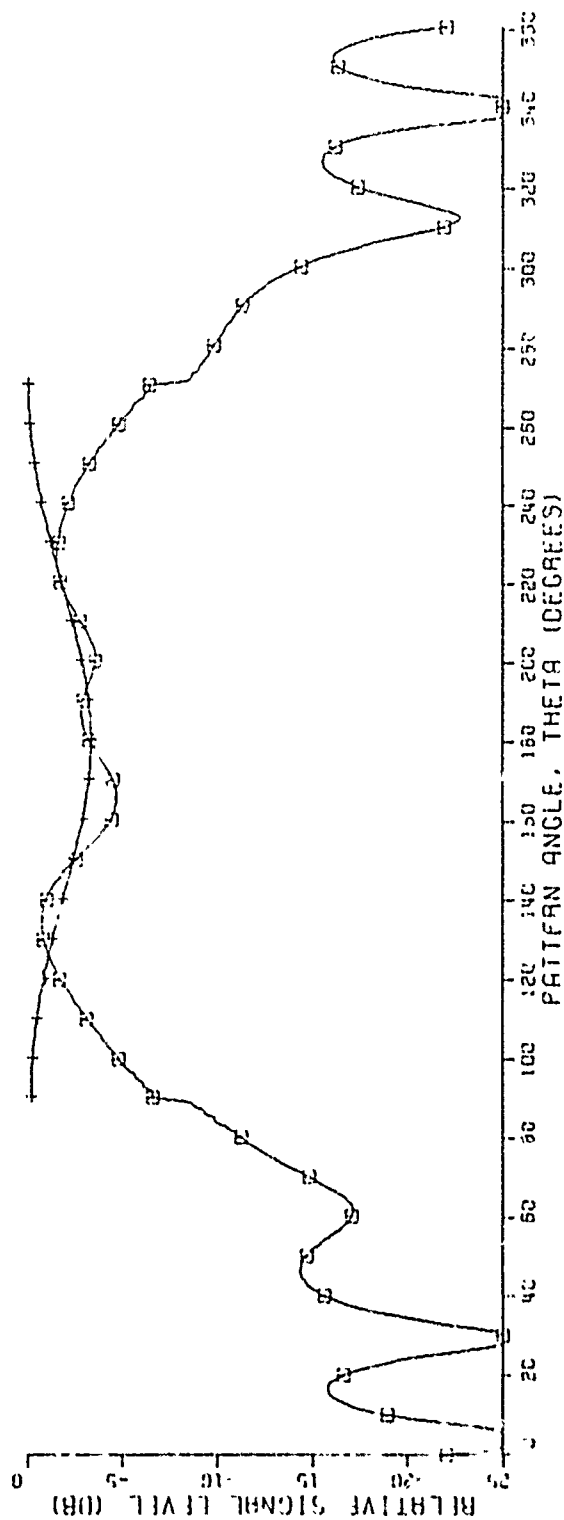
FREQUENCY=900.0 MHZ

OF FIELD INCLUDING EDGE DIFFRACTION

+ FIELD FROM ANT. ON INFINITE GROUND PLANE

Fig. 4-22b.





30" 12 0" 0.3" 18.0" 270" ANGLE OF ELEMENTS=30.0 DEGREES  
 WAVELENGTH=0.29 WAVELENGTHS  
 FREQUENCY=1000.0 MHZ

+ FIELD INCLUDING EDGE DIFFRACTION  
 + FIELD FROM ANT. ON INFINITE GROUND PLANE

Fig. 4-22c.

## CHAPTER V

### SUMMARY AND CONCLUSIONS

This research and development effort, which investigates the radiation patterns of a proposed UHF satellite antenna, has utilized a combination of two powerful computational techniques, the Method of Moments and the Geometrical Theory of Diffraction (GTD), combined into a Hybrid Technique. The Hybrid Technique allows us to investigate the performance of the satellite antenna at various locations on a 28" by 28" panel without making an assumption about the current distribution in amplitude or phase as one would normally do in a pure GTD approach to the problem. Instead, the current distribution is treated as an unknown in the moment method part of the hybrid technique.

The radiation pattern results presented in Chapter IV have been checked against an independent computer program and against measurements in the literature. In all cases agreement is good, giving one the necessary confidence in the data and the conclusions that can be drawn from them. It is surprisingly apparent from the data that the best location for the UHF antenna is near one edge of the panel, rather than near the center.

There are, of course, other antennas and scattering objects on the panel that will redirect some of the energy and cause perturbations in the radiation patterns from those shown here. The method we used here and the associated computer program can be extended to include these effects. It is recommended that such an effort be undertaken.

## REFERENCES

- [1] T. Newhouse and G. A. Thiele, "A New Method for Combining the Method of Moments with the Geometrical Theory of Diffraction," Report 3468-4, March 1974, The Ohio State University ElectroScience Laboratory, Department of Electrical Engineering; prepared under Contract N00014-67-A-0232-0018 for Office of Naval Research (Naval Research Laboratory). (AD 780055)
- [2] G. A. Thiele and T. H. Newhouse, "A Hybrid Technique for Combining the Method of Moments with the Geometrical Theory of Diffraction," IEEE Transactions on Antennas and Propagation, Vol. AP-23, No. 1, January 1975.
- [3] G. A. Thiele, "Wire Antennas," Chapter 2 of Computer Techniques for Electromagnetics, R. Mittra, Ed., Pergamon Press, London, 1973.
- [4] J. H. Richmond, "Radiation and Scattering by Thin-Wire Structures in the Complex Frequency Domain," from notes for "Short Course on Application of GTD and Numerical Techniques to the Analysis of Electromagnetic and Acoustic Radiation and Scattering," September 1973, The Ohio State University, Columbus, Ohio.
- [5] G. A. Richards, "Reaction Formulation and Numerical Results for Multiturn Loop Antennas and Arrays," Dissertation, Spring 1970, The Ohio State University, Columbus, Ohio.
- [6] R. C. Rudduck, Notes for a "Short Course on Application of GTD and Numerical Techniques to the Analysis of Electromagnetic and Acoustic Radiation and Scattering," September 1973, The Ohio State University, Columbus, Ohio.
- [7] V. H. Rumsey, "Reaction Concept in Electromagnetic Theory," Physical Review, Vol. 94, (June 1954), pp. 1483-1491.
- [8] J. H. Richmond, "Computer Program for Thin-Wire Structures in a Homogeneous Conducting Medium," from notes for "Short Course on Application of GTD and Numerical Techniques to the Analysis of Electromagnetic and Acoustic Radiation and Scattering," September 1973, The Ohio State University, Columbus, Ohio.
- [9] S. A. Schelkunoff, "On Diffraction and Radiation of Electromagnetic Waves," Physical Review, Vol. 56, August 15, 1939.

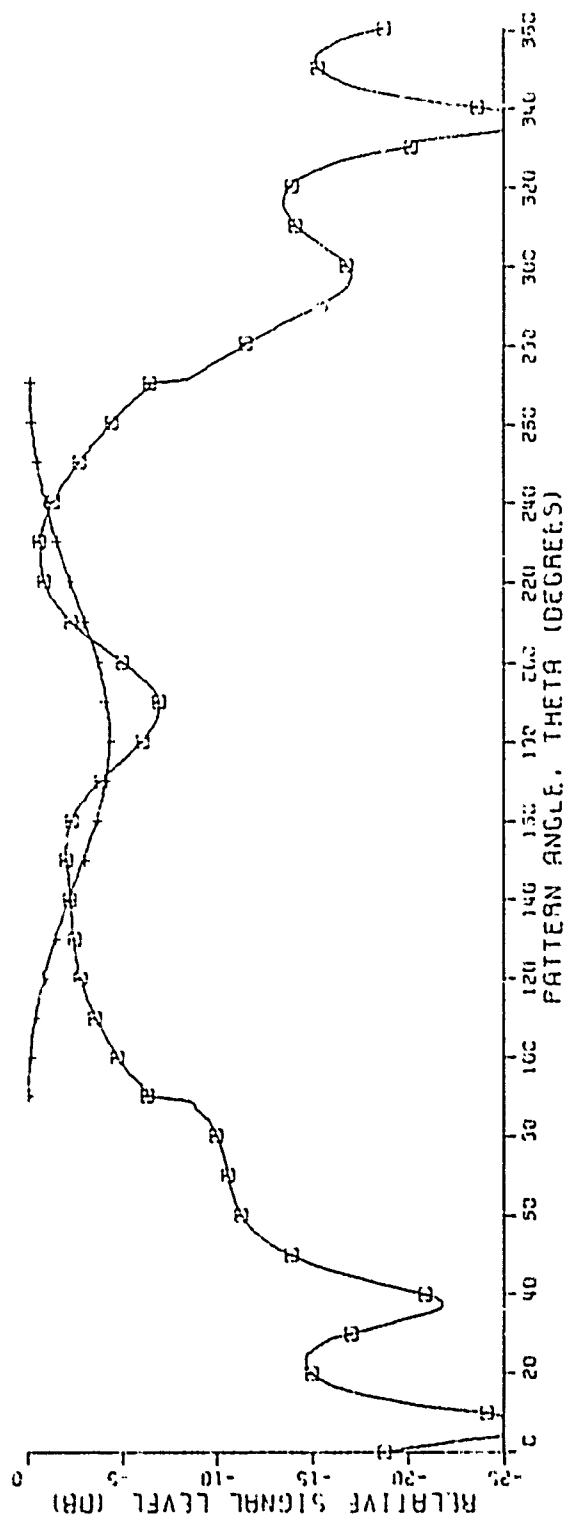
- [10] J. R. Carson, "An Generalization of the Reciprocity Theory," Bell System Technical Journal, Vol. 3, July 1924, pp. 393-399.
- [11] A. Sommerfeld, Optics, Academic Press, Inc., New York, 1954, pp. 245-265.
- [12] W. Pauli, "On Asymptotic Series for Functions in the Theory of Diffraction of Light," Phys. Rev., Vol. 54, 1 December 1968, pp. 924-931.
- [13] J. B. Keller, "Geometrical Theory of Diffraction," J. Opt. Soc. Am., 52, No. 2, February 1962, pp. 116-130.
- [14] D. L. Hutchins and R. G. Kouyoumjian, "A New Asymptotic Solution to the Diffraction by a Wedge," URSI 1967 Spring Meeting, Ottawa, Canada, pp. 154-155.
- [15] P. H. Pathak and R. G. Kouyoumjian, "The Dyadic Diffraction Coefficient for a Perfectly Conducting Wedge," Report 2183-4, 5 June 1970, The Ohio State University ElectroScience Laboratory, Department of Electrical Engineering; prepared under Contract AF 19(628)-5929 for Air Force Cambridge Research Laboratories. (AFCRL-69-0546) (AD 707 827).
- [16] A. R. Lopez, "The Geometrical Theory of Diffraction Applied to Antenna Pattern and Impedance Calculations," IEEE Transaction on Antennas and Propagation, Vol. AP-14, No. 1, January 1966, p. 40.
- [17] W. D. Burnside, R. J. Marhefka, C. L. Yu, "Roll-Plane Analysis of On-Aircraft Antennas," IEEE Trans. on Antennas and Propagation, Vol. AP-21, Number 6, November 1973.

## APPENDIX I

The patterns contained in this appendix are those of a two monopole array with the array center located 12 inches from one ground plane edge and 16 inches from the opposite edge.

Figures I-1a-e are patterns for various element spacings at 800 MHz. The angle of the elements is 30 degrees. Figures I-2a-e and Figs. I-3a-e have the same geometric set ups as Figs. I-1a-e but the frequency is 900 and 1000 MHz respectively.

Figures I-4a-f, I-5a-f, and I-6a-f are patterns for various element spacings with the angle of the elements set at 45 degrees. Figures I-4a-f are at 800 MHz while Figs. I-5a-f and Figs. I-6a-f are at 900 and 1000 MHz respectively.



190

12.0" 0.2" 15 C" 270

ANGLE OF ELEMENTS = 30.0 DEGREES

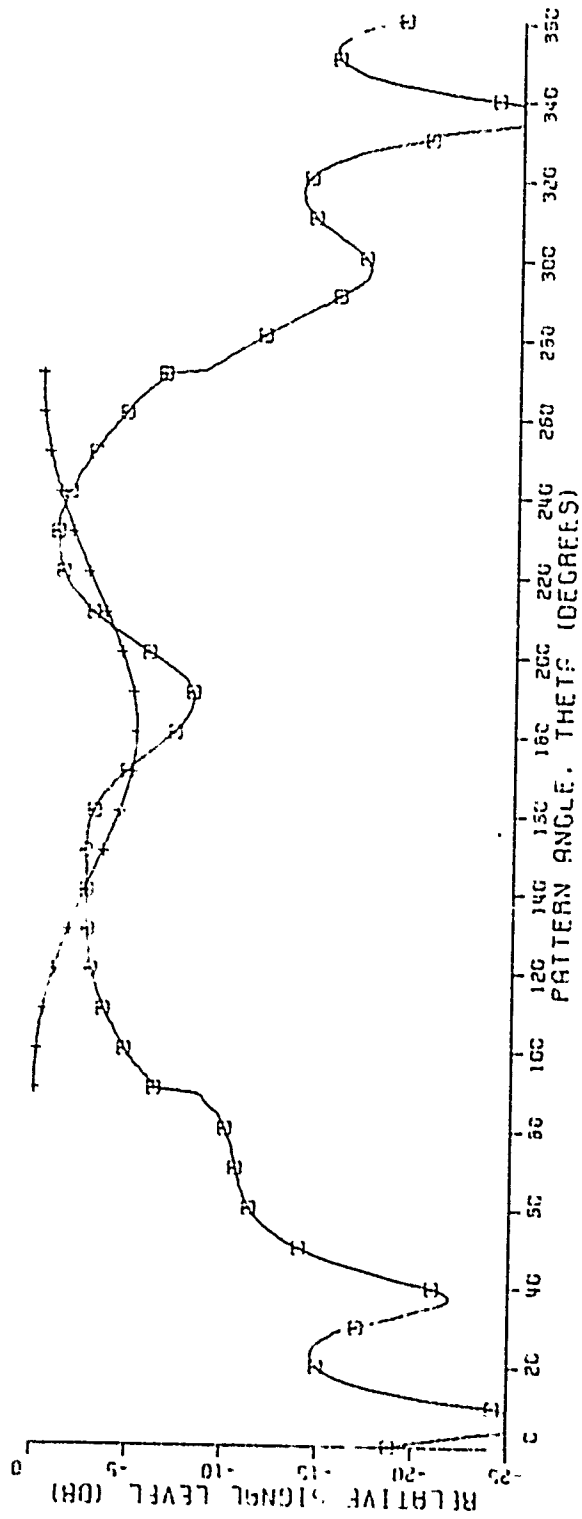
MONOPOLE LENGTH = 0.22 WAVELENGTHS

FREQUENCY = 300.0 MHZ

W FIELD INCLUDING EDGE DIFFRACTION

+ FIELD FROM ANT. ON INFINITE GROUND PLANE

Fig. I-1a.



180

90 12.0" 15.0" 270

ANGLE OF ELEMENTS=30.0 DEGREES

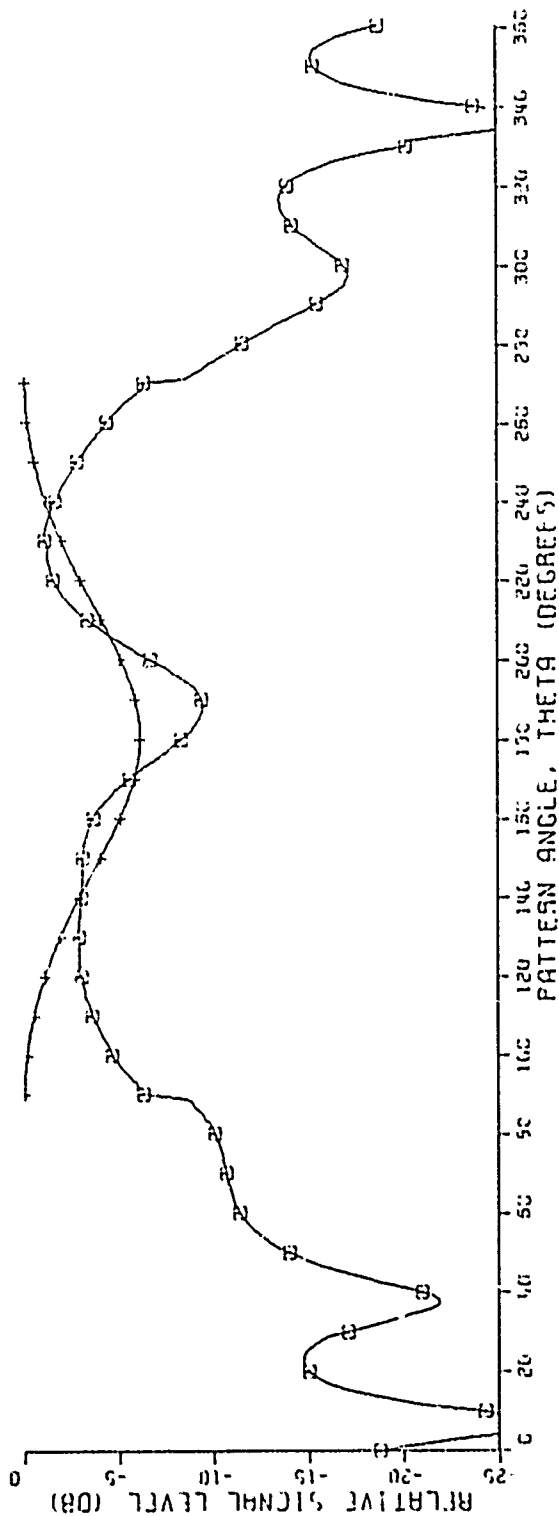
MONOPOLE LENGTH=0.22 WAVELENGTHS

FREQUENCY=800.0 MHZ

FIELD INCLUDING EDGE DIFFRACTION

+ FIELD FROM ANT. ON INFINITE GROUND PLANE

Fig. I-1b.



180

30 12.0" 1.0" 15 0" 270 ANGLE OF ELEMENTS=30.0 DEGREES

MONOPOLE LENGTH=0.22 WAVELENGTHS

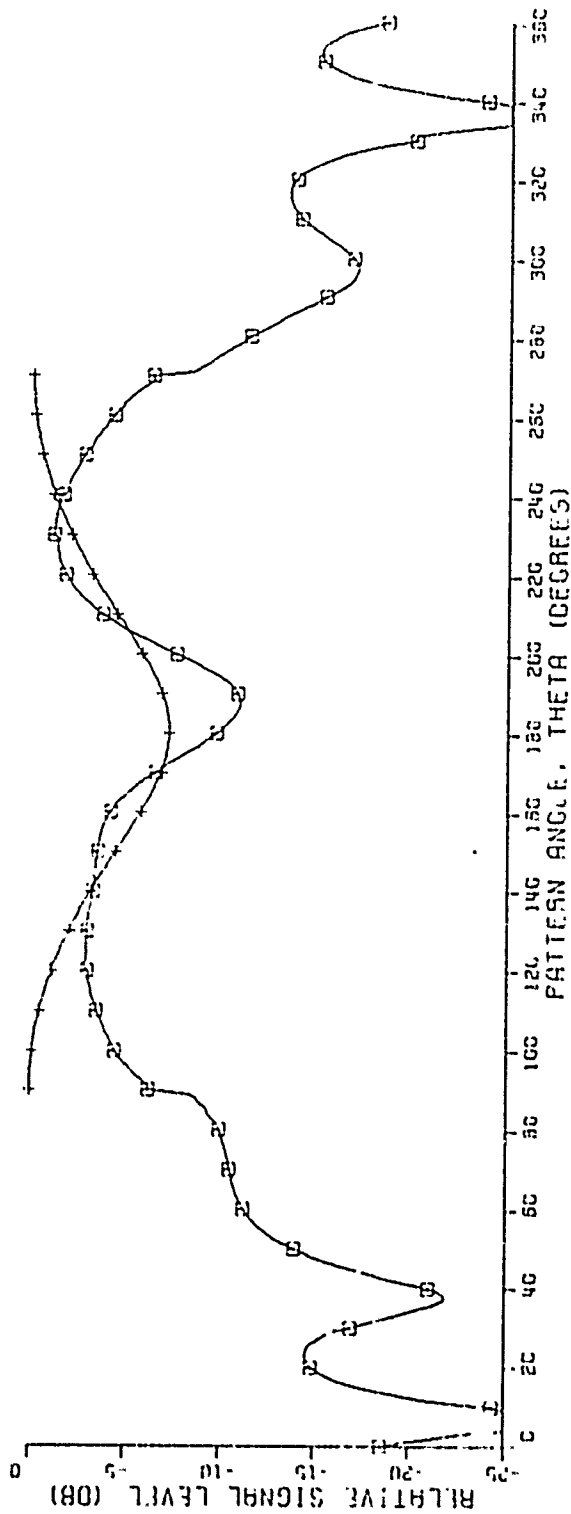
FREQUENCY=800.0 MHZ

W FIELD INCLUDING EDGE DIFFRACTION

+ FIELD FROM ANT. ON INFINITE GROUND PLANE

Fig. I-1c.





180°

90° 2.0" 15.0" 270° ANGLE OF ELEMENTS-30.0 DEGREES

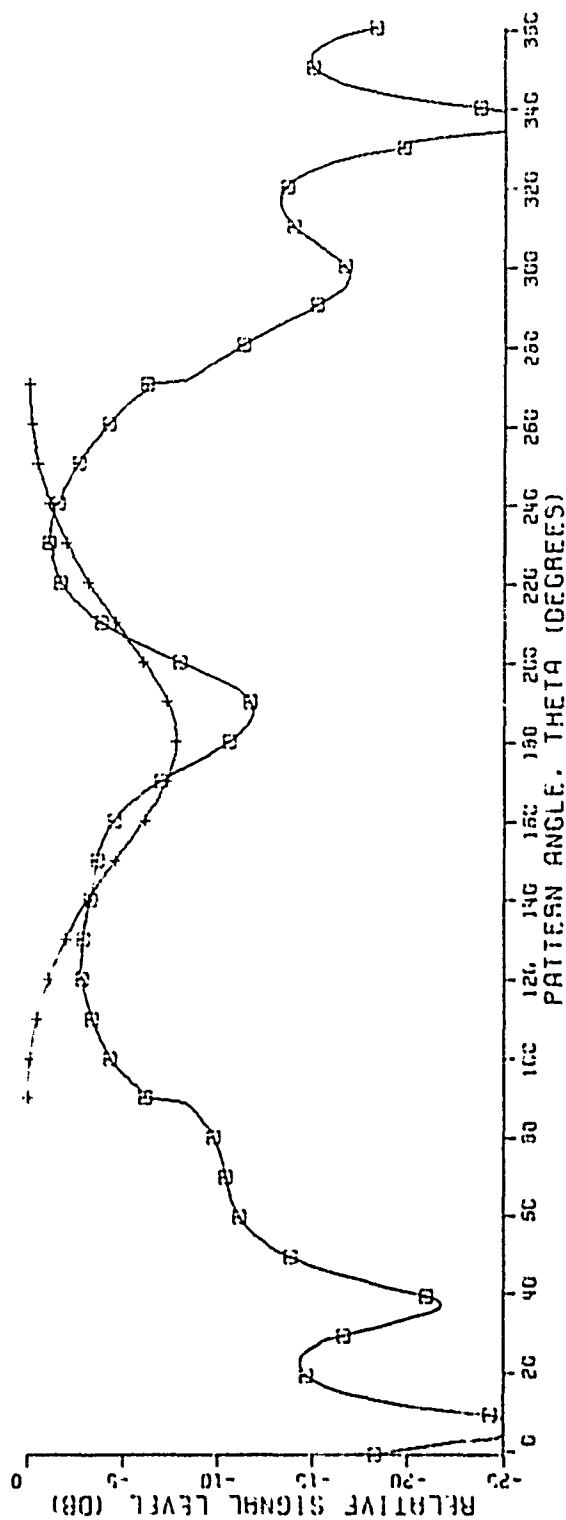
MONOPOLE LENGTH=0.22 WAVELENGTHS

FREQUENCY-300.0 MHZ

□ FIELD INCLUDING EDGE DIFFRACTION

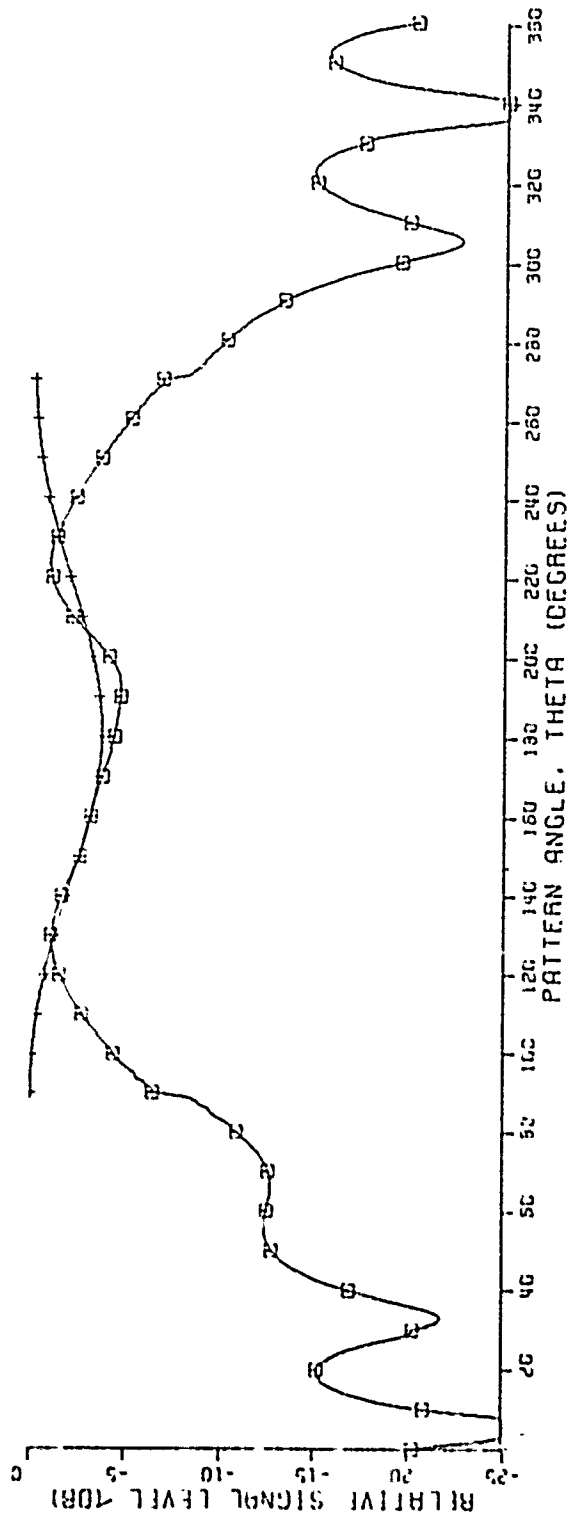
+ FIELD FROM ANT. ON INFINITE GROUND PLANE

Fig. I-1d.



150  
 120" 3 3" 150" 270 ANGLE OF ELEMENTS=30.0 DEGREES  
 MONOPOLE LENGTH=0.22 WAVELENGTHS  
 FREQUENCY=800.0 MHZ  
 E FIELD INCLUDING EDGE DIFFRACTION  
 + FIELD FROM ANT. ON INFINITE GROUND PLANE

Fig. I-1e,



180

90 12 0" 0.2" 15.0" 270

ANGLE OF ELEMENTS=30.0 DEGREES

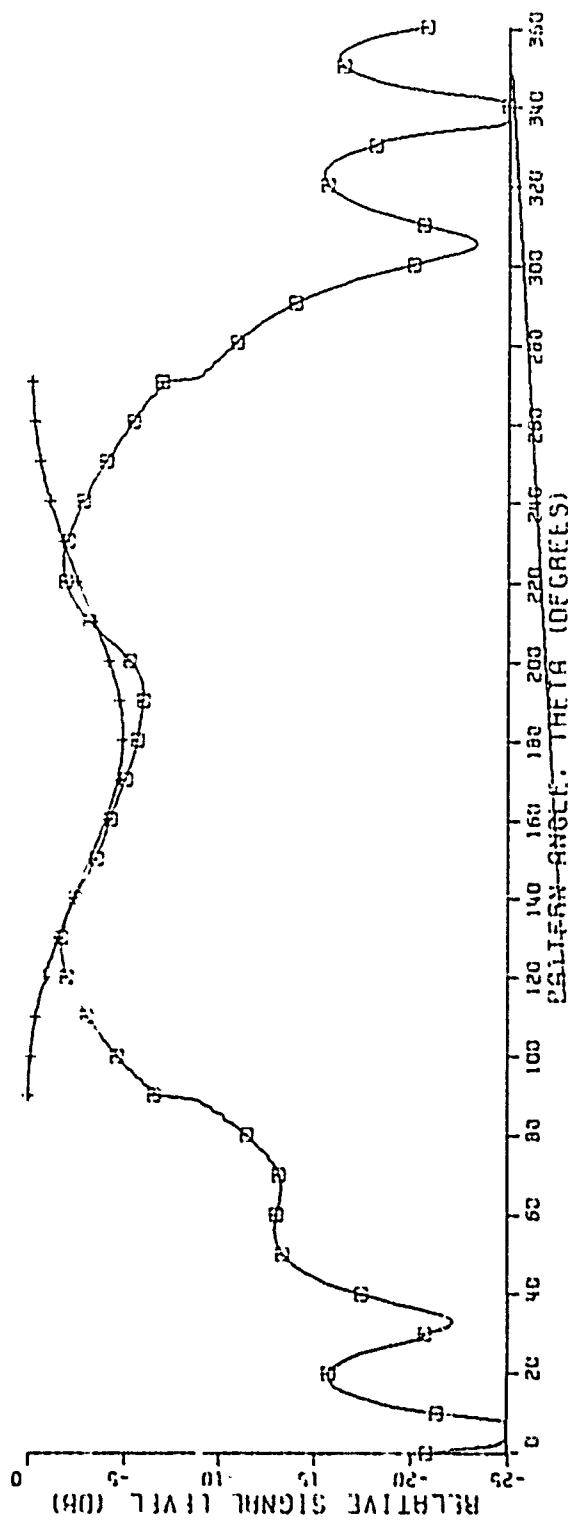
MONOPOLE LENGTH=0.25 WAVELENGTHS

FREQUENCY=900.0 MHZ

W FIELD INCLUDING EDGE DIFFRACTION

+ FIELD FROM ANT. ON INFINITE GROUND PLANE

Fig. I-2a.



150

12 0" 0.5" 16.0" 270

ANGLE OF ELEMENTS = 30.0 DEGREES

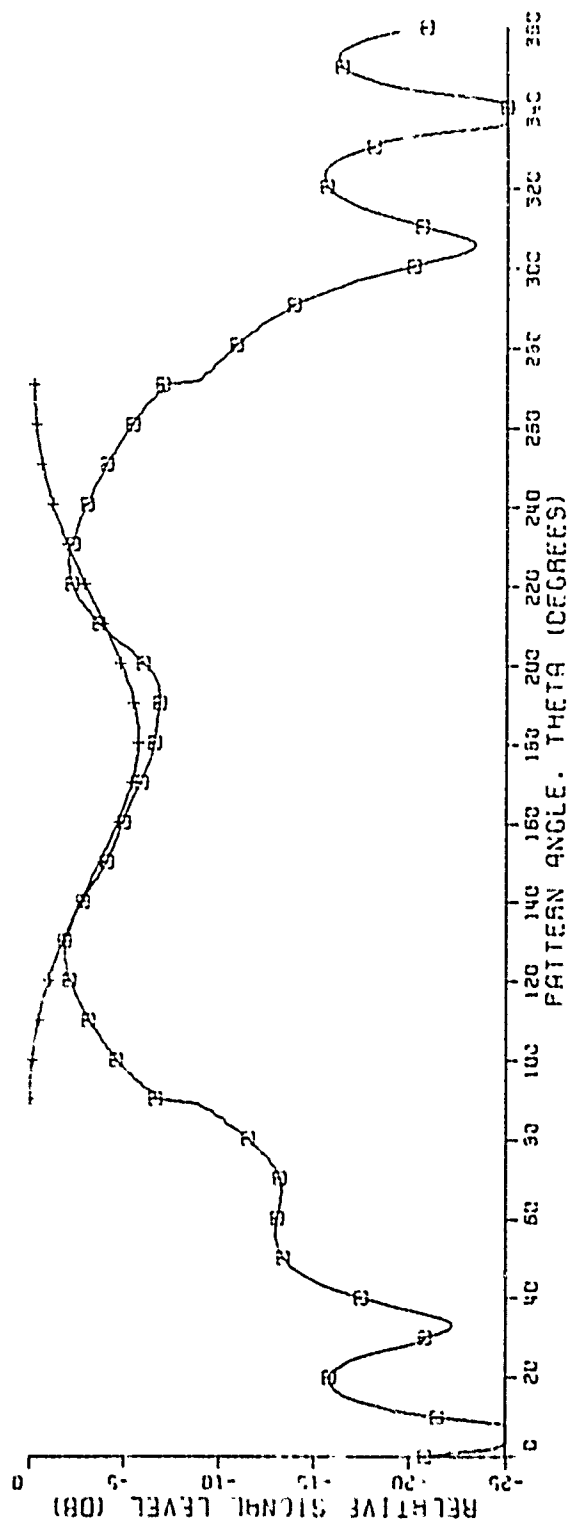
MONOPOLE LENGTH = 0.25 WAVELENGTHS

FREQUENCY = 900.0 MHZ

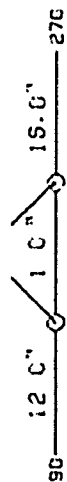
FIELD INCLUDING EDGE DIFFRACTION

+ FIELD FROM CNT. ON INFINITE GROUND PLANE

Fig. I-2b.



150



ANGLE OF ELEMENTS=30.0 DEGREES

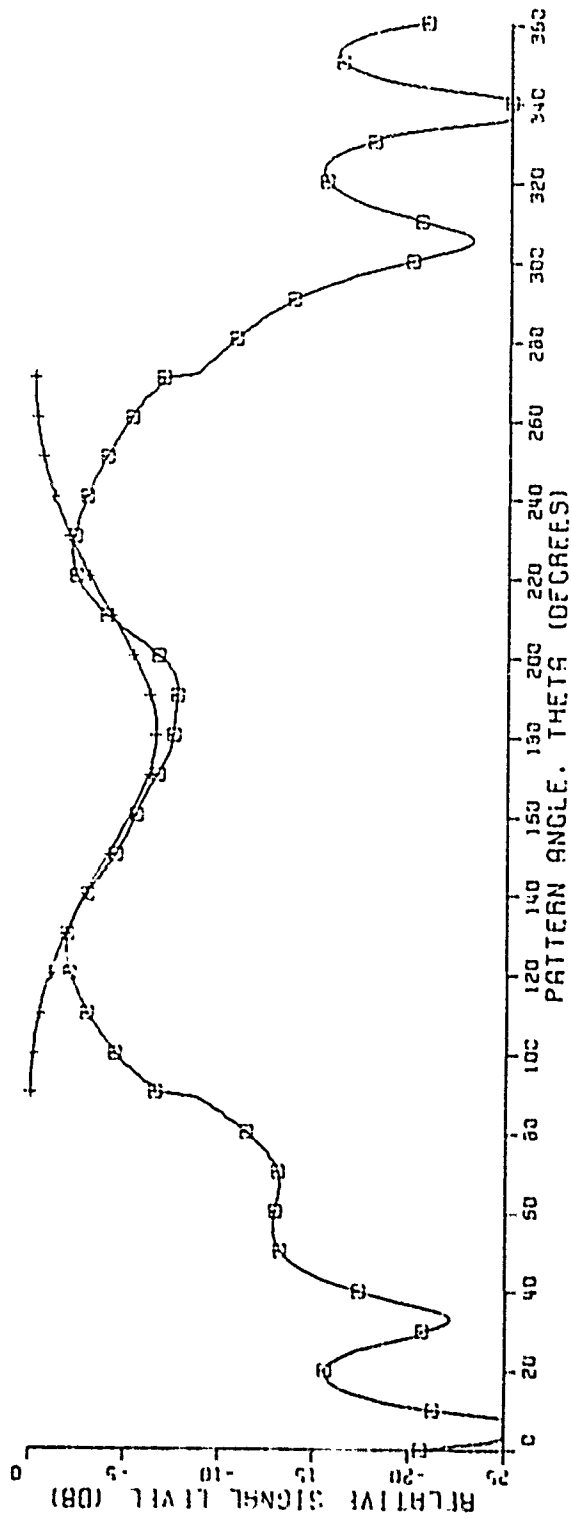
MONOPOLE LENGTH=0.25 WAVELENGTHS

FREQUENCY=900.0 MHZ

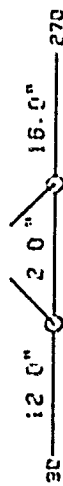
± FIELD INCLUDING EDGE DIFFRACTION

+ FIELD FROM ANT. ON INFINITE GROUND PLANE

Fig. I-2c.



180



ANGLE OF ELEMENTS=30.0 DEGREES

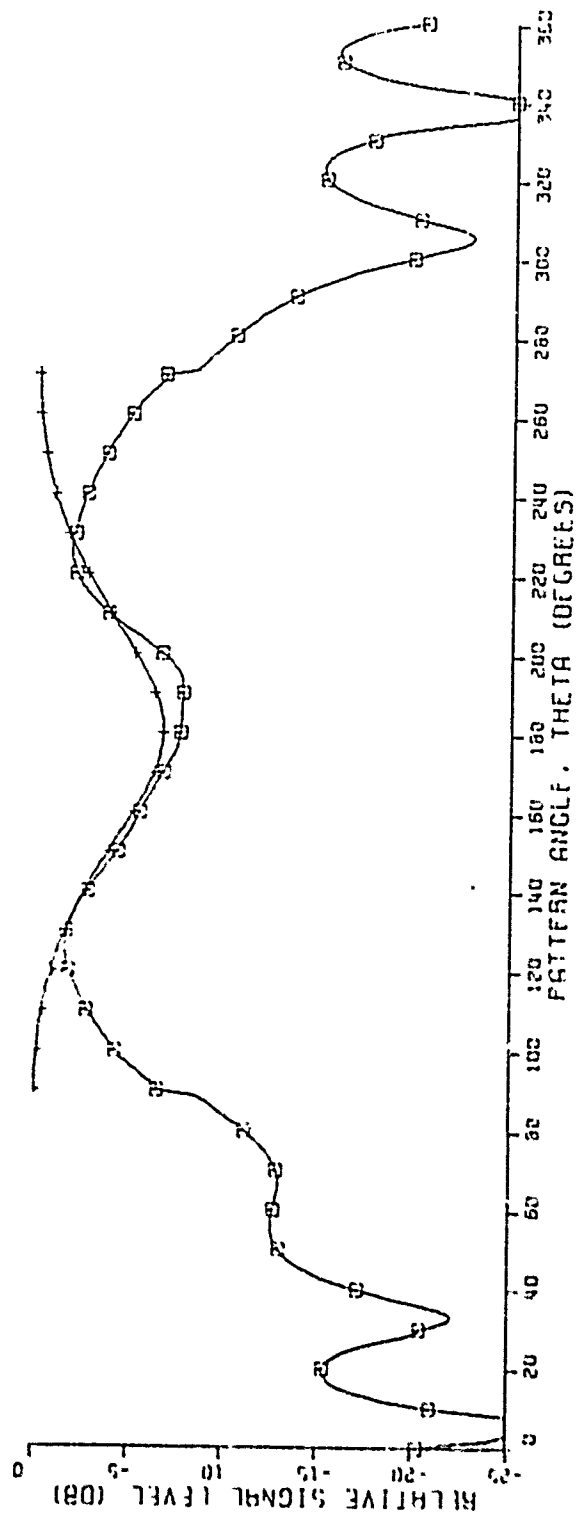
MONOPOLE LENGTH=0.25 WAVELENGTHS

FREQUENCY=300.3 MHZ

FIELD INCLUDING EDGE DIFFRACTION

+ FIELD FROM ANT. ON INFINITE GROUND PLANE

Fig. I-2d.



180

90 — .2 0" — 3 3" — 15.0" — 270

MONOPOLE LENGTH = 0.25 WAVELENGTHS

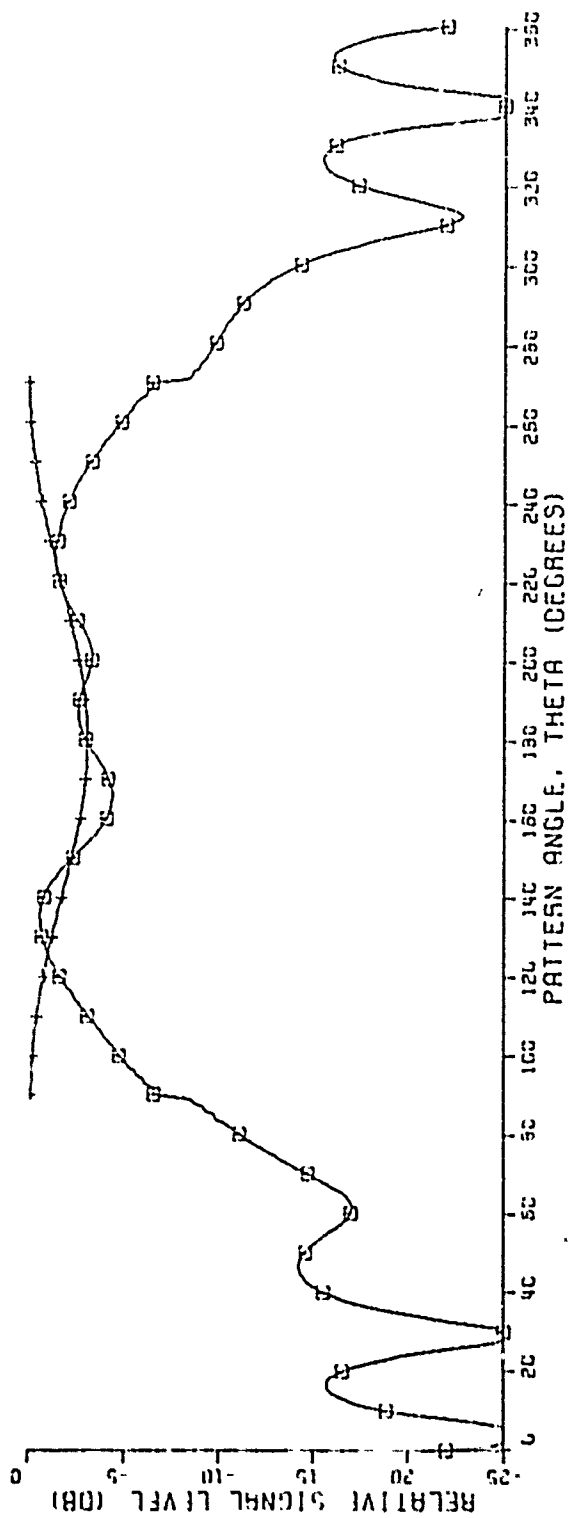
FREQUENCY = 301.0 MHZ

W FIELD INCLUDING FOC OF DIFFRACTION

+ FIELD FROM ANT. ON INFINITE GROUND PLANE

ANGLE OF ELEMENTS = 30.6 DEGREES

Fig. I-2e.



120

12 0" C. 2" 16.0" 270 ANGLE OF ELEMENTS=30.0 DEGREES

MONOPOLE LENGTH=0.28 WAVELENGTHS

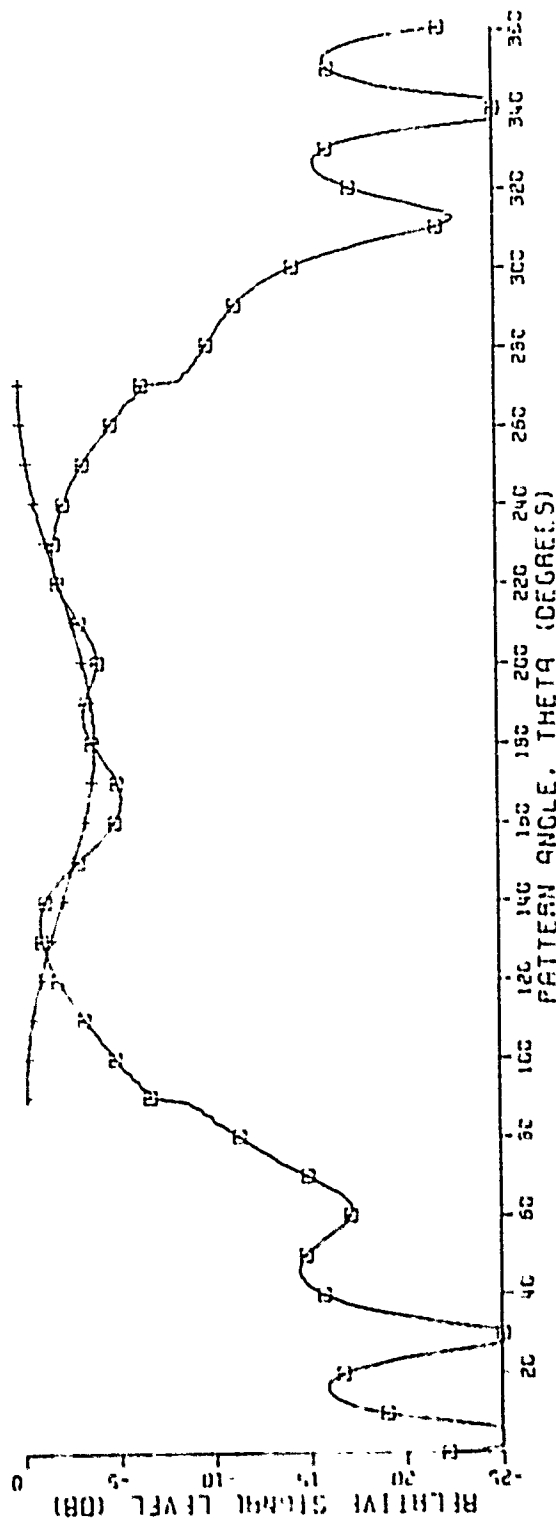
FREQUENCY=1000.0 MHZ

2 FIELD INCLUDING EDGE DIFFRACTION

+ FIELD FROM ANT. ON INFINITE GROUND PLANE

Fig. I-3a.





192

12 0" 0.5" 18.0" 270 ANGLE OF ELEMENTS=30.0 DEGREES

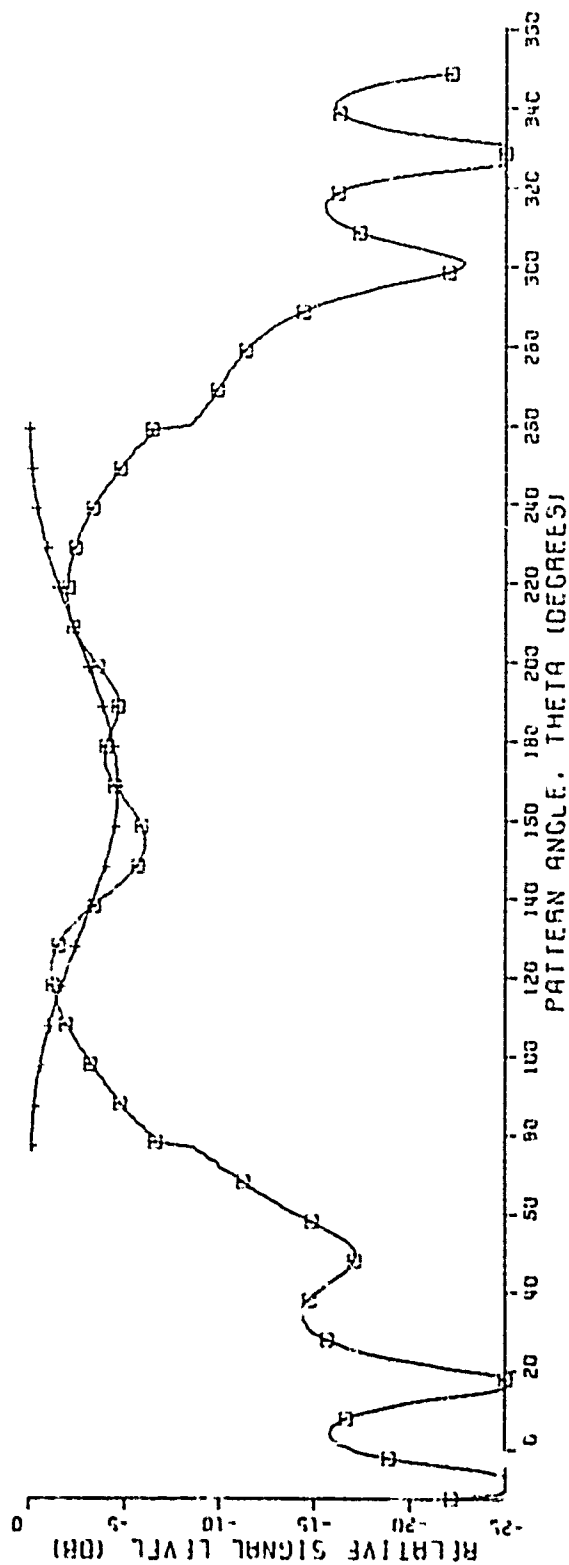
MONOPOLE LENGTH=0.25 WAVELENGTHS

FREQUENCY=1000.0 MHZ

± FIELD INCLUDING EDGE DIFFRACTION

+ FIELD FROM ANT. ON INFINITE GROUND PLANE

Fig. I-3b.



150

2.0" 1.0" 15.0" 270

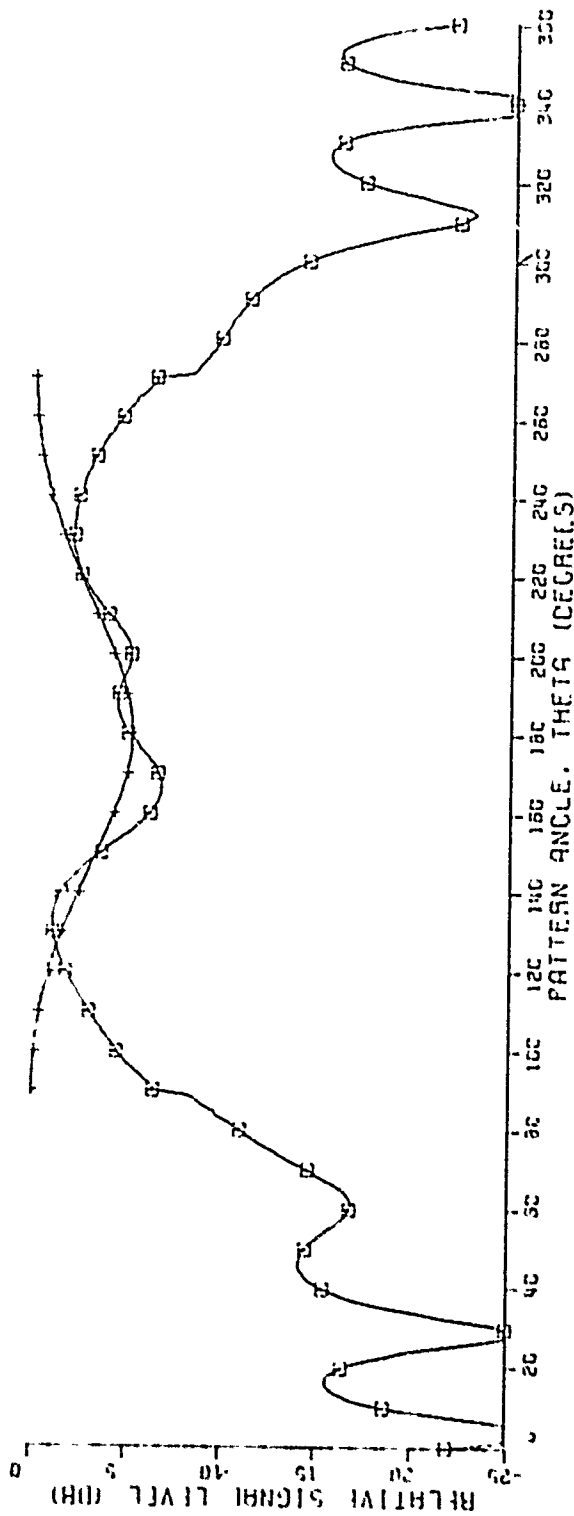
MONOPOLE LENGTH=0.23 WAVELENGTHS

FREQUENCY=1000.0 MHZ

FIELD INCLUDING EDGE DIFFRACTION

— FIELD FROM ANT. ON INFINITE GROUND PLANE

Fig. I-3c.



150

30 12 0" 2 0" 15.0" 270 ANGLE OF ELEMENTS=30.0 DEGREES

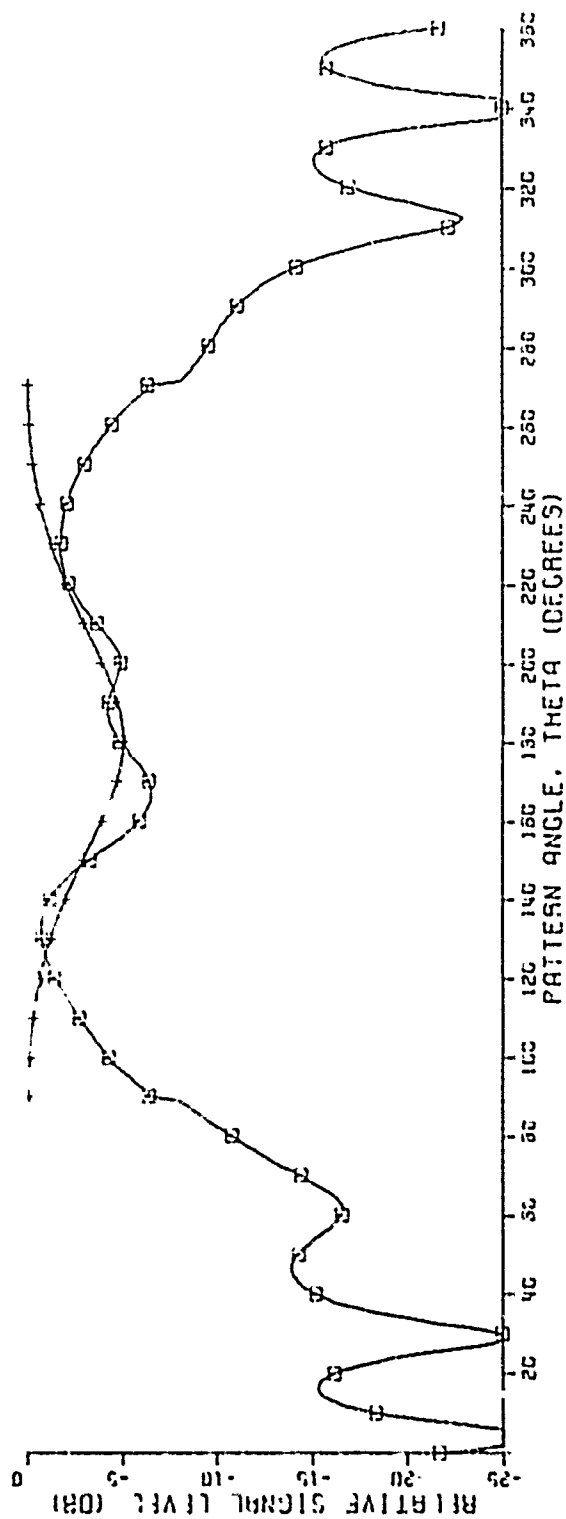
MONOPOLE LENGTH=0.28 WAVELENGTHS

FREQUENCY=1000.0 MHZ

FIELD INCLUDING EDGE DIFFRACTION

+ FIELD FROM ANT. ON INFINITE GROUND PLANE

Fig. I-3d.



180

90 12.0" 3 3" 15.0" 270 ANGLE OF ELEMENTS=30.0 DEGREES

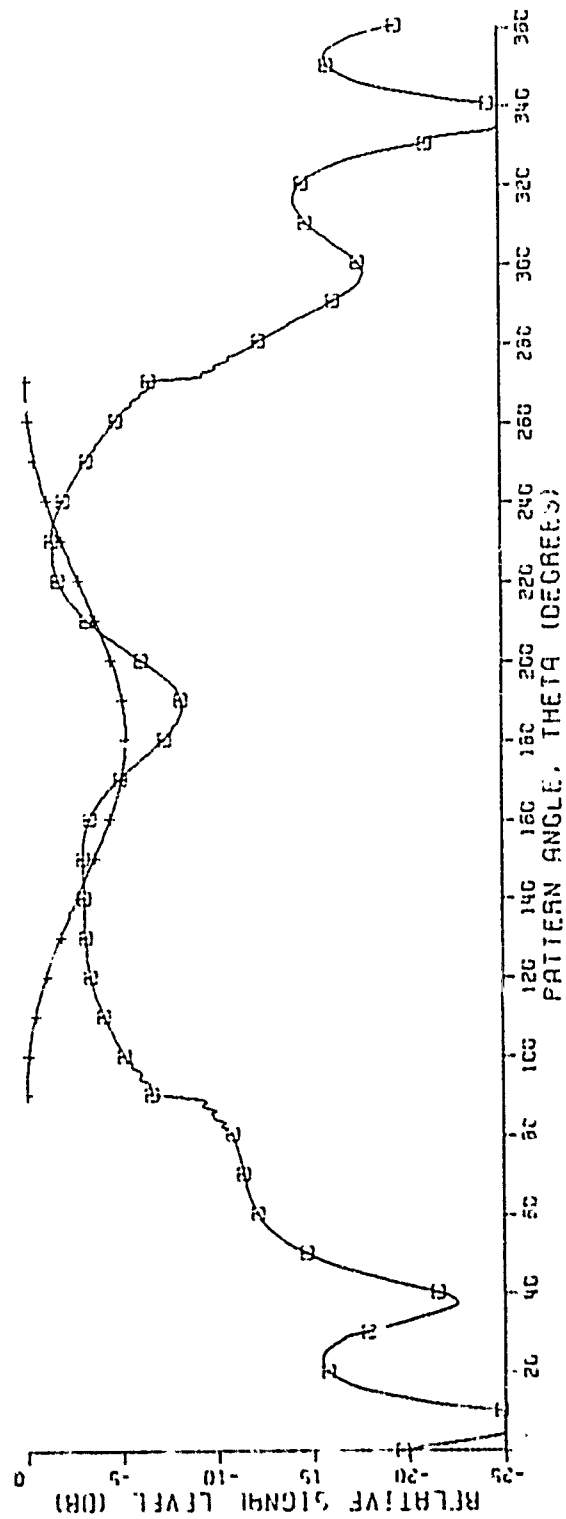
MONOPOLE LENGTH=0.28 WAVELENGTHS

FREQUENCY=1000.0 MHZ

□ FIELD INCLUDING EDGE DIFFRACTION

+ FIELD FROM ANT. ON INFINITE GROUND PLANE

Fig. I-3e.



180

30 12.0" 0.2" 15.0" 270

ANGLE OF ELEMENTS=45.0 DEGREES

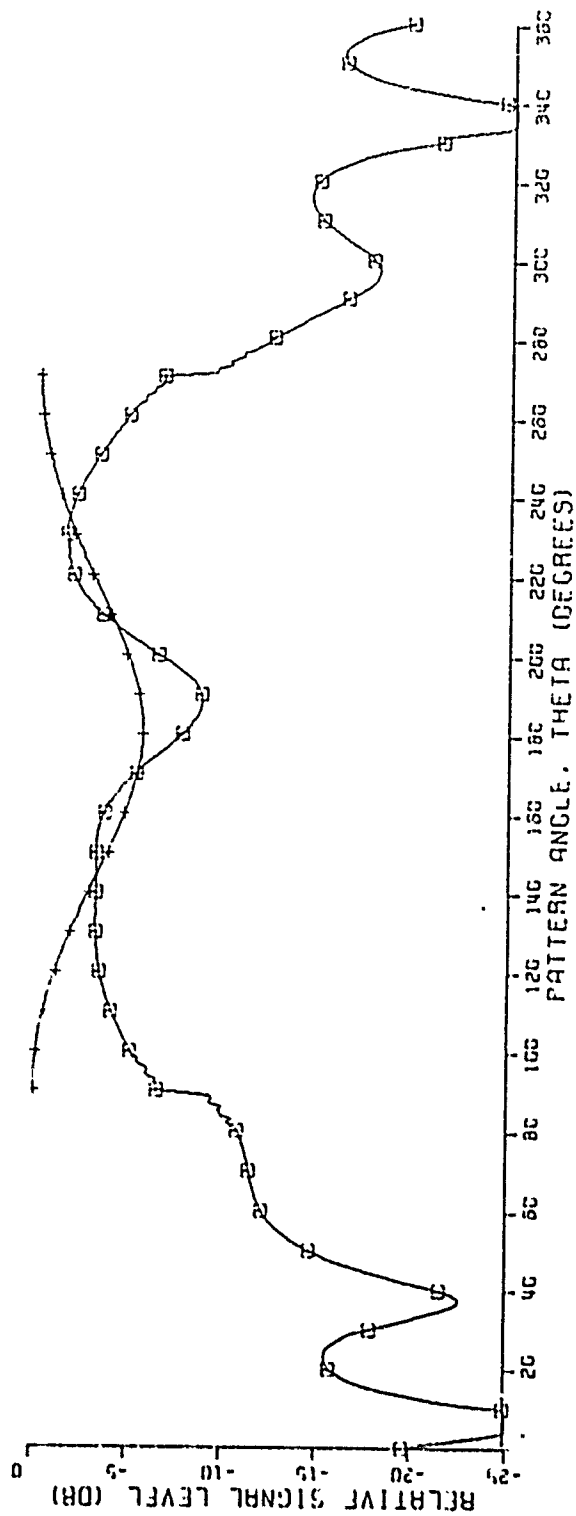
MONOPOLE LENGTH=0.22 WAVELENGTHS

FREQUENCY=800.0 MHZ

FIELD INCLUDING EDGE DIFFRACTION

+ FIELD FROM ANT. ON INFINITE GROUND PLANE

Fig. I-4a.



180  
 90 12.0" 0.3" 15.0" 270  
 ANGLE OF ELEMENTS=45.0 DEGREES

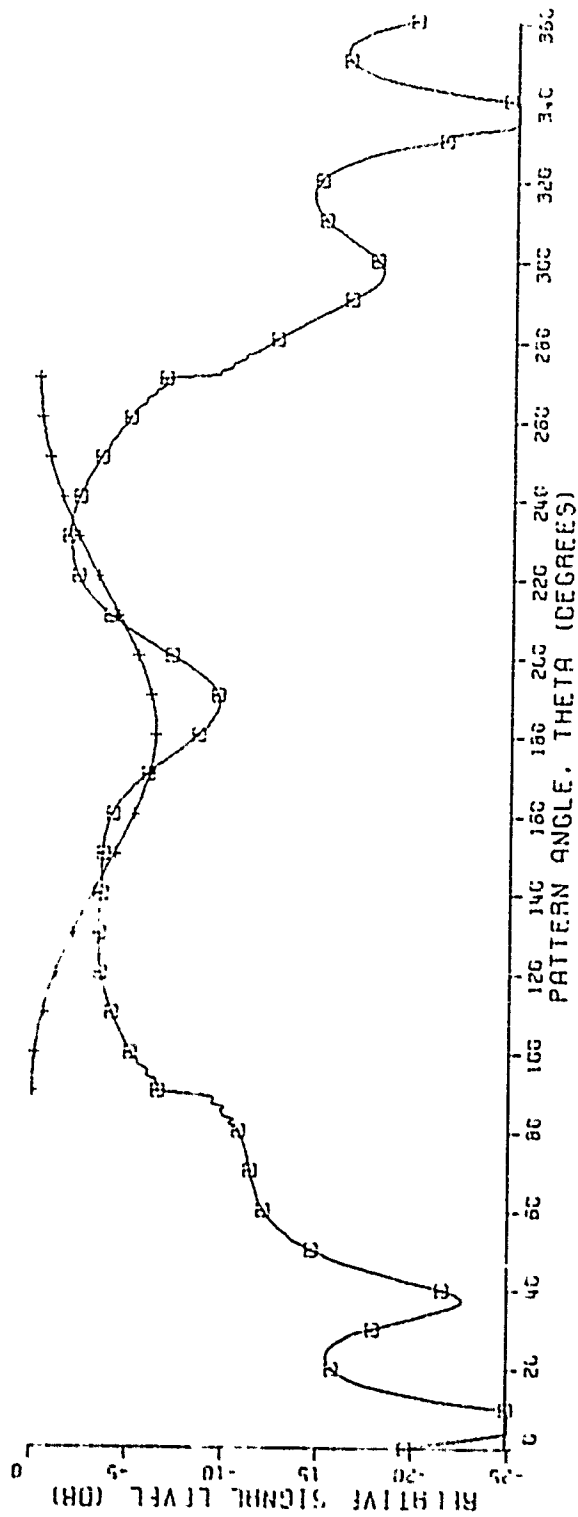
MONOPOLE LENGTH=0.22 WAVELENGTHS

FREQUENCY=800.0 MHZ

○ FIELD INCLUDING EDGE DIFFRACTION

+ FIELD FROM ANT. ON INFINITE GROUND PLANE

Fig. I-4b.



13C



ANGLE OF ELEMENTS=45.0 DEGREES

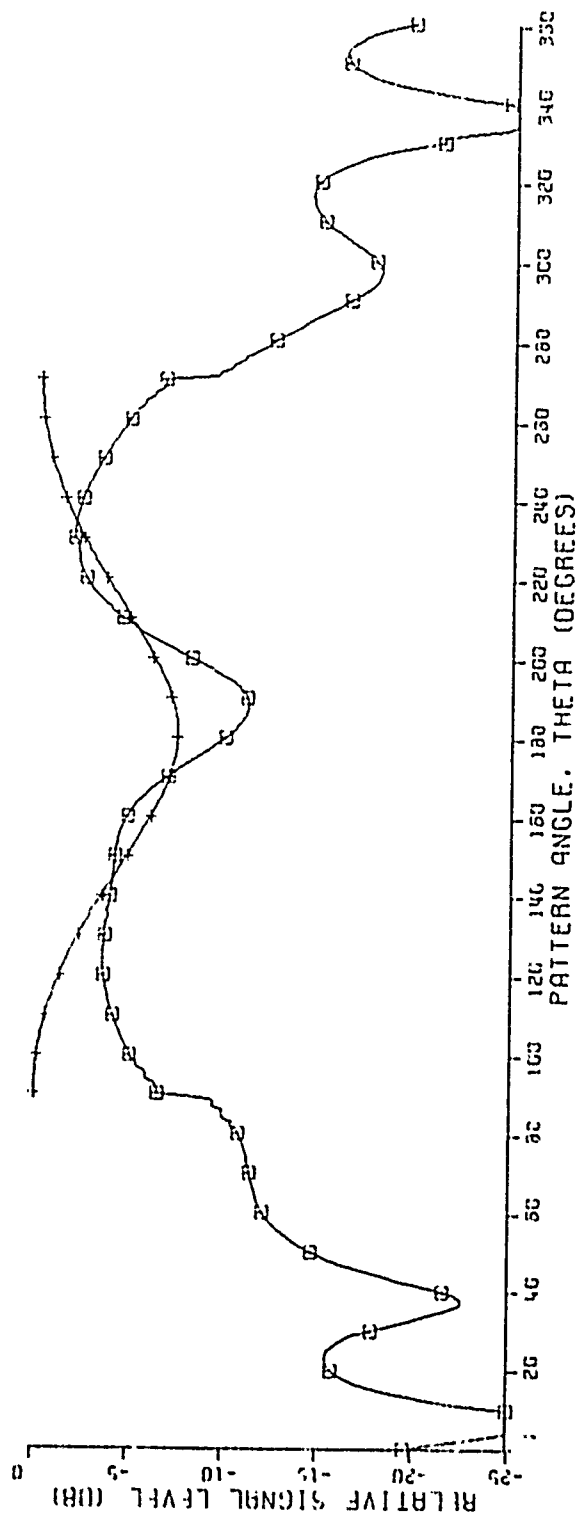
MONOPOLE LENGTH=0.22 WAVELENGTHS

FREQUENCY=900.0 MHZ

FIELD INCLUDING EDGE DIFFRACTION

+ FIELD FROM ANT. ON INFINITE GROUND PLANE

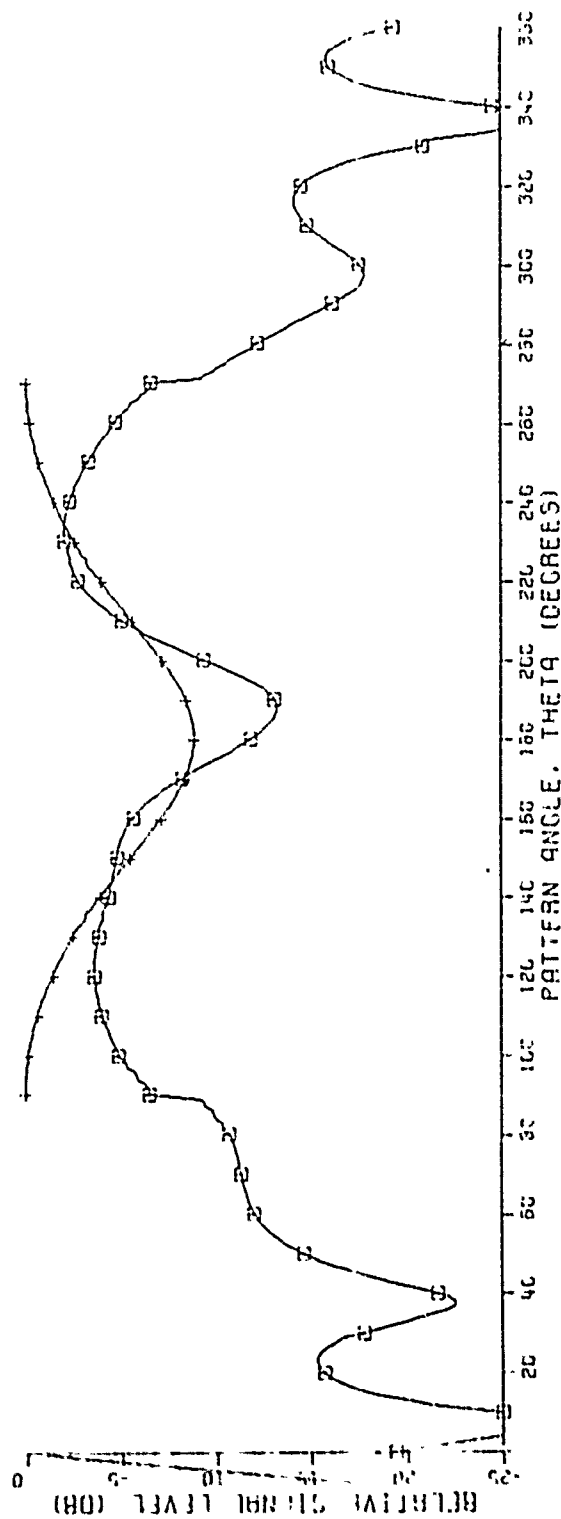
Fig. I-4c.



180  
 90 12 0" 1 0" 16.0" 270 ANGLE OF ELEMENTS=45.0 DEGREES  
 MONOPOLE LENGTH=C.22 WAVELENGTHS  
 FREQUENCY=800.0 MHZ  
 O FIELD INCLUDING EDGE DIFFRACTION  
 + FIELD FROM ANT. ON INFINITE GROUND PLANE

Fig. I-4d.





180

90 12.0" 2.0" 16.0" 270

ANGLE OF ELEMENTS = 45.0 DEGREES

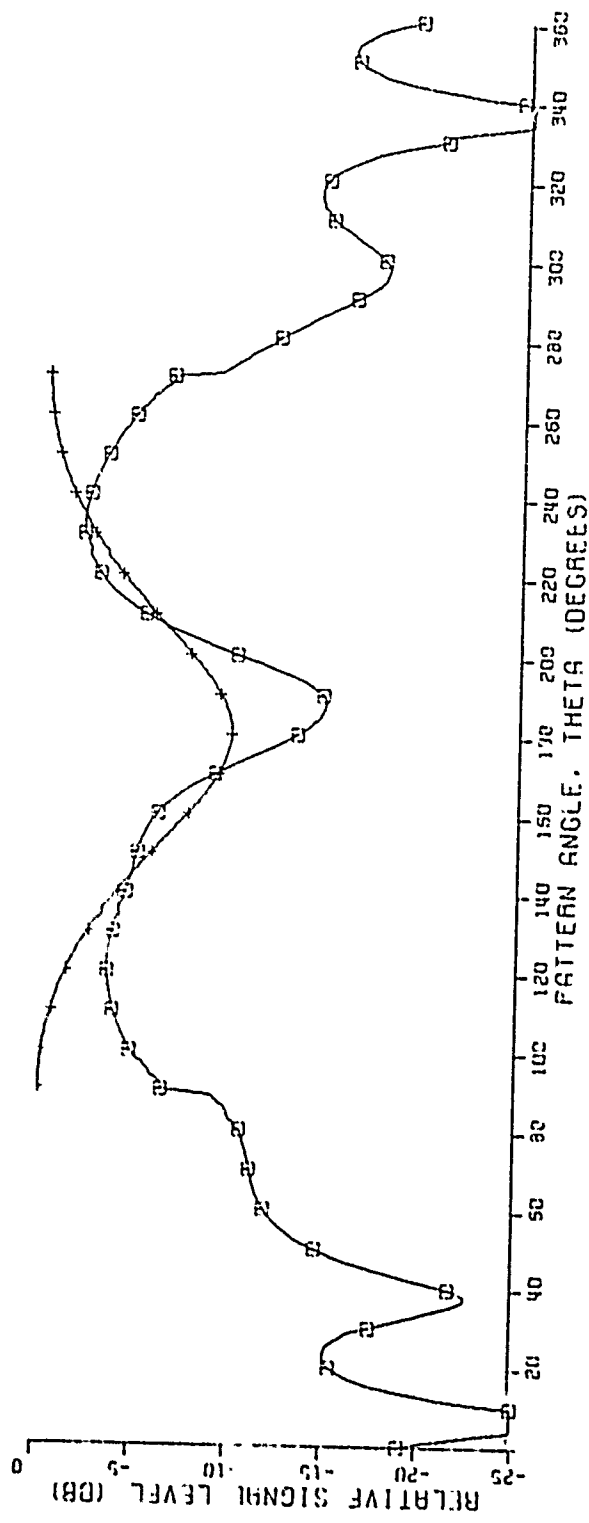
MONOPOLE LENGTH = 0.22 WAVELENGTHS

FREQUENCY = 900.0 MHZ

FIELD INCLUDING EDGE DIFFRACTION

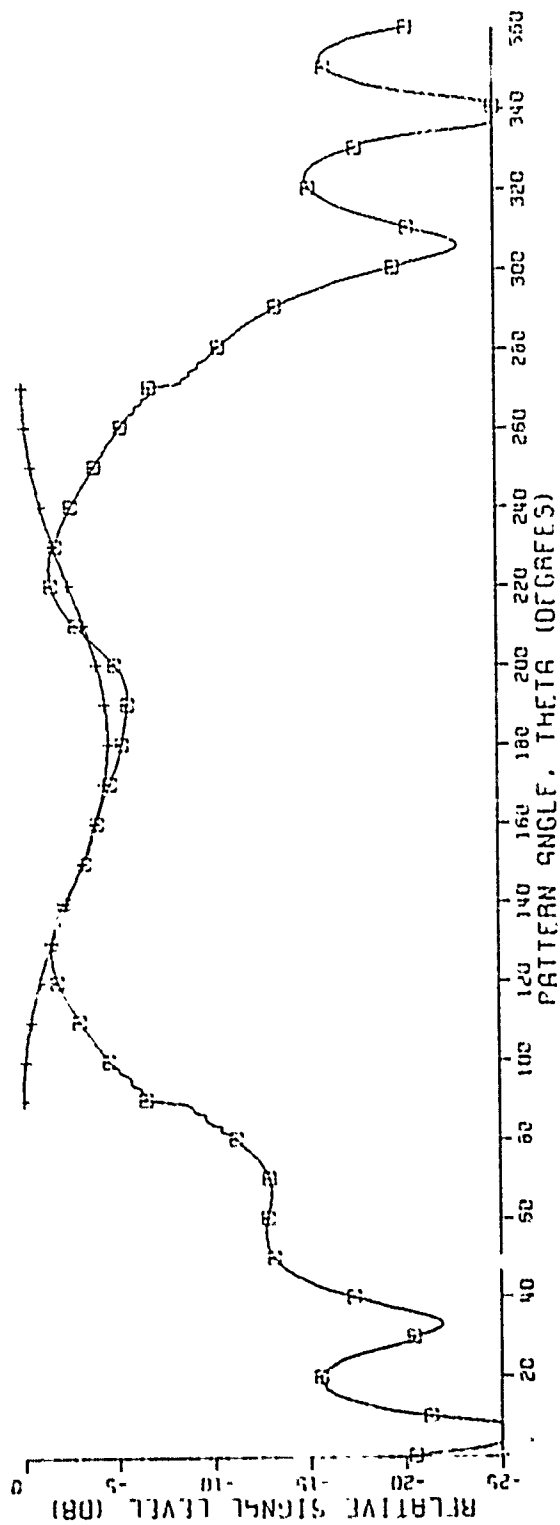
+ FIELD FROM ANT. ON INFINITE GROUND PLANE

Fig. I-4e.



180  
 12.0" 3 3" 16.0" 270  
 ANGLE OF ELEMENTS=45.0 DEGREES  
 MONOPOLE LENGTH=0.22 WAVELENGTHS  
 FREQUENCY=800.0 MHZ  
 □ FIELD INCLUDING EDGE DIFFRACTION  
 + FIELD FROM ANT. ON INFINITE GROUND PLANE

Fig. I-4f.



190

90

12.0"

0 2"

15.0"

270

ANGLE OF ELEMENTS=45.0 DEGREES

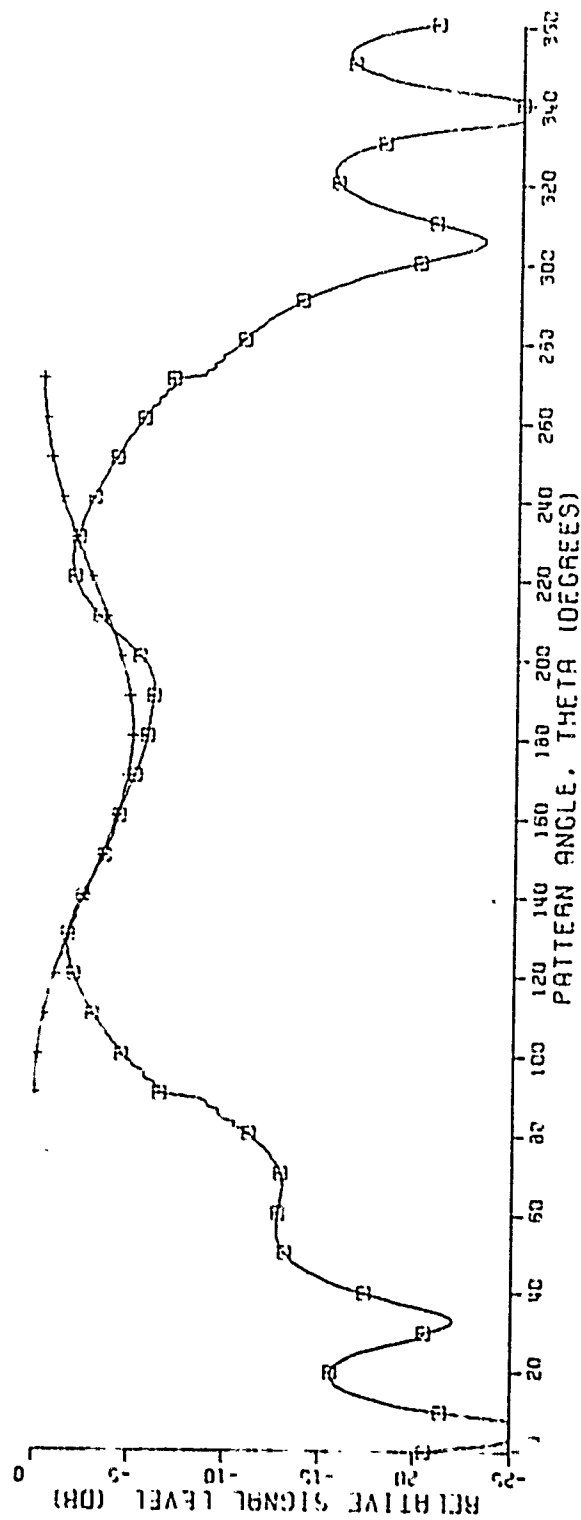
MONOPOLE LENGTH=0.25 WAVELENGTHS

FREQUENCY=900.0 MHz

W FIELD INCLUDING EDGE DIFFRACTION

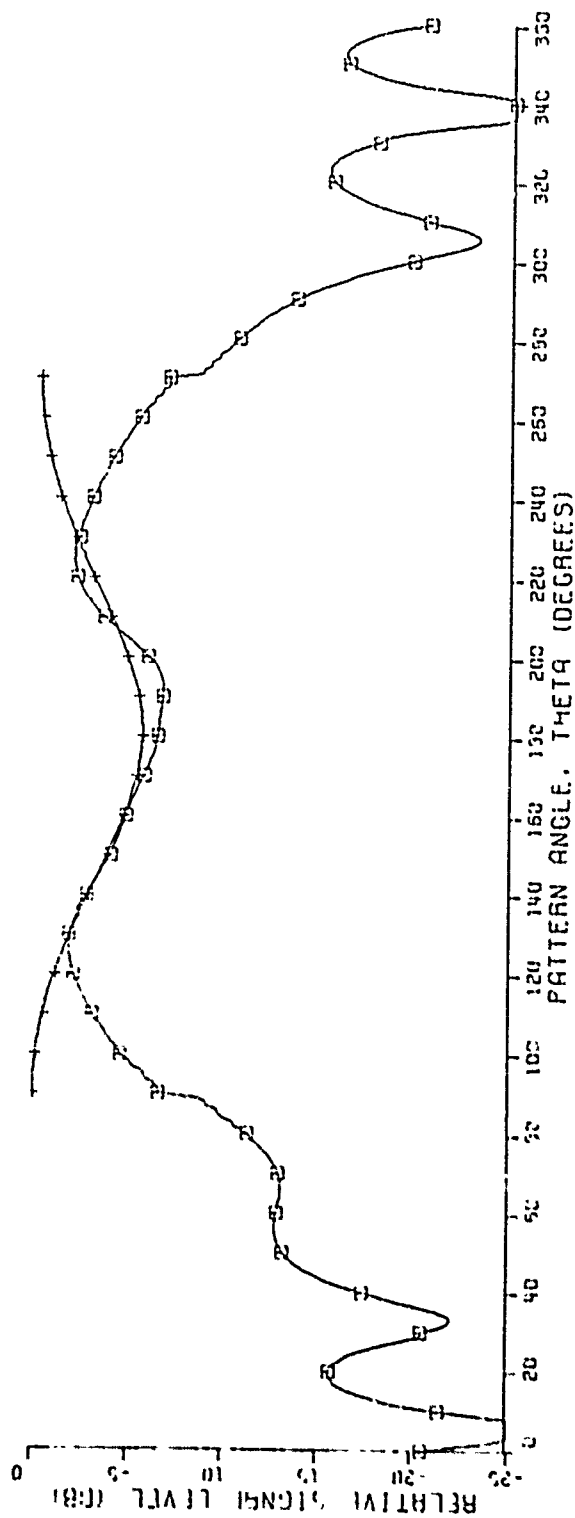
+ FIELD FROM ANT. ON INFINITE GROUND PLANE

Fig. I-5a.



150  
 90 12.0" 0 3" 15.0" 270  
 MONOPOLE LENGTH=0.25 WAVELENGTHS  
 FREQUENCY=900.0 MHZ  
 + FIELD INCLUDING EDGE DIFFRACTION  
 + FIELD FROM ANT. ON INFINITE GROUND PLANE

Fig. I-5b.



192

30° 12 0" 15 0" 270° ANGLE OF ELEMENTS=45.0 DEGREES

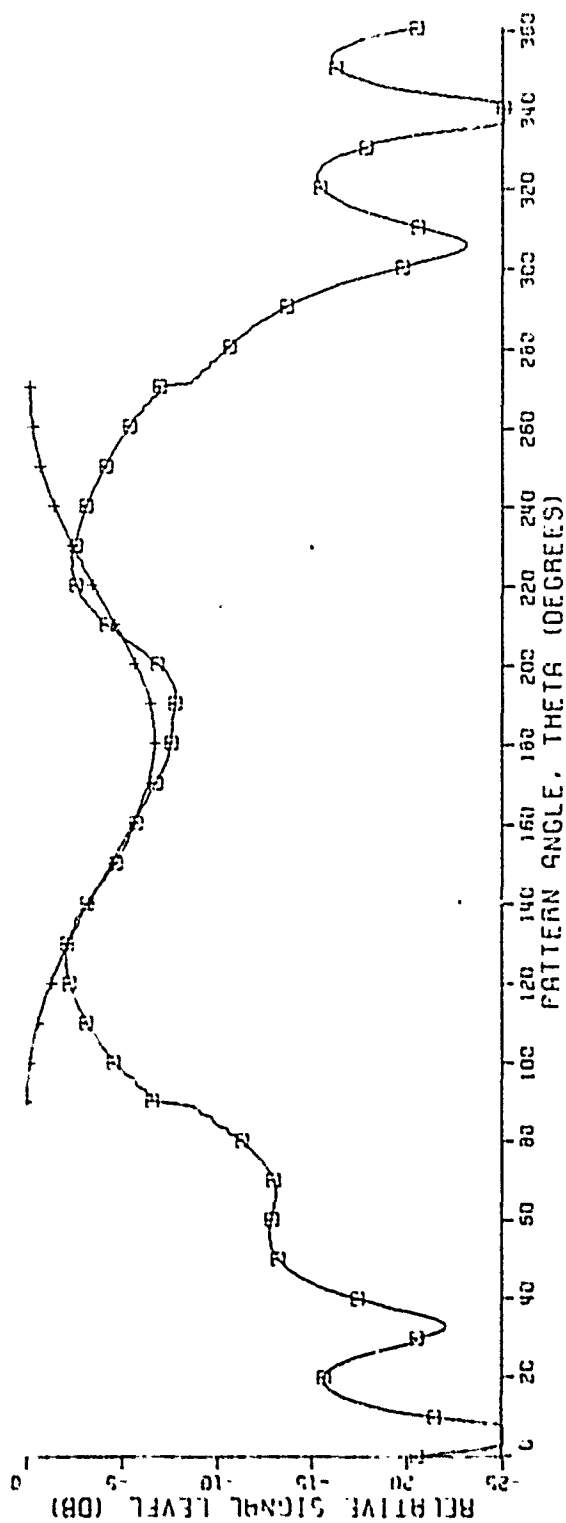
MONOPOLE LENGTH=0.25 WAVELENGTHS

FREQUENCY=300.0 MHZ

W FIELD INCLUDING EDGE DIFFRACTION

+ FIELD FROM ANT. ON INFINITE GROUND PLANE

Fig. I-5c.



160

90 12.0" 1 0" 16.0" 270 ANGLE OF ELEMENTS=45.0 DEGREES

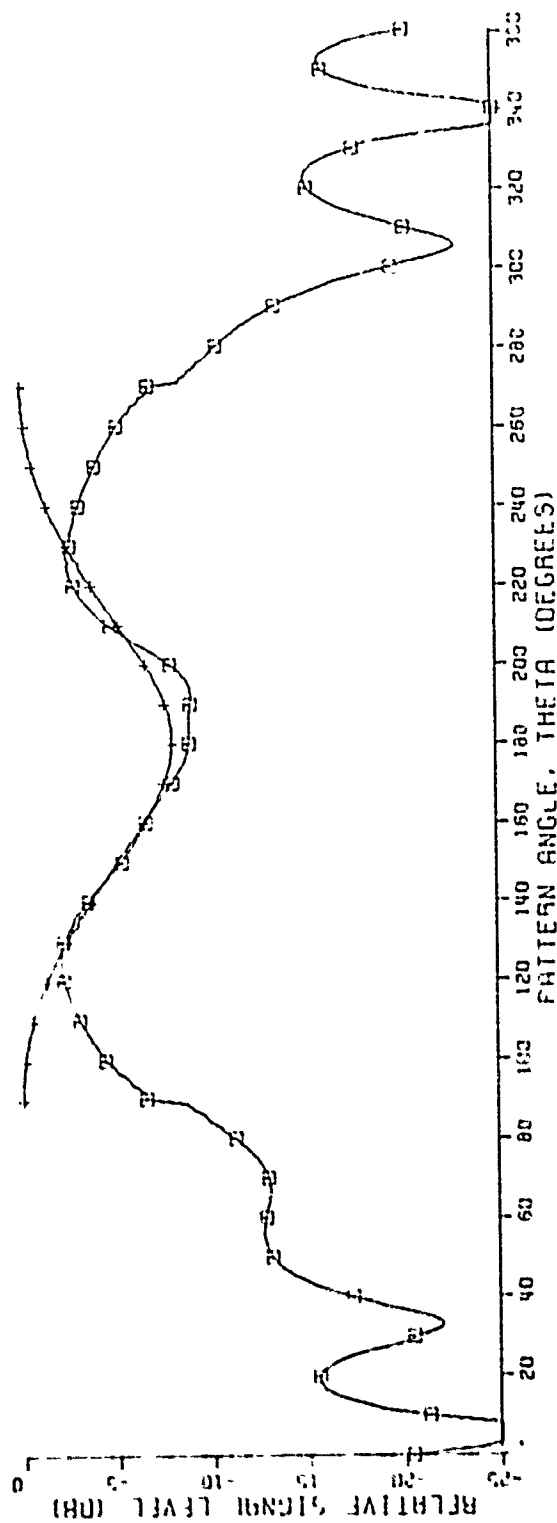
MONOPOLE LENGTH=0.25 WAVELENGTHS

FREQUENCY=900.0 MHZ

W FIELD INCLUDING EDGE DIFFRACTION

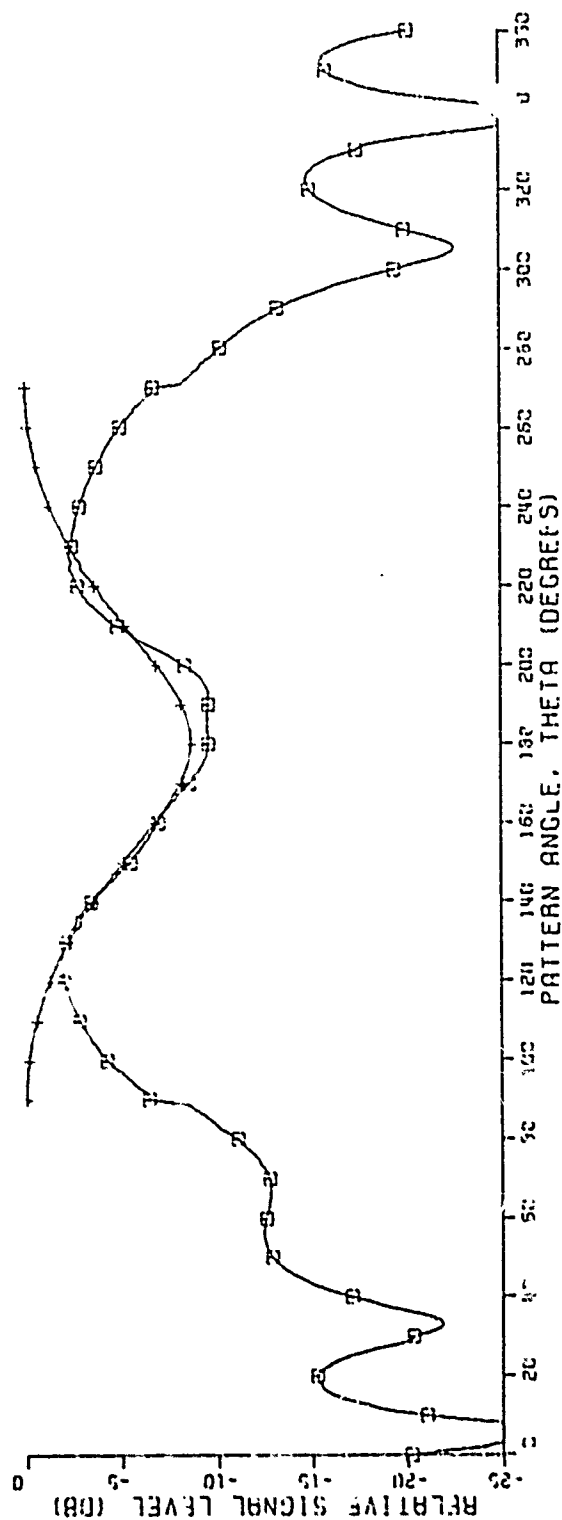
+ FIELD FROM ANT. ON INFINITE GROUND PLANE

Fig. I-5d.



160  
 90 12 0" 2.0" 16.0" 270  
 ANGLE OF ELEMENTS=45.0 DEGREES  
 MONOPOL LENGTH=0.25 WAVELENGTHS  
 FREQUENCY=900.0 MHZ  
 E FIELD INCLUDING EDGE DIFFRACTION  
 + FIELD FROM ANT. ON INFINITE GROUND PLANE

Fig. I-5e.



190

90 120° 3 3" 16.0" 270

ANGLE OF ELEMENTS=45.0 DEGREES

MONOPOLE LENGTH=0.25 WAVELENGTHS

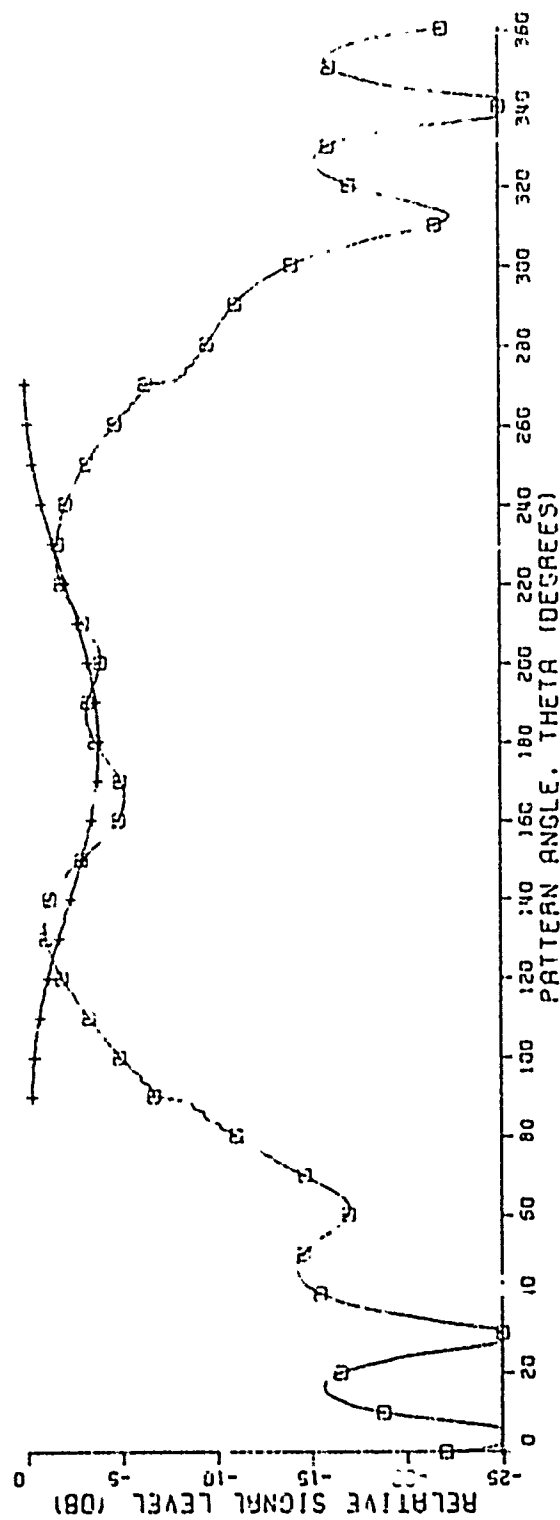
FREQUENCY=300.0 MHZ

Ø FIELD INCLUDING EDGE DIFFRACTION

+ FIELD FROM ANT. ON INFINITE GROUND PLANE

Fig. I-5f.





130

50---12.0" 0.2" 16.0" 270

ANGLE OF ELEMENTS=45.0 DEGREES

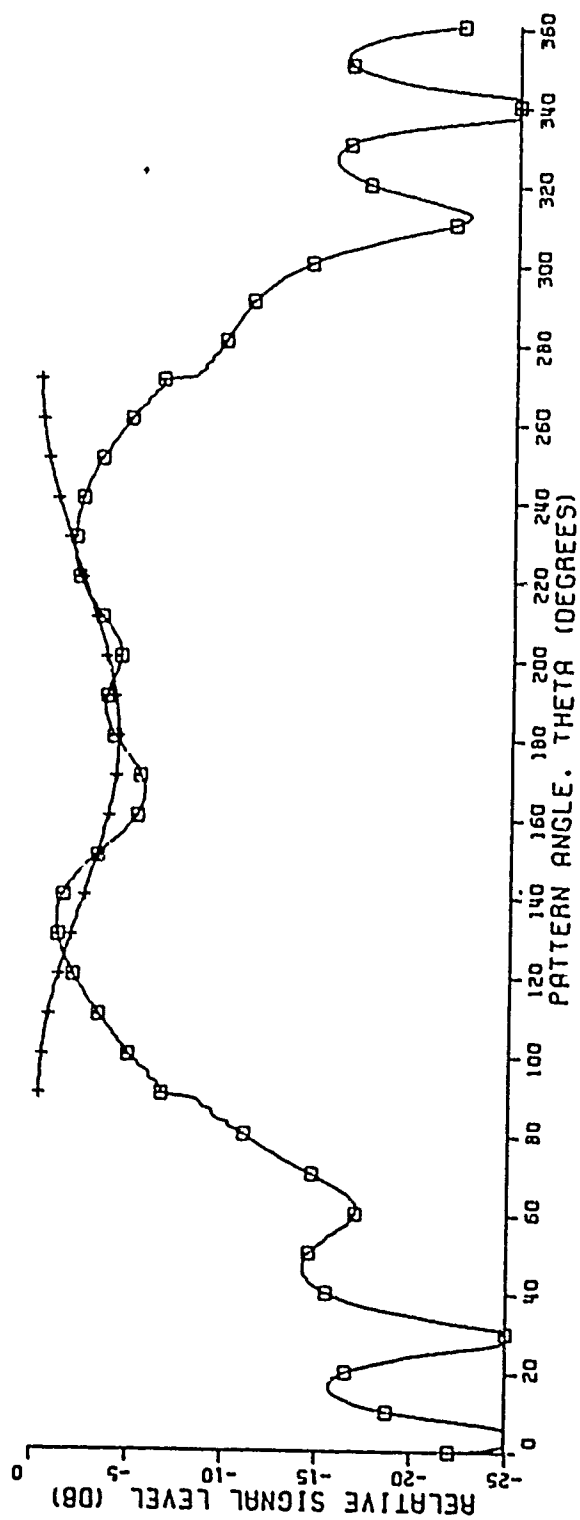
MONOPOLE LENGTH=0.28 WAVELENGTHS

FREQUENCY=1000.0 MHZ

0" FIELD INCLUDING EDGE DIFFRACTION

+ FIELD FROM ANT. ON INFINITE GROUND PLANE

Fig. 1-6a.



180  
 90 12.0" 0.3" 16.0" 270  
 ANGLE OF ELEMENTS=45.0 DEGREES

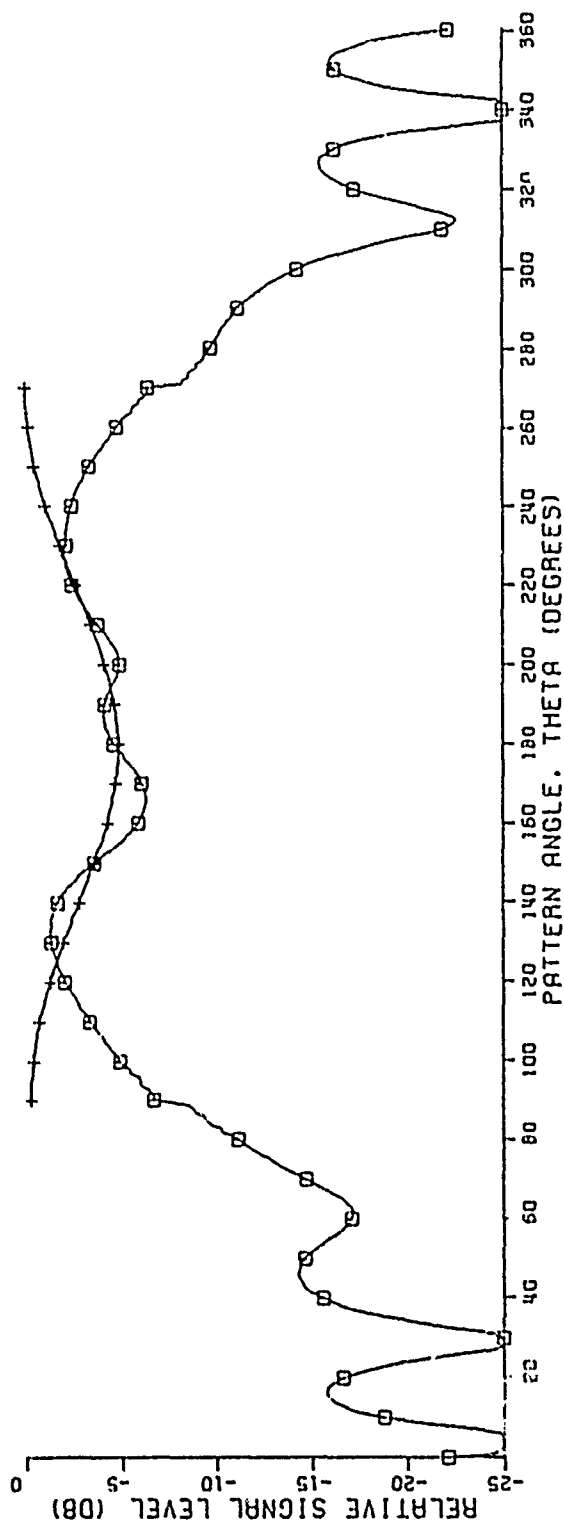
MONOPOLE LENGTH=0.28 WAVELENGTHS

FREQUENCY=1000.0 MHZ

□ FIELD INCLUDING EDGE DIFFRACTION

+ FIELD FROM ANT. ON INFINITE GROUND PLANE

Fig. 1-65.



100

90 12.0" 0.5" 16.0" 270

ANGLE OF ELEMENTS=45.0 DEGREES

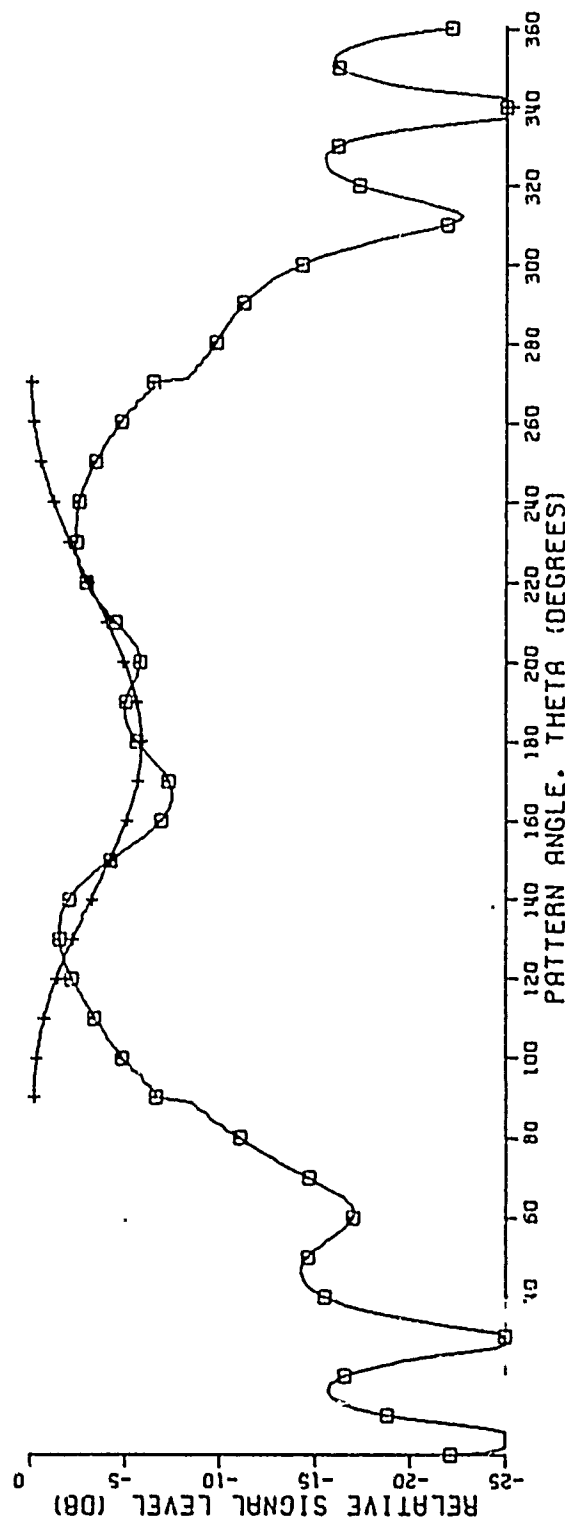
MONOPOLE LENGTH=0.28 WAVELENGTHS

FREQUENCY=1000.0 MHZ

Ø FIELD INCLUDING EDGE DIFFRACTION

+ FIELD FROM ANT. ON INFINITE GROUND PLANE

Fig. I-6c.



180

90 12.0" 1.0" 16.0" 270

ANGLE OF ELEMENTS=45.0 DEGREES

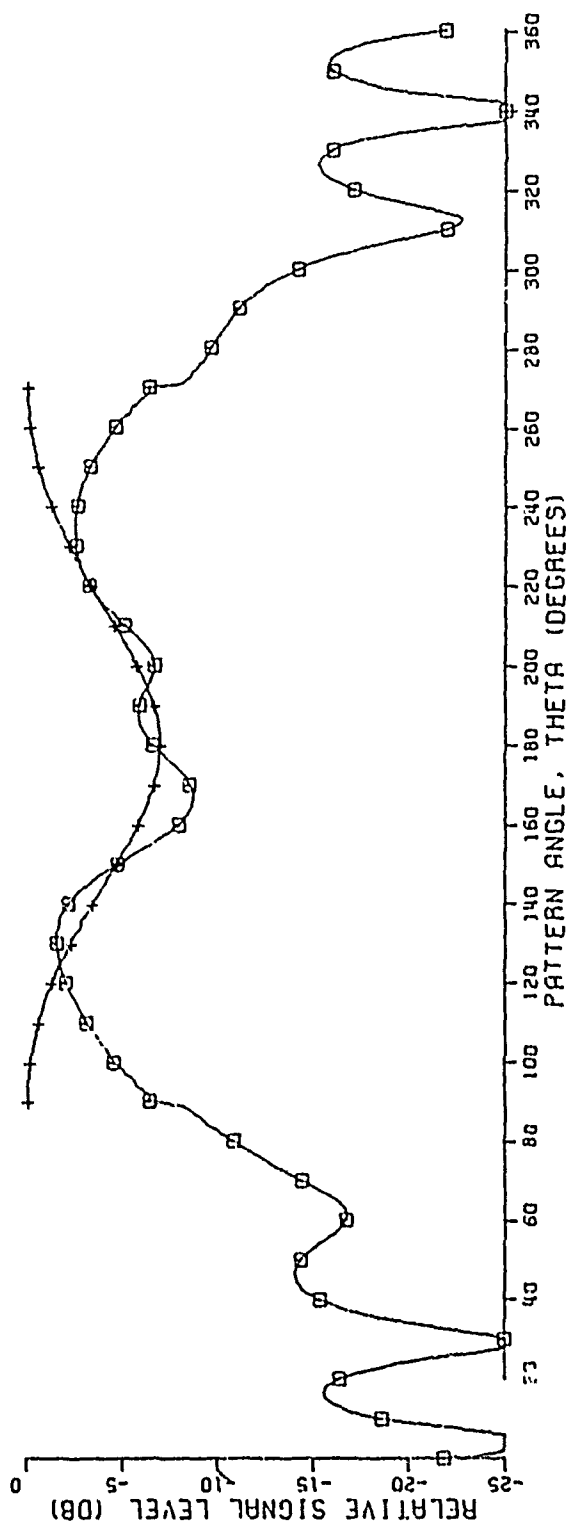
MONOPOLE LENGTH=0.28 WAVELENGTHS

FREQUENCY=1000.0 MHZ

○ FIELD INCLUDING EDGE DIFFRACTION

+ FIELD FROM ANT. ON INFINITE GROUND PLANE

Fig. I-6d.



180

90 12.0" 2.0" 15.0" 70

ANGLE OF ELEMENTS=45.0 DEGREES

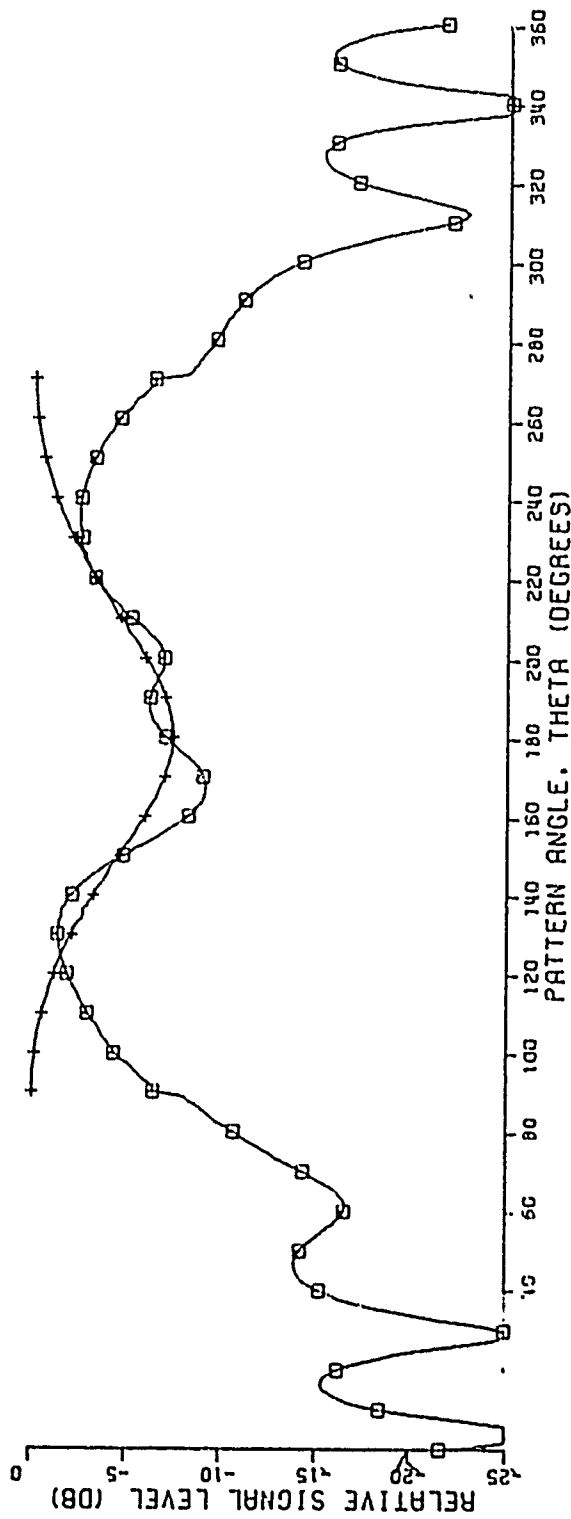
MONOPOLE LENGTH=0.28 WAVELENGTHS

FREQUENCY=1000.0 MHZ

□ FIELD INCLUDING EDGE DIFFRACTION

+ FIELD FROM ANT. ON INFINITE GROUND PLANE

Fig. I-6e.

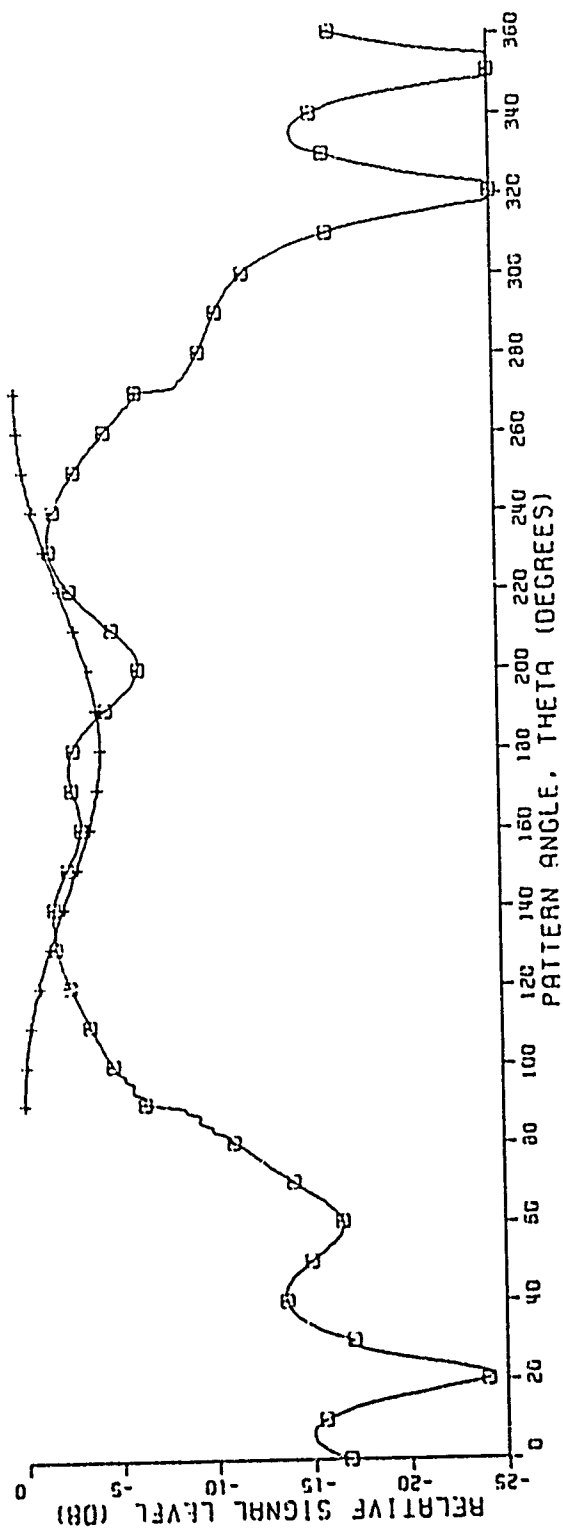


150  
 90 12.0" 3.3" 16.0" 270  
 ANGLE OF ELEMENTS=45.0 DEGREES  
 MONOPOLE LENGTH=0.28 WAVELENGTHS  
 FREQUENCY=1000.0 MHZ  
 □ FIELD INCLUDING EDGE DIFFRACTION  
 + FIELD FROM ANT. ON INFINITE GROUND PLANE

Fig. I-6f.

## APPENDIX II

The patterns contained in this appendix are those of a two monopole array with the array center located at 8 inches from one ground plane edge and 20 from the opposite edge. The angle of the monopoles with respect to the ground plane is 30 degrees. Figures II-1a-e are at 800 MHz while Figs. II-2a-d and Figs. II-3a-e are at 900 and 1000 MHz respectively.



180

90 8.0" 0.2" 20.0" 270

ANGLE OF ELEMENTS=30.0 DEGREES

MONOPOLE LENGTH=0.22 WAVELENGTHS

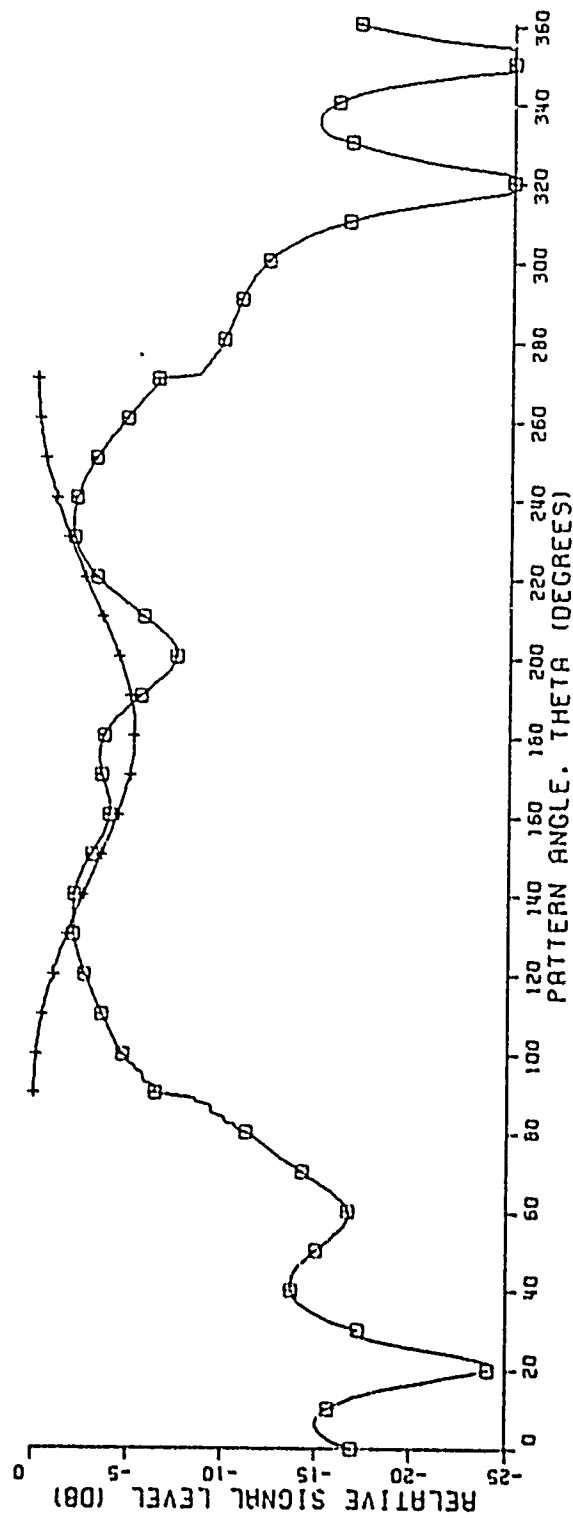
FREQUENCY=900.0 MHZ

○ FIELD INCLUDING EDGE DIFFRACTION

+ FIELD FROM ANT. ON INFINITE GROUND PLANE

Fig. II-1a.





150  
 8.0" 0.5" 20.0" 270  
 ANGLE OF ELEMENTS=30.0 DEGREES

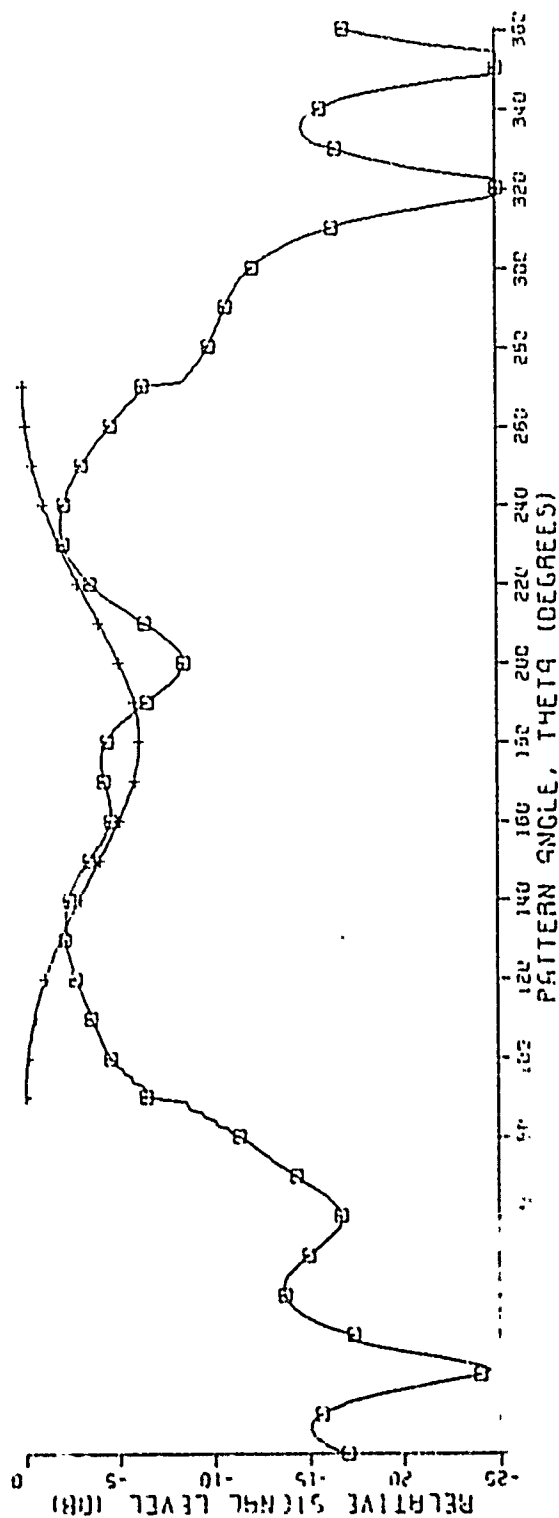
MONOPOLE LENGTH=0.22 WAVELENGTHS

FREQUENCY=800.0 MHZ

○ FIELD INCLUDING EDGE DIFFRACTION

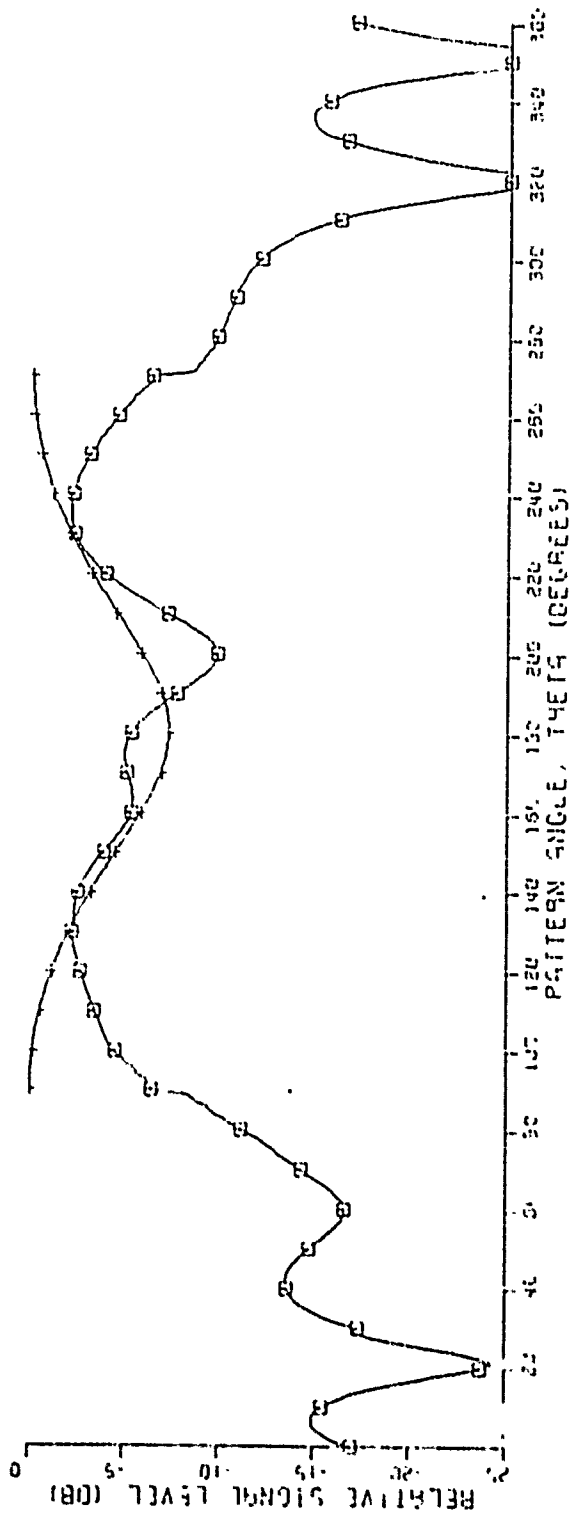
+ FIELD FROM ANT. ON INFINITE GROUND PLANE

Fig. II-1b.



150  
 90° 10° 20.0° 270° ANGLE OF ELEMENTS - 30.0 DEGREES  
 MONOPOLE LENGTH = 0.22 WAVELENGTHS  
 FREQUENCY = 900.0 MHz  
 E FIELD INCLUDING EDGE DIFFRACTION  
 + FIELD FROM ANT. ON INFINITE GROUND PLANE

Fig. II-1c.



150

90° 20.0° 270° ANGLE OF ELEMENTS - 30.0 DEGREES

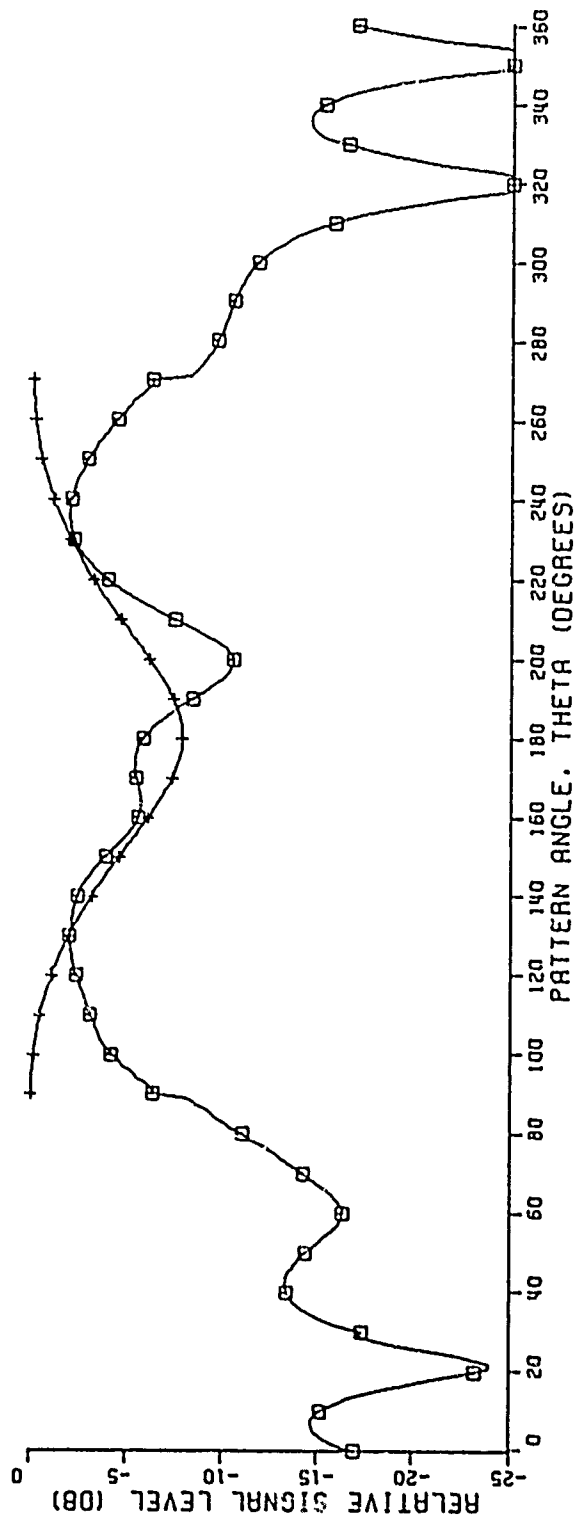
MONOPOLE LENGTH = 0.22 WAVELENGTHS

FREQUENCY = 500.0 MHZ

W FIELD INCLUDING EDGE DIFFRACTION

+ FIELD FROM ANT. ON INFINITE GROUND PLANE

Fig. II-1d.



180

90 8.0" 3.3" 20.0" 270

ANGLE OF ELEMENTS=30.0 DEGREES

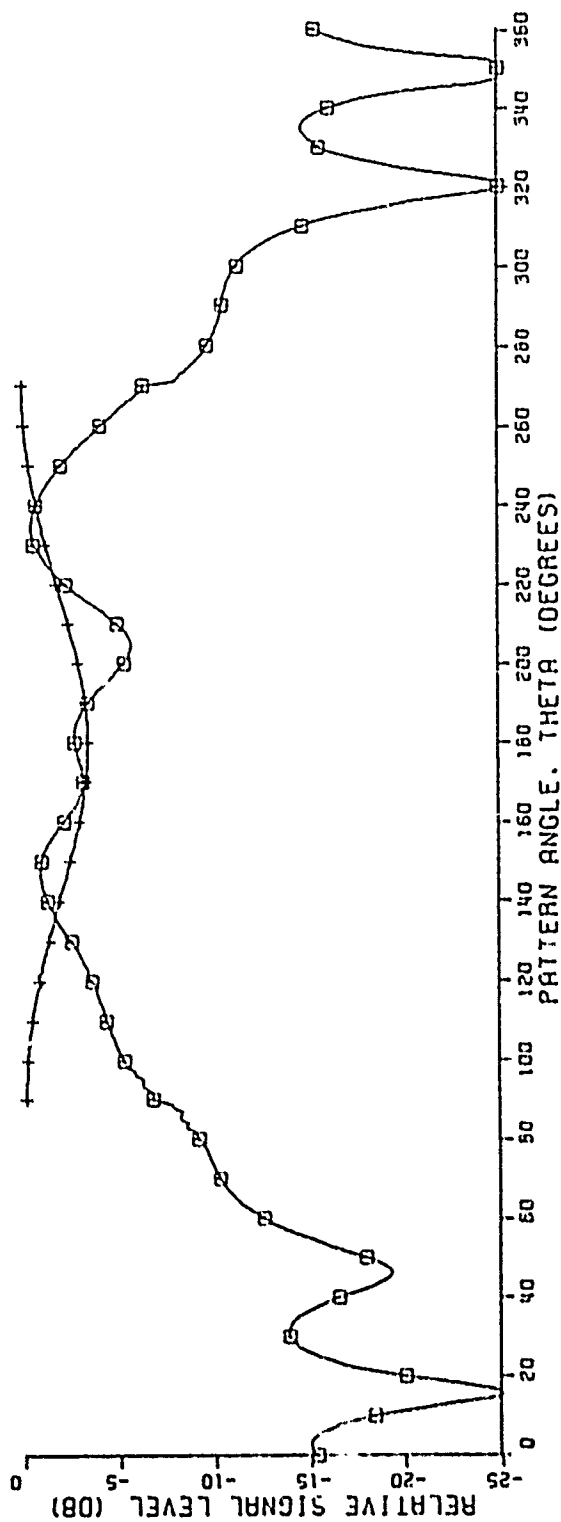
MONOPOLE LENGTH=0.22 WAVELENGTHS

FREQUENCY=800.0 MHZ

□ FIELD INCLUDING EDGE DIFFRACTION

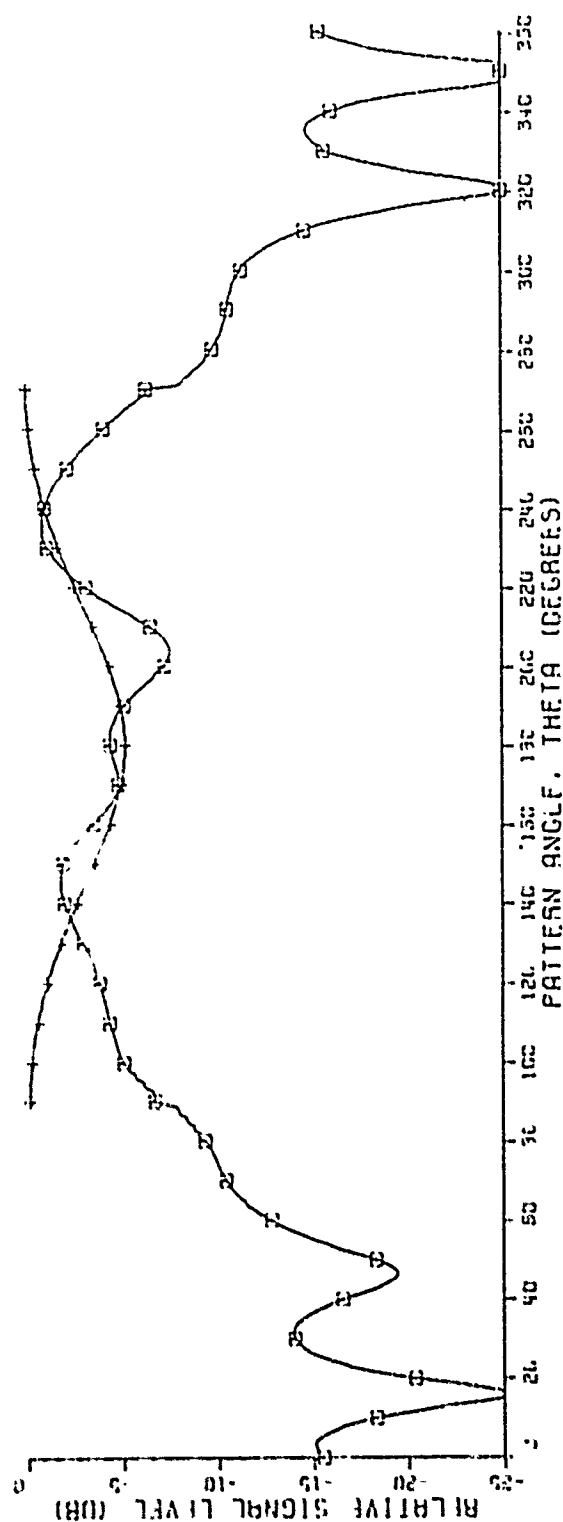
+ FIELD FROM ANT. ON INFINITE GROUND PLANE

Fig. II-1e.



180  
 90 8.0" 0.2" 20.0" 270  
 MONOPOLE LENGTH=0.25 WAVELENGTHS  
 FREQUENCY=900.0 MHZ  
 □ FIELD INCLUDING EDGE DIFFRACTION  
 + FIELD FROM ANT. ON INFINITE GROUND PLANE

Fig. II-2a.



180

90 20.0" 1.0" 20.0" 270 ANGLE OF ELEMENTS = 30.0 DEGREES

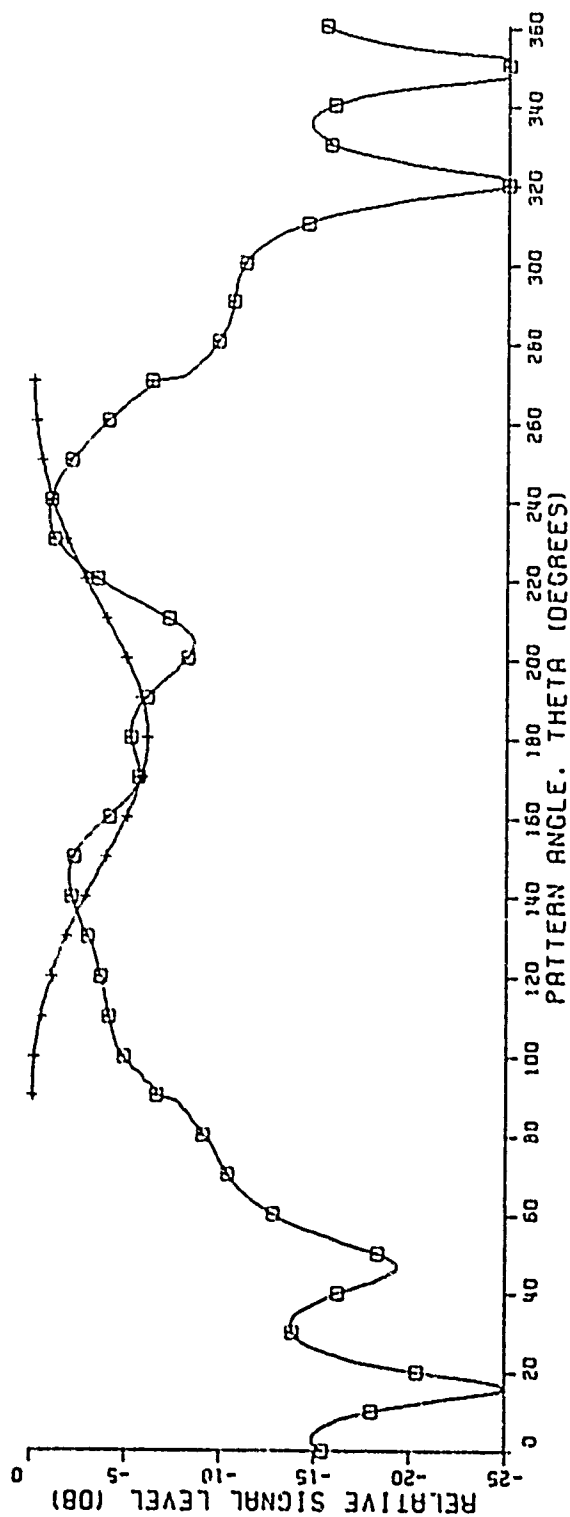
MONOPOLE LENGTH = 0.25 WAVELENGTHS

FREQUENCY = 900.0 MHz

FIELD INCLUDING EDGE DIFFRACTION

+ FIELD FROM ANT. ON INFINITE GROUND PLANE

Fig. II-25b.



180  
 90 — 8.0" — 2.0" — 20.0" — 270  
 ANGLE OF ELEMENTS = 30.0 DEGREES

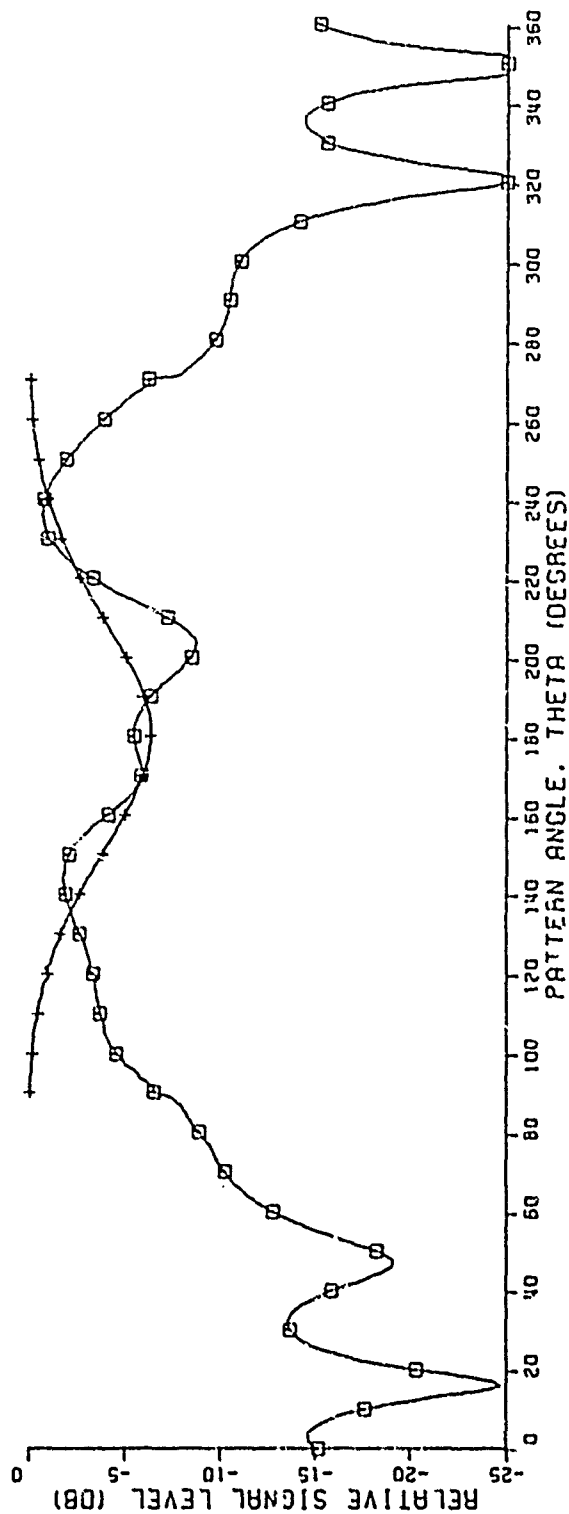
MONOPOLE LENGTH = 0.25 WAVELENGTHS

FREQUENCY = 900.0 MHZ

○ FIELD INCLUDING EDGE DIFFRACTION

+ FIELD FROM ANT. ON INFINITE GROUND PLANE

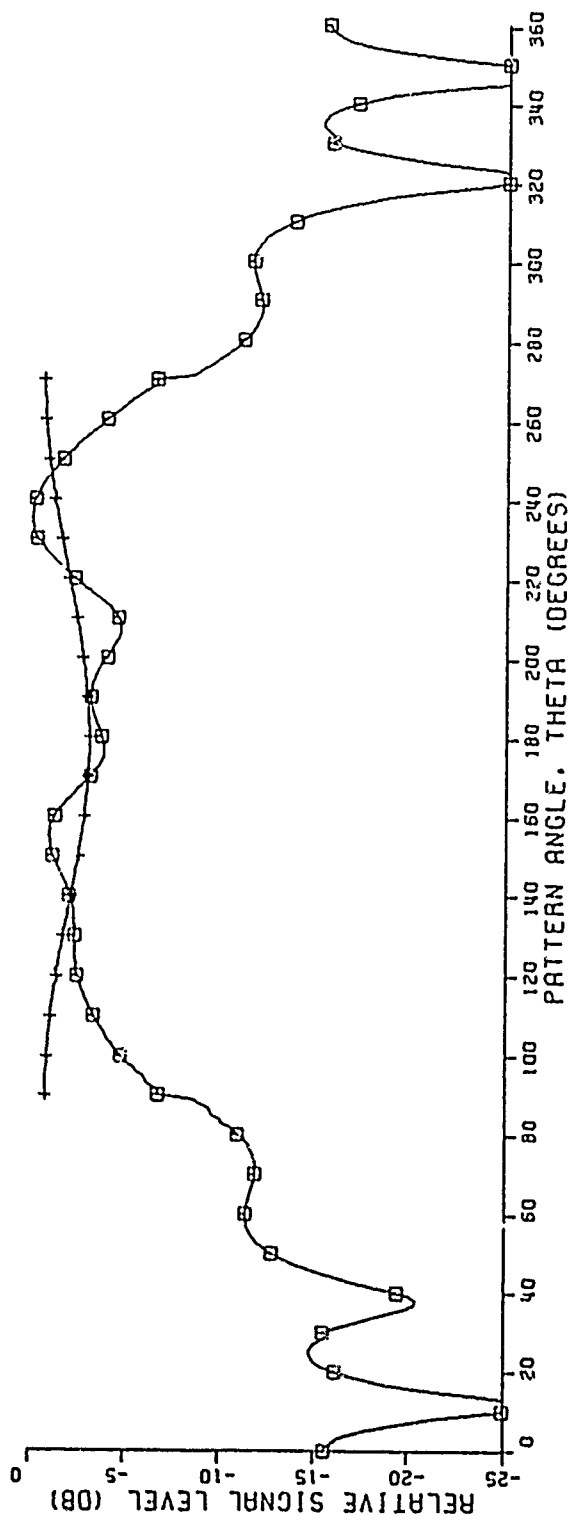
Fig. JI-2c.



180  
 90 8.0" 3.3" 20.0" 270  
 ANGLE OF ELEMENTS=30.0 DEGREES  
 MONOPOLE LENGTH=0.25 WAVELENGTHS  
 FREQUENCY=900.0 MHZ  
 O FIELD INCLUDING EDGE DIFFRACTION  
 + FIELD FROM ANT. ON INFINITE GROUND PLANE

Fig. II-2d.





180

90 8.0" 0.2" 20.0" 270

ANGLE OF ELEMENTS=30.0 DEGREES

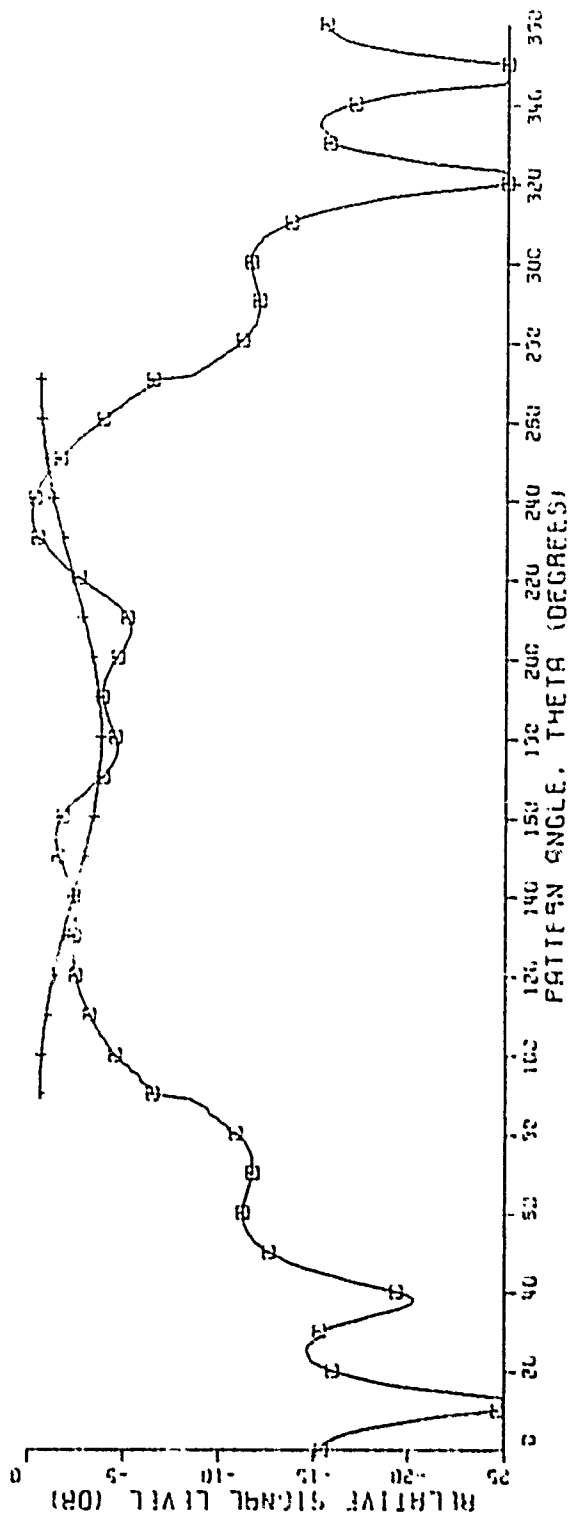
MONOPOLE LENGTH=0.28 WAVELENGTHS

FREQUENCY=1000.0 MHZ

□ FIELD INCLUDING EDGE DIFFRACTION

+ FIELD FROM ANT. ON INFINITE GROUND PLANE

Fig. II-3a.



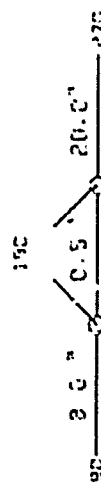
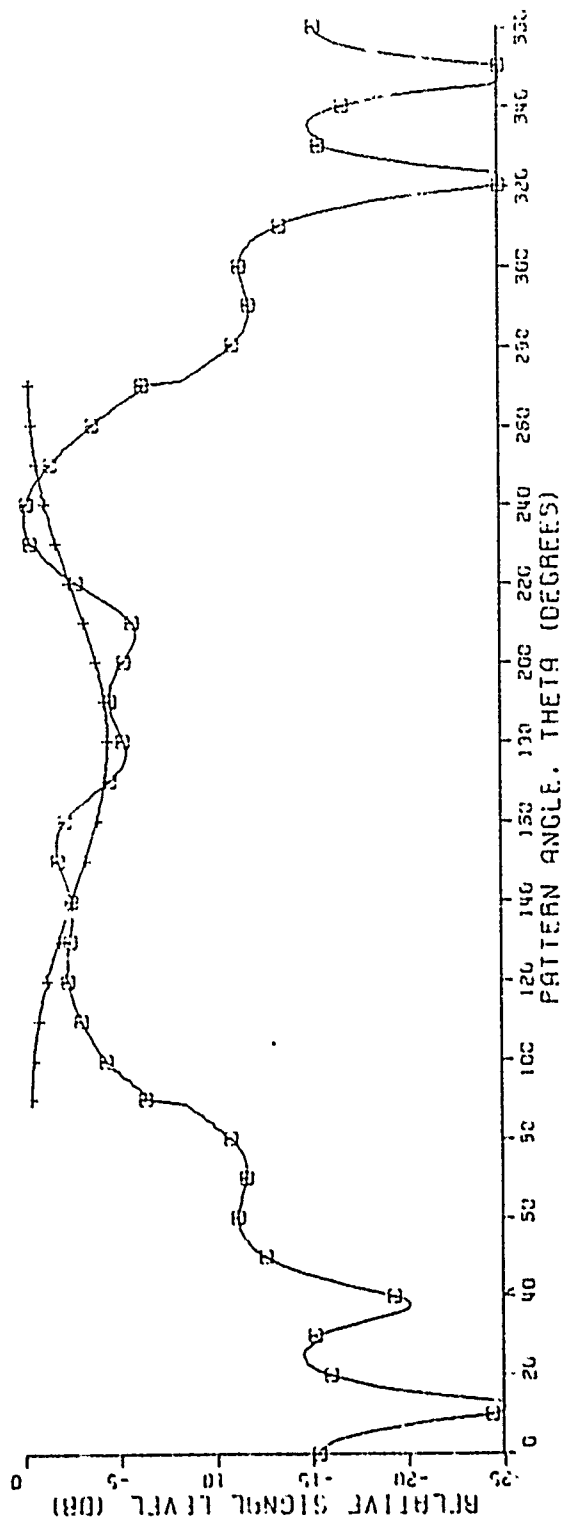

  
 MONOPOLE LENGTH=0.25 WAVELENGTHS  
 FREQUENCY=1000.0 MHZ  
 + FIELD INCLUDING EDGE DIFFRACTION  
 + FIELD FROM ANT. ON INFINITE GROUND PLANE

Fig. II-3b.



19C

30 0 0 20.0 270 ANGLE OF ELEMENTS=30.0 DEGREES

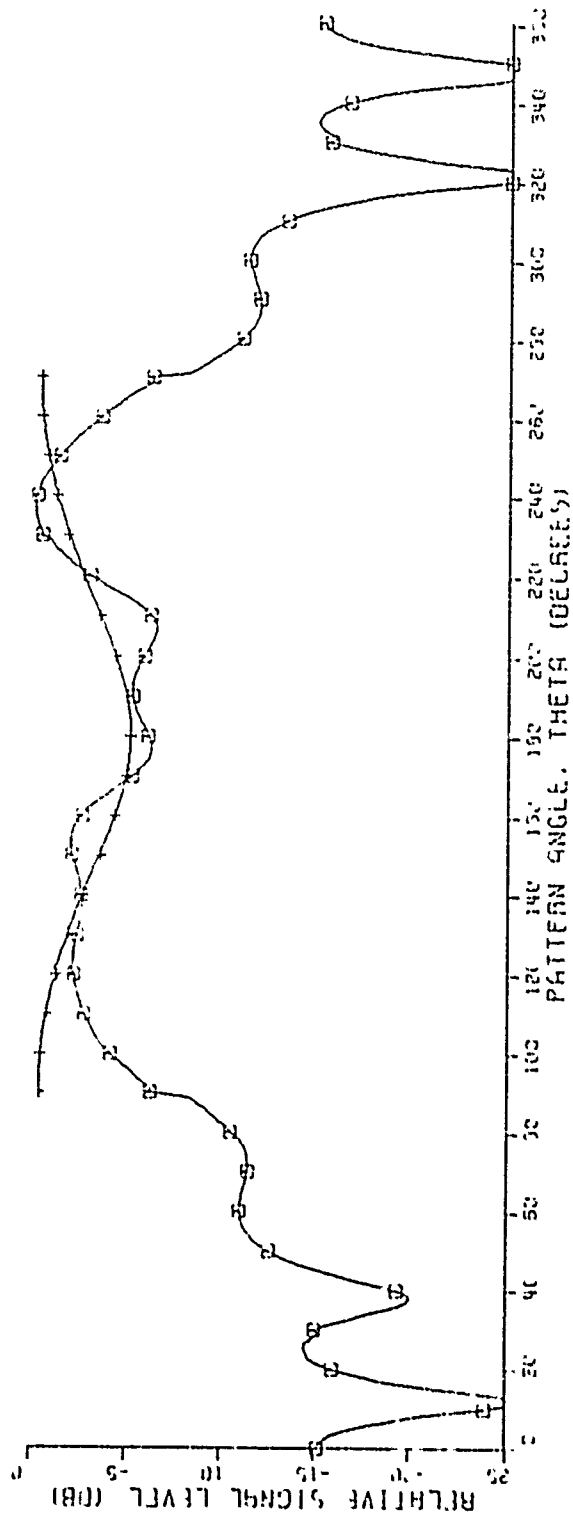
MONOPOLE LENGTH=0.28 WAVELENGTHS

FREQUENCY=1000.0 MHZ

+ FIELD INCLUDING EDGE DIFFRACTION

+ FIELD FROM ANT. ON INFINITE GROUND PLANE

Fig. II-3c.



150

30" 20" 20" 270 ANGLE OF ELEMENTS=30.0 DEGREES

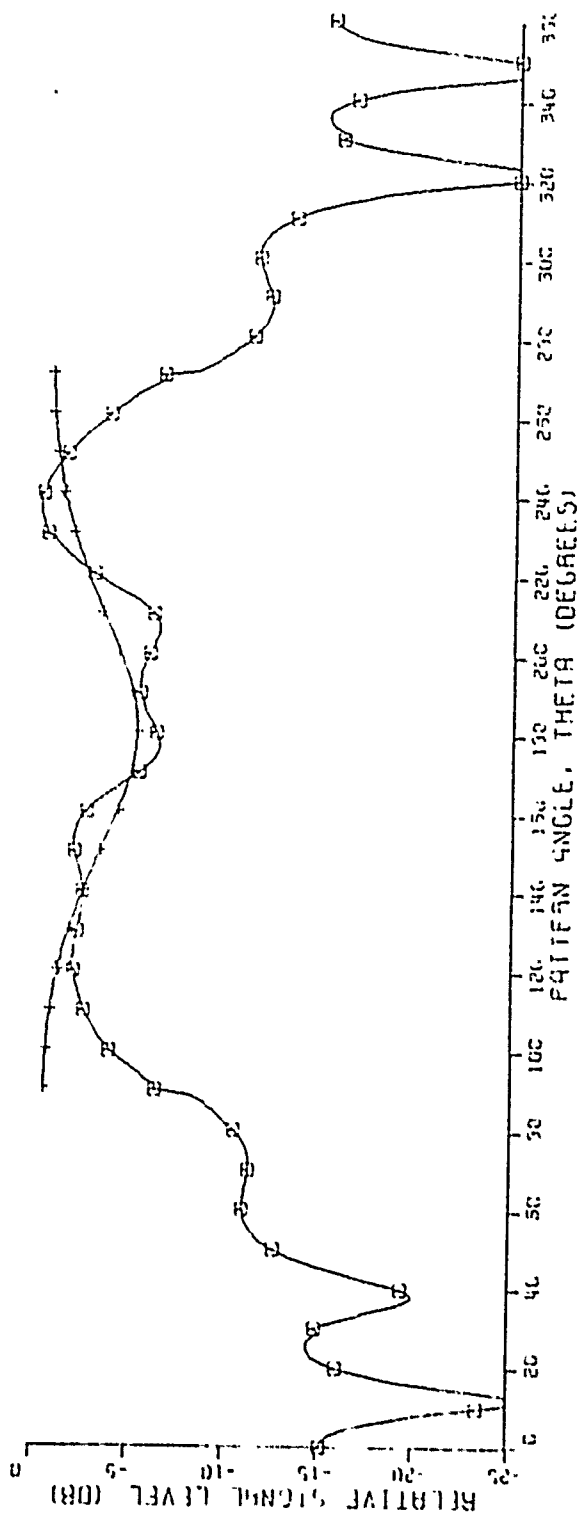
MONOPOLE LENGTH=0.20 WAVELENGTHS

FREQUENCY=1000.0 MHZ

E FIELD INCLUDING EDGE DIFFRACTION

+ FIELD FROM ANT. ON INFINITE GROUND PLANE

Fig. II-3d.



19C

30° 30' 20.0' 270° ANGLE OF ELEMENTS - 30.0 DEGREES

WAVELENGTH = 0.28

FREQUENCY = 1000.0 MHZ

W FIELD INCLUDING EDGE DIFFRACTION

+ FIELD FROM GNT. ON INFINITE GROUND PLANE

Fig. II-3e.